
COOLOCE debris bed experiments
and simulations investigating the
coolability of cylindrical beds
with different materials
and flow modes

Eveliina Takasuo, Tuomo Kinnunen, Stefan Holmström, Taru Lehtikuusi

VTT Technical Research Centre of Finland

Abstract

The COOLOCE experiments aim at investigating the coolability of debris beds of different geometries, flow modes and materials. A debris bed may be formed of solidified corium as a result of a severe accident in a nuclear power reactor.

The COOLOCE-8 test series consisted of experiments with a top-flooded test bed with irregular gravel as the simulant material. The objective was to produce comparison data useful in estimating the effects of different particle materials and the possible effect of the test arrangement on the results. It was found that the dryout heat flux (DHF) measured for the gravel was lower compared to previous experiments with spherical beads, and somewhat lower compared to the early STYX experiments. The difference between the beads and gravel is at least partially explained by the smaller average size of the gravel particles.

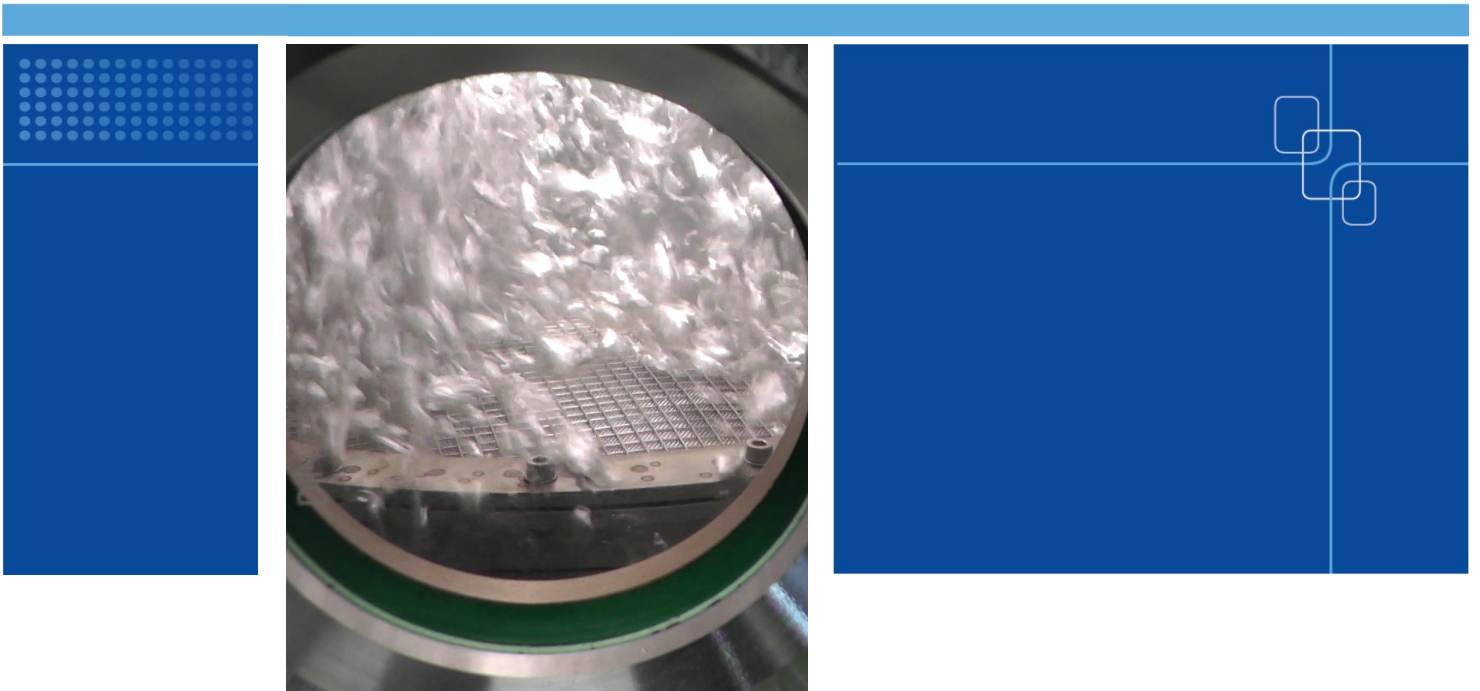
The COOLOCE-9 test series included scoping experiments examining the effect of subcooling of the water pool in which the debris bed is immersed. The experiments with initially subcooled pool suggest that the subcooling may increase DHF and increase coolability. The aim of the COOLOCE-10 experiments was to investigate the effect of lateral flooding on the DHF a cylindrical test bed. The top of the test cylinder and its sidewall were open to water infiltration. It was found that the DHF is increased compared to a top-flooded cylinder by more than 50%. This suggests that coolability is notably improved.

2D simulations of the top-flooded test beds have been run with the MEWA code. Prior to the simulations, the effective particle diameter for the spherical beads and the irregular gravel was estimated by single-phase pressure loss measurements performed at KTH in Sweden. Parameter variations were done for particle size and porosity used as input in the models. It was found that with the measured effective particle diameter and porosity, the simulation models predict DHF with a relatively good accuracy in the case of spherical particles. In the case of irregular gravel, for which the uncertainties of porosity and particle diameter are larger, the discrepancy between the simulations and experiments is greater.

Key words

severe accident, core debris, coolability, dryout, COOLOCE experiments, MEWA code

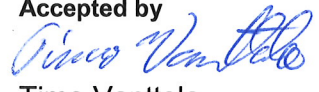
NKS-286
ISBN 978-87-7893-361-4
Electronic report, July 2013
NKS Sekretariat
P.O. Box 49
DK - 4000 Roskilde, Denmark
Phone +45 4677 4041
www.nks.org
e-mail nks@nks.org



COOLOCE debris bed experiments and simulations investigating the coolability of cylindrical beds with different materials and flow modes

Authors: Eveliina Takasuo, Tuomo Kinnunen, Stefan Holmström, Taru Lehtikuusi

Confidentiality: Public

Report's title	
COOLOCE debris bed experiments and simulations investigating the coolability of cylindrical beds with different materials and flow modes	
Customer, contact person, address	Order reference
SAFIR2014 Finnish Research Programme on Nuclear Power Plant Safety	2/2012SAF
Project name	Project number/Short name
Core debris coolability	77466/COOLOCE-E
Author(s)	Pages
Eveliina Takasuo, Tuomo Kinnunen, Stefan Holmström, Taru Lehtikuusi	58 p./3 appendices
Keywords	Report identification code
severe accident, core debris, coolability, dryout, COOLOCE experiments, MEWA code	VTT-R-04306-13
Summary	
<p>The COOLOCE experiments aim at investigating the coolability of debris beds of different geometries, flow modes and materials. A debris bed may be formed of solidified corium as a result of a severe accident in a nuclear power reactor.</p> <p>The COOLOCE-8 test series consisted of experiments with a top-flooded test bed with irregular gravel as the simulant material. The objective was to produce comparison data useful in estimating the effects of different particle materials and the possible effect of the test arrangement on the results. It was found that the dryout heat flux (DHF) measured for the gravel was lower compared to previous experiments with spherical beads, and somewhat lower compared to the early STYX experiments. The difference between the beads and gravel is at least partially explained by the smaller average size of the gravel particles.</p> <p>The COOLOCE-9 test series included scoping experiments examining the effect of subcooling of the water pool in which the debris bed is immersed. The experiments with initially subcooled pool suggest that the subcooling may increase DHF and increase coolability. The aim of the COOLOCE-10 experiments was to investigate the effect of lateral flooding on the DHF a cylindrical test bed. The top of the test cylinder and its sidewall were open to water infiltration. It was found that the DHF is increased compared to a top-flooded cylinder by more than 50%. This suggests that coolability is notably improved.</p> <p>2D simulations of the top-flooded test beds have been run with the MEWA code. Prior to the simulations, the effective particle diameter for the spherical beads and the irregular gravel was estimated by single-phase pressure loss measurements performed at KTH in Sweden. Parameter variations were done for particle size and porosity used as input in the models. It was found that with the measured effective particle diameter and porosity, the simulation models predict DHF with a relatively good accuracy in the case of spherical particles. In the case of irregular gravel, for which the uncertainties of porosity and particle diameter are larger, the discrepancy between the simulations and experiments is greater.</p>	
Confidentiality	Public
Espoo 14.6.2013	
Written by	Reviewed by
	
Eveliina Takasuo Senior Scientist	Mikko Ilvonen Team Leader
	Accepted by
	
	Timo Vanttola Technology Manager
VTT's contact address	
PO Box 1000, 02044-VTT, Finland	
Distribution (customer and VTT)	
SAFIR2014 Reference Group 5, NKS Management Board	
<p><i>The use of the name of the VTT Technical Research Centre of Finland (VTT) in advertising or publication in part of this report is only permissible with written authorisation from the VTT Technical Research Centre of Finland.</i></p>	

Contents

Contents.....	3
1. Introduction.....	5
2. Experimental set-up.....	6
2.1 Particle size distribution.....	9
2.2 Bed porosity.....	10
2.3 Test matrix.....	11
2.4 The test procedures.....	11
2.4.1 Saturated initial conditions.....	11
2.4.2 Subcooled initial conditions.....	12
2.5 Estimation of dryout power by steam flow.....	13
3. COOLOCE-8 and -9 results.....	14
3.1 COOLOCE-8a and 8aR.....	14
3.2 COOLOCE-8b.....	17
3.3 COOLOCE-8c.....	18
3.4 COOLOCE-8d.....	20
3.5 COOLOCE-8e.....	21
3.6 COOLOCE-8f.....	23
3.6.1 COOLOCE-9a.....	24
3.7 COOLOCE-9b.....	27
4. COOLOCE-8 and -9 discussion.....	34
4.1 Effect of particle material.....	34
4.2 Effect of experimental set-up.....	34
4.3 Effect of pool subcooling.....	36
5. COOLOCE-10 results.....	38
5.1 COOLOCE-10a.....	38
5.2 COOLOCE-10b.....	39
5.3 COOLOCE-10c.....	41
6. COOLOCE-10 discussion.....	43
6.1 Effect of lateral flooding.....	44
7. 2D simulations of top-flooded beds.....	45
7.1 Goal.....	45
7.2 Simulant materials in the experiments.....	45
7.3 Simulation specifications.....	46
7.3.1 Drag force models for porous medium.....	46
7.3.2 Simulation set-up.....	48
7.4 Simulation results.....	50
7.4.1 Cylindrical debris beds with gravel (COOLOCE-8 and STYX).....	50
7.4.2 Cylindrical debris beds with spherical particles (COOLOCE-3-5).....	52
7.4.3 Conical debris bed with spherical particles (COOLOCE-6-7).....	53
7.5 Discussion of the simulation results.....	54
7.5.1 Model limitations.....	55
8. Conclusions.....	56
9. References.....	56
APPENDIX A. Heater arrangement in the COOLOCE cylinder.....	A

APPENDIX B. Thermocouple arrangement in the COOLOCE cylinder.....	B
APPENDIX C. Dryout heat flux and power density in the experiments and simulations	C

1. Introduction

A debris bed (particle bed) that consists of solidified corium may be formed as a result of a core melt accident in a nuclear power reactor. Depending on the design of the reactor, such a debris bed may be formed in the containment, e.g. in the flooded lower drywell of the Finnish BWR's after the failure of the reactor pressure vessel, or inside the pressure vessel. In order to ensure the coolability of the core debris and to prevent dryout and possible re-melting of the material, decay heat has to be removed from the material. The issue of corium coolability has received considerable attention since the accident at Fukushima which apparently resulted in various degrees of core melting in Units 1–3.

The COOLOCE test facility is used to investigate the coolability of porous particle beds of different geometries, focusing on ex-vessel cases. The main objective of the experimental programme in 2011 was to compare the dryout power of a conical (heap-like) particle bed configuration to that of a cylindrical (evenly distributed) configuration [1-5]. This report describes the test series COOLOCE-8-10.

The test series COOLOCE-8 and -9 extended the investigations to (1) experiments with the irregular gravel used in the STYX experiments and (2) experiments with a subcooled pool. In COOLOCE-10, a flow mode variation was considered: the test cylinder was modified to allow water infiltration through the cylinder sidewall, in addition to the top flooding through the cylinder top surface. The COOLOCE-8 and -9 test series were conducted with irregular alumina gravel as the debris simulant material. The other COOLOCE experiments, including COOLOCE-10, have been conducted with spherical ceramic beads. While the spherical beads are poor representation of the realistic particles expected to form in reactor conditions, they are adequate for comparison experiments investigating the effect of geometry and flow mode on coolability (since the relative coolability can be assumed independent of the material).

The main objective of COOLOCE-8 was to clarify the role of the heating arrangement and the selection of particle material in the experiments. The alumina gravel that was used in the STYX experiments [6-8] can be considered more representative to the debris formed in the postulated reactor scenario as its size distribution is based on several FCI experiments [6]. Analyses that combine the results obtained by the COOLOCE and STYX facilities as well as those by the POMECO facility at KTH in Stockholm [9-10] are expected to produce a comprehensive understanding about the effect of the particle material and the effect of the different types of heating systems utilized in the different experiments. This will help to evaluate the representativeness of the results considering reactor scenarios and to reduce the uncertainties of the experiments.

The COOLOCE-9 experiments were motivated by another unknown issue in the reactor scenario. The severe accident management strategies of the Finnish and Swedish BWRs rely on quenching and coolability of the debris bed in a deep water pool in the lower drywell of the containment. Before the melt discharge the pool temperature is well below saturation temperature. Recent studies have suggested that the degree of pool subcooling has an effect of the melt fragmentation and debris bed formation, largely determining the size and shape of the particles in the established debris bed (fully quenched and settled) [11-12]. On the other hand, previous studies on the coolability of an established debris bed have mainly assumed saturated initial conditions. Thus, it is of interest to examine whether the subcooling of the water surrounding the debris bed – in addition to the possible effect of the pool dynamics in general – helps to maintain coolability after the initial quenching and bed formation.

Prior to the COOLOCE-8 experiment, a sieve analysis was performed for the alumina gravel in order to estimate the particle size distribution and, preferably, to achieve a similar distribution as in the original STYX experiments. The test facility was modified for the

subcooled pool experiments by installing additional thermocouples into the water volume of the test vessel.

The COOLOCE-10 test series investigated the effect of lateral flooding in a cylindrical bed. The main objective was to complement the experimental database of dryout heat flux measurements in cases of multi-dimensional flooding. The cylindrical test bed with lateral flooding (water infiltration through all surfaces except bottom), roughly approximates a mound-like bed: a representative debris bed geometry which has not been previously investigated experimentally.

The flow conditions in the laterally flooded cylinder are analogous to those in the conical bed but with a constant cross-sectional area, through which the steam flows upwards. In the conical geometry, it has been shown by simulations that dryout typically occurs in the tip (apex) of the cone where the cross-sectional area is approaching zero, and the dryout zone is inherently very small. In the laterally flooded cylinder, there is no such restriction for the dryout zone size by the geometry and it is expected that the evaluation of simulation results against the experimental ones might be easier.

The final part of the report consists of simulations performed using the MEWA code which is a severe accident code developed at the University of Stuttgart. The simulation results are compared to the results of COOLOCE-8 and the other cylindrical bed experiments. The experiments with the conical test bed geometry are also modelled with variations of particle size and porosity. The effective particle diameter for both materials, gravel and the spherical beads, has been estimated based on single-phase pressure loss and constant porosity. The dryout heat flux obtained with these effective parameter values has been compared to the experimental results.

2. Experimental set-up

The main components of the COOLOCE test facility are the pressure vessel which houses the test particle bed, the feed water and steam removal systems and instrumentation. The custom-designed pressure vessel has a volume of 270 dm³ and design pressure of 7 bar (overpressure). The schematic of the arrangement is presented in *Fig. 1*. A photograph of the experimental set-up is shown in *Fig. 2*.

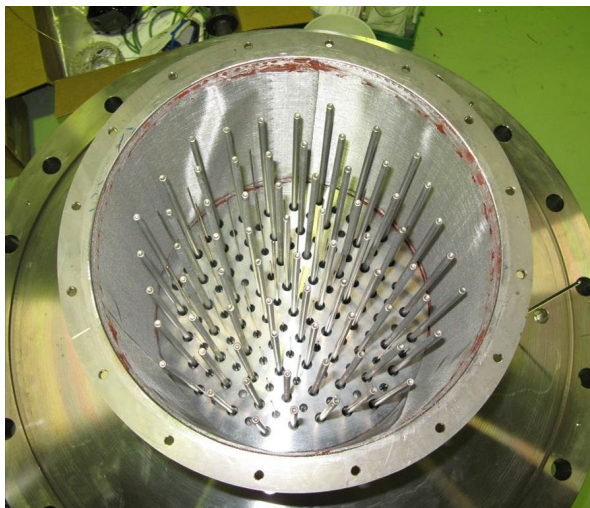
The cylindrical test bed is 305 mm in diameter and 270 mm in height with the total volume being 19.7 dm³. Due to the installation of a wire net to constrain the bed sidewalls, the diameter is about 5 mm smaller than in the previous arrangement used in COOLOCE-3-5 (that had a volume 20.4 dm³). In COOLOCE-8 and -9, the sidewall was closed so that only top flooding was allowed. For COOLOCE-10, the sidewall was opened in order to achieve multi-dimensional flow mode in which water would infiltrate through the sidewall as well as the top surface.

The test particle bed in COOLOCE-8 and -9 consisted of irregular alumina gravel (Al₂O₃) which was the same material as in the STYX experiments. The test bed in COOLOCE-10 consisted of spherical zirconia/silica beads (ZrO₂ ≥ 65%, SiO₂ ≤ 35%) that were used in COOLOCE-3-5, the reference experiments for COOLOCE-10. The test bed is heated by Ø 6.3 mm vertically installed cartridge heaters. There is a 40 mm layer of unheated particles above the heaters. In the cylindrical test bed, all the heaters have a heated length of approximately 230 mm. The configuration aims at a power distribution as uniform as possible with this type of heating system with no heat-generating particles.

To measure the particle bed temperature and detect dryout, K type thermocouples are installed in a distributed configuration striving for maximal coverage of the particle bed



Fig. 2. COOLOCE experimental set-up: 1) feed water pre-heater, 2) feed water control valve, 3) connection box for the heaters, 4) pressure vessel, 5) steam line condenser and scale, 6) sightglass with video monitoring, 7) water level and pressure gauges.



a)



b)

Fig. 3. a) The heater and thermocouple arrangement and b) the test bed filled with particles for the COOLOCE-8 and 9 experiments. Note that the open side wall was sealed and the top covered with a wire net before test runs. In COOLOCE-10, the set-up is similar but the test bed is filled with ceramic beads.

2.1 Particle size distribution

One of the main objectives of the experiments is to compare the results to the STYX experiments. Thus, the similarity of the particle size distribution in the batch to be used in the experiments with the original size distribution had to be investigated, and a sieve analysis was done for the alumina gravel prior to the experiments. The results of the analysis, i.e. the old and new particle size distributions are shown in *Fig. 4*.

The original distribution did not contain particles smaller than 0.25 mm but a small fraction of these was found in the new analysis. The origin of these might be the layer of small particles used in the STYX experiments with a stratified test bed. Even though the fraction of the smallest particles (0.0-0.25 mm) is small, it contributes to the area-weighted average size and possibly to the bed porosity. Thus, the smallest particles were removed before COOLOCE-8 experiments.

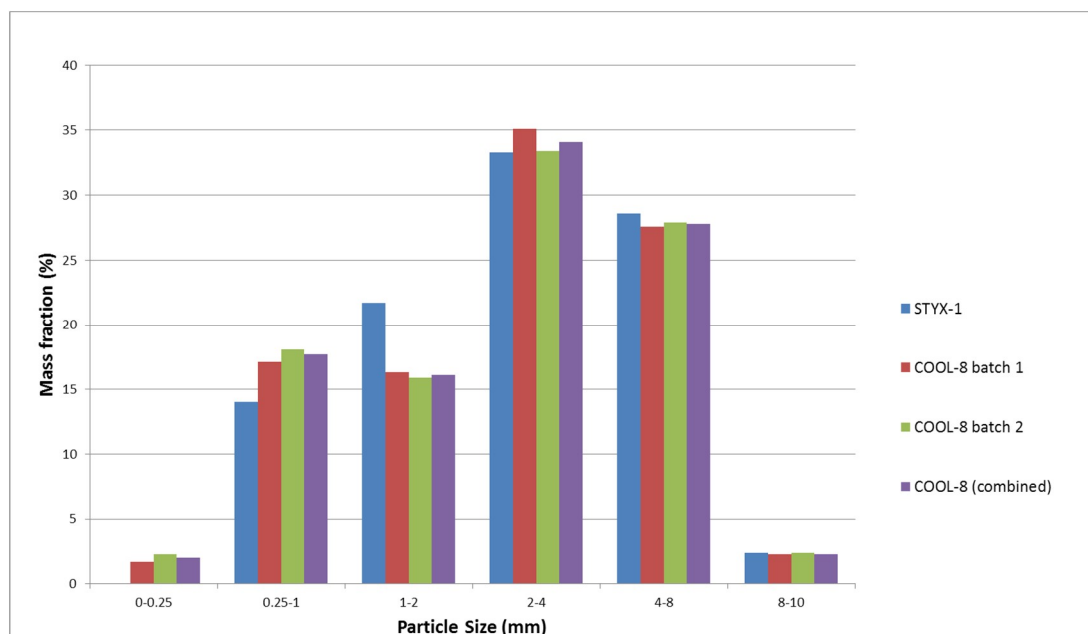


Fig. 4. Size distribution of the alumina gravel before the STYX and COOLOCE experiments (measured in 2000 and 2012). The smallest size group was removed before the COOLOCE experiments.

Due to the irregular shape of the particles, it is usually difficult to define a single average particle diameter (based on e.g. number of particles or surface weighted averages) that would be representative for modeling purposes. Instead, an effective particle diameter obtained by single-phase pressure loss measurements and the Ergun equation [13] is often a good choice for modeling purposes. The original effective particle diameter for the STYX test bed according to single phase pressure loss measurement was about 0.8 mm for 40% porosity [6].

After the sieve analysis, a batch of the gravel was sent to KTH (Royal Institute of Technology) in Stockholm, Sweden, for re-evaluation of effective particle diameter with the POMECO-FL test facility. According to the measurement, the effective particle diameter was biased towards smaller particles even though the smallest batch had been removed from the gravel prior to the measurements: For a porosity of 40.8%, the effective particle diameter was 0.65 mm. The results of the measurements are illustrated in *Fig. 5*. For higher flow velocities, the pressure drop was greater than the one predicted by the Ergun's equation.

The average size of the spherical beads used in COOLOCE-3–5 and made of zirconia/silica composition ($ZrO_2 \geq 65\%$, $SiO_2 \leq 35\%$) is somewhat greater, 0.97 mm. The size distribution is rather uniform. Note that in the previous COOLOCE publications, the particle size is reported as 0.8 – 1.0 mm as given by the manufacturer. Later estimation by using image processing software revealed that the particles are actually slightly larger, the measured range being 0.815 – 1.126 mm.

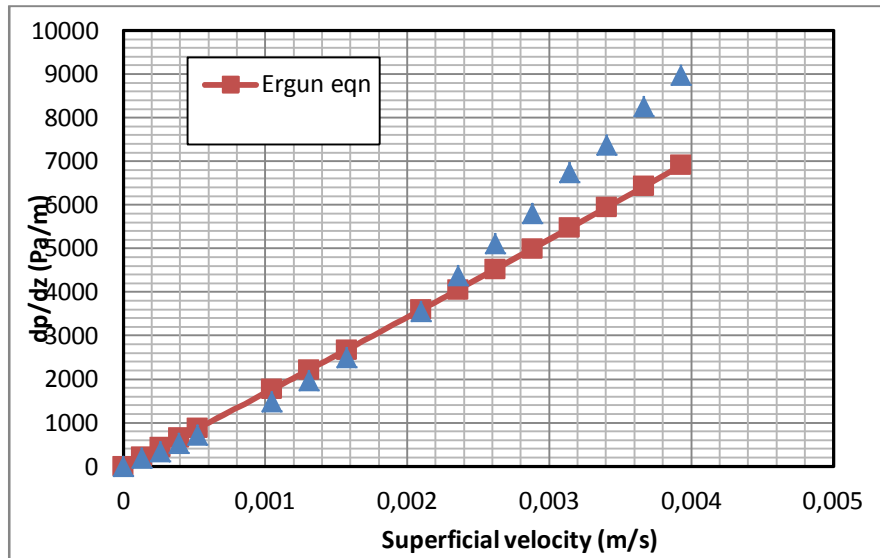


Fig. 5. Pressure loss for the alumina gravel as a function of superficial fluid velocity [14].

2.2 Bed porosity

The bed porosity was estimated based on the weight of the gravel in the cylinder which yielded the approximate porosity of 39%. The density of the material is approximately 3900 kg/m^3 . Porosity was also estimated by flooding the gravel with water in the test bed and in a separate container but these measurements cannot be considered reliable since it was apparent that the material was not fully wetted. Pockets of air remained in the porous material and the resulting porosity, i.e. the volume fraction of water, was only about 32%.

The test bed was not purposefully packed as dense as possible before the experiments (as was the case also with the STYX test beds) because this might have caused artificial particle size stratification. The measured porosity of 39% is reasonable considering the range estimated for the STYX experiments: 34-41% (34-37% by flooding the test bed and 40-41% with separate batches of particles [6]). After the experiments, it was seen that no significant reduction in the apparent bed volume had occurred during the experiments.

For the test bed filled with spherical beads, the porosity is estimated to be 38-40%. In this case, porosity measurement in a separate container suggested fully wetted particles. Based on the weight of the particles in the cylindrical test bed, the porosity is 39.2%. (Note that in this calculation, the heaters are not considered as part of the porous structure, i.e. they are subtracted from the total volume.)

2.3 Test matrix

The experiments conducted in 2012 are listed in *Table 1*. The experimental series are numbered according to their chronological order. However, the separate dryout points at different pressures such as 8a – 8f are not always measured in the order of increasing pressure, rather, the naming convention is selected for better clarity. The details of the test runs are presented in the result Chapter.

Table 1. The COOLOCE experiments in 2012.

Experiment	Date (2012)	Type of test procedure	Pressure [bar abs]
COOLOCE-8a	July 2	<ul style="list-style-type: none"> • saturated initial conditions • irregular gravel particles • top flooding 	1.1
COOLOCE-8aR			1.1
COOLOCE-8b			2.1
COOLOCE-8c			3.0
COOLOCE-8d			4.0
COOLOCE-8e			5.0
COOLOCE-8f			7.0
COOLOCE-9a	July 5	<ul style="list-style-type: none"> • subcooled initial conditions 	1.0
COOLOCE-9b	August 22		1.0
COOLOCE-9c	August 24	<ul style="list-style-type: none"> • irregular gravel particles • top flooding 	1.0
COOLOCE-9d	August 24		1.0
COOLOCE-10a	December 18	<ul style="list-style-type: none"> • saturated initial conditions • ceramic beads • lateral and top flooding 	1.3
COOLOCE-10b	December 18		2.0
COOLOCE-10c	December 19		3.0

2.4 The test procedures

2.4.1 Saturated initial conditions

The normal test procedure consists of a heat-up sequence and the main test sequence. Generally, these are similar for the cylindrical and conical bed experiments. Prior to the experiments, the test pressure vessel is filled with pre-heated demineralized water to a level of approximately 300 mm above the test bed surface. During the heat-up sequence the facility is heated up to the saturation temperature and steady-state boiling is reached. The power level of the heat-up sequence depends on e.g. the test pressure and the expected dryout power.

In the test sequence, a stepwise power increase is conducted until a dryout is indicated by one or more thermocouples within the test bed. Dryout is seen as a stable increase of the sensor temperature from the saturation temperature. A holding time of 20 to 30 minutes is applied for each power step. This is necessary because the boil-off of liquid inside the particle bed after the critical power level has been reached takes some time (the time depends on the excess power as will be discussed in Chapter 4.3).

The size of the power increments is 1 kW - 2 kW. The power increase scheme for each test sequence is documented in the power and temperature figures in Chapter 3. During the test

sequence, the water level and pressure in the test vessel are controlled by the feed water and steam line control valves according to given set points. These process variables are also shown in Chapter 3 and Chapter 5.

The heating power is manually controlled by adjusting the output voltage of a purpose-tailored power transformer. The heaters are arranged in three groups according to the electrical phase. The heater locations are presented in Appendix A. Five of the heaters are equipped with temperature sensors which help to detect possible overheating. (In the previous experiments, there were three heaters with thermocouples). The thermocouple map is presented in Appendix B. The thermocouples numbered 100-45 and 400-8 have multiple measuring points and the other thermocouples have a single measuring point at the upper end. Total number of sensors is 70, excluding the heater measuring points.

The heat-up sequence typically lasts from 1 to 2 hours during which the temperature is gradually increased up to the saturation temperature at the pressure of the experiment to be conducted. The temperatures near the bottom plate of the pressure vessel tend to increase more slowly than in the other parts of the test bed. The bottom plate temperature remains slightly below the saturation temperature in steady-state conditions due to heat losses.

2.4.2 Subcooled initial conditions

In the subcooled pool experiments, there is no heat-up sequence. At the beginning of the test runs, the power level is rapidly increased up to - or above - the expected dryout power in saturated conditions. Then, the power is held constant until dryout occurs and the time to dryout is examined. It is also possible that no dryout occurs in case the pool subcooling increases dryout power. The test procedure was adopted after the first experiment, a scoping test with the purpose of evaluating the possibilities of subcooled pool measurements with the current experimental set-up.

The pool temperature cannot be controlled during the test runs since there is no arrangement for continuous water circulation. Thus, the pool temperature gradually increases until saturation temperature is reached, at which time the test run is terminated. After each measured dryout point, the power is turned off to allow the test bed to reflood and the temperatures to stabilize (to some extent) before the next constant power step aiming for dryout.

Because of the increasing temperature (and decreasing subcooling), the dryout power at constant amounts of pool subcooling cannot be quantified. Moreover, the pool tends to be thermally stratified during the experiments. However, the effect of the pool temperature (average or at a certain measuring point) on dryout power may be estimated based on the waiting times to dryout and observing whether a dryout occurs at all at a constant power level.

The experiments have been conducted at atmospheric pressure. For greater pressure levels, the test vessel would have to be pressurized with air because there is no flow in the steam line with the pressure control valve (steam is condensed in the subcooled water unless the pool temperature is very close to saturation temperature). A multi-point thermocouple is installed into the pressure vessel specifically to monitor the pool temperature in the annular space between the test bed and the vessel wall (between 67 - 217 mm height). The pool temperature is also measured at the height of 317 mm and the steam volume at 760 mm.

2.5 Estimation of dryout power by steam flow

As described in the previous COOLOCE reports [1-5], the condensate flow that exits from the facility can be calculated using a bench scale connected to the condenser outlet. It is possible to verify the power level of the experiments and estimate the heat losses assuming that the water which is collected to the scale per unit of time is equal to the mass flux evaporated by the heated test bed. The difference between the power calculated from the measurements of mass (*calculated power*) and the *control power* gives an estimate of the heat losses and uncertainty in the recorded control power. This method is not applicable to the experiments with initially subcooled pool because steam is condensed in the water pool and does not exit from the test vessel.

For the COOLOCE-8 and -10 test series, the difference between the control power and calculated power is 1-5 kW (10-20%) and it increases with increasing pressure. Since the power generation by the test bed heaters has to compensate for the heat losses, in addition to being able to boil the water, the control power is greater than the calculated power. Based on the estimates of condensate accumulation at the dryout power steps, the difference is similar to the one observed in the previous COOLOCE experiments.

Due to the unknown (and possible pressure-dependent) effect of direct contact condensation in the test vessel and other uncertainties in the condensate mass flow rate, we consider only the control power in the following Chapters. The values of control power serve as well-defined reference points for the different comparisons between the experiments conducted with COOLOCE and STYX facilities. (The STYX facility did not have a measurement for condensate mass flow).

3. COOLOCE-8 and -9 results

3.1 COOLOCE-8a and 8aR

The COOLOCE-8a test run at atmospheric pressure was the first performed with the alumina gravel. The power and temperature histories which illustrate the progress and dryout points of the test run are shown in Fig. 6. The parameters of the test run, i.e. pressure, water level in the test vessel and the feed water temperature are shown in Fig. 7. The temperatures shown in Fig. 6 are taken from the sensors that indicated dryout in the COOLOCE-8 series, mostly located below 100 mm in the test bed.

The heat-up sequence is included in the data, shown before 80 minutes in the test run. Two dryout points are seen in the test run at approximately 80 minutes and 130 minutes. The latter dryout point represents the final measured dryout power for the test run since it turned out that a clear excess power was applied in the heat-up sequence and in the first “approach” to dryout.

The dryout control power in this test run at 1.1 bar (abs.) pressure was 12.9 kW. Three temperature sensors located 40-120 mm from the test bed bottom indicated dryout.

The test run was repeated after the experiments with higher pressures to verify the dryout power of the first measurement at atmospheric pressure. The dryout power for the new test run, COOLOCE-8aR was 13.6 kW which is consistent with the first measurement considering the accuracy achieved with 2 kW power steps. The power and temperature histories during the second test run are presented in Fig. 8. The pressure and water level in the test vessel as well as the feed water temperature are shown in Fig. 9.

The results show a widespread dryout, 15 temperature sensors located in the lower region of the test bed (below 110 mm) indicated excursion from saturation temperature. The maximum temperature reached was above 200°C. The power was switched off when the heater temperatures in VY36 and VY37 (see Appendix B, measured in the heater sheath at 110 mm height) reached 300°C.

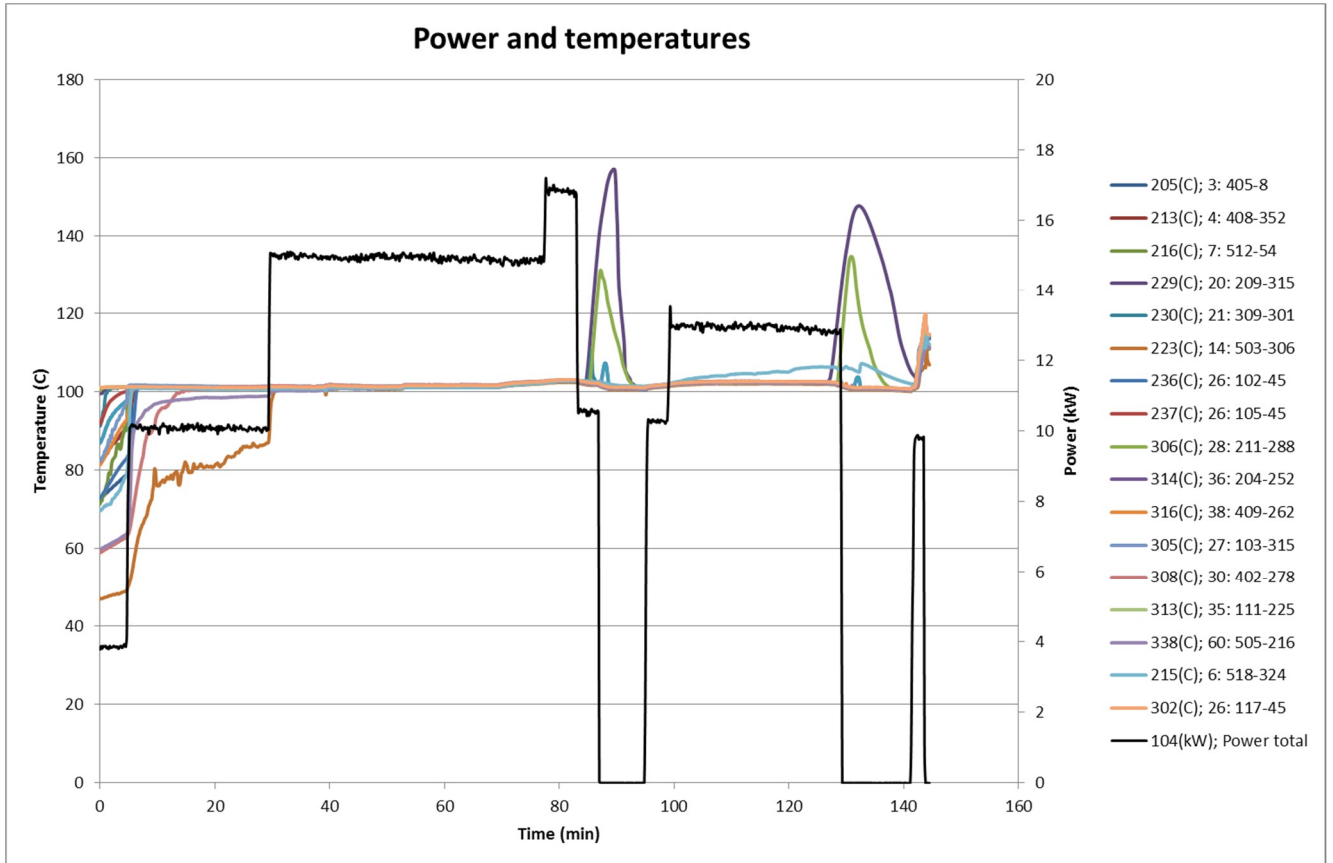


Fig. 6. Control power and temperature log in the COOLOCE-8a experiment.

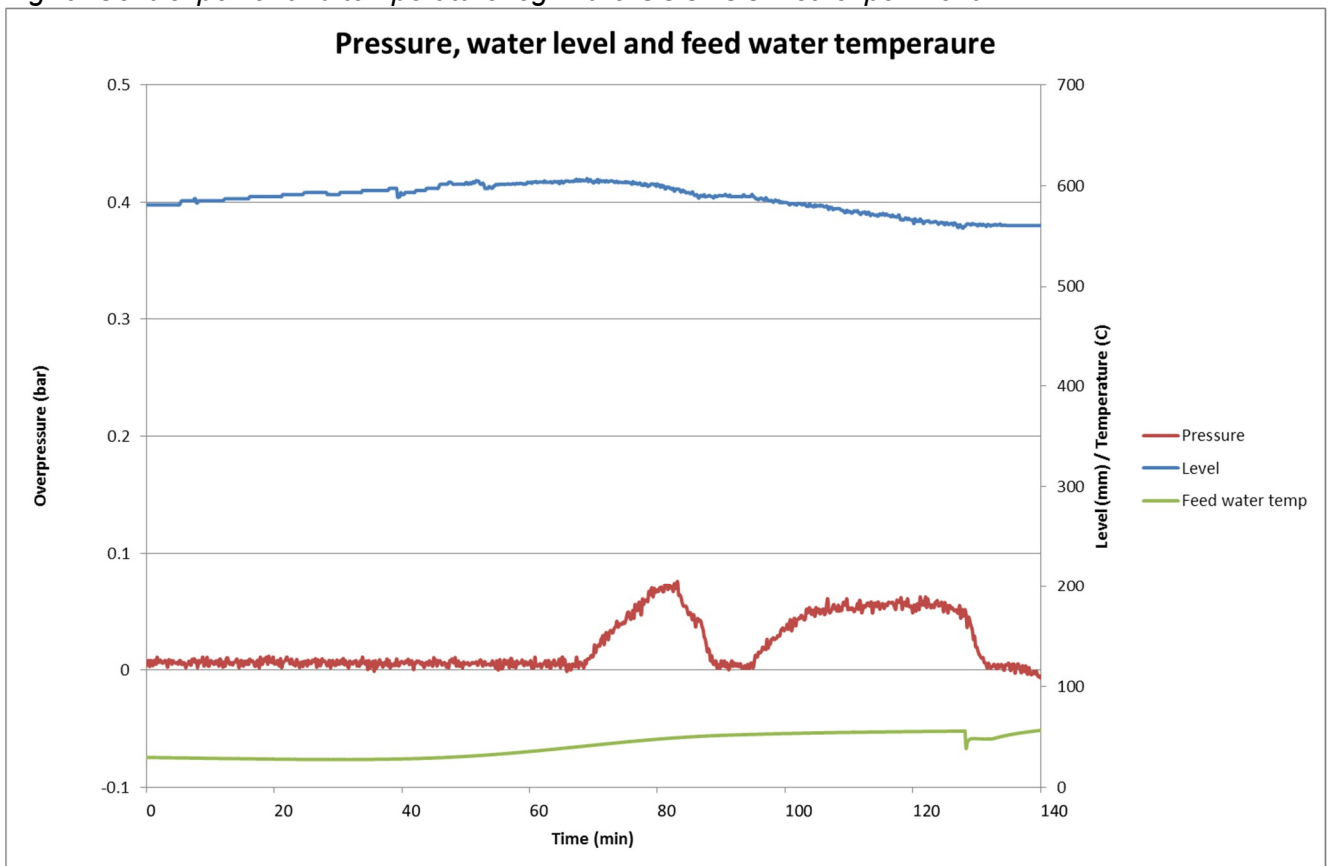


Fig. 7. Pressure and water level in the test vessel and the feed water temperature in the COOLOCE-8a experiment.

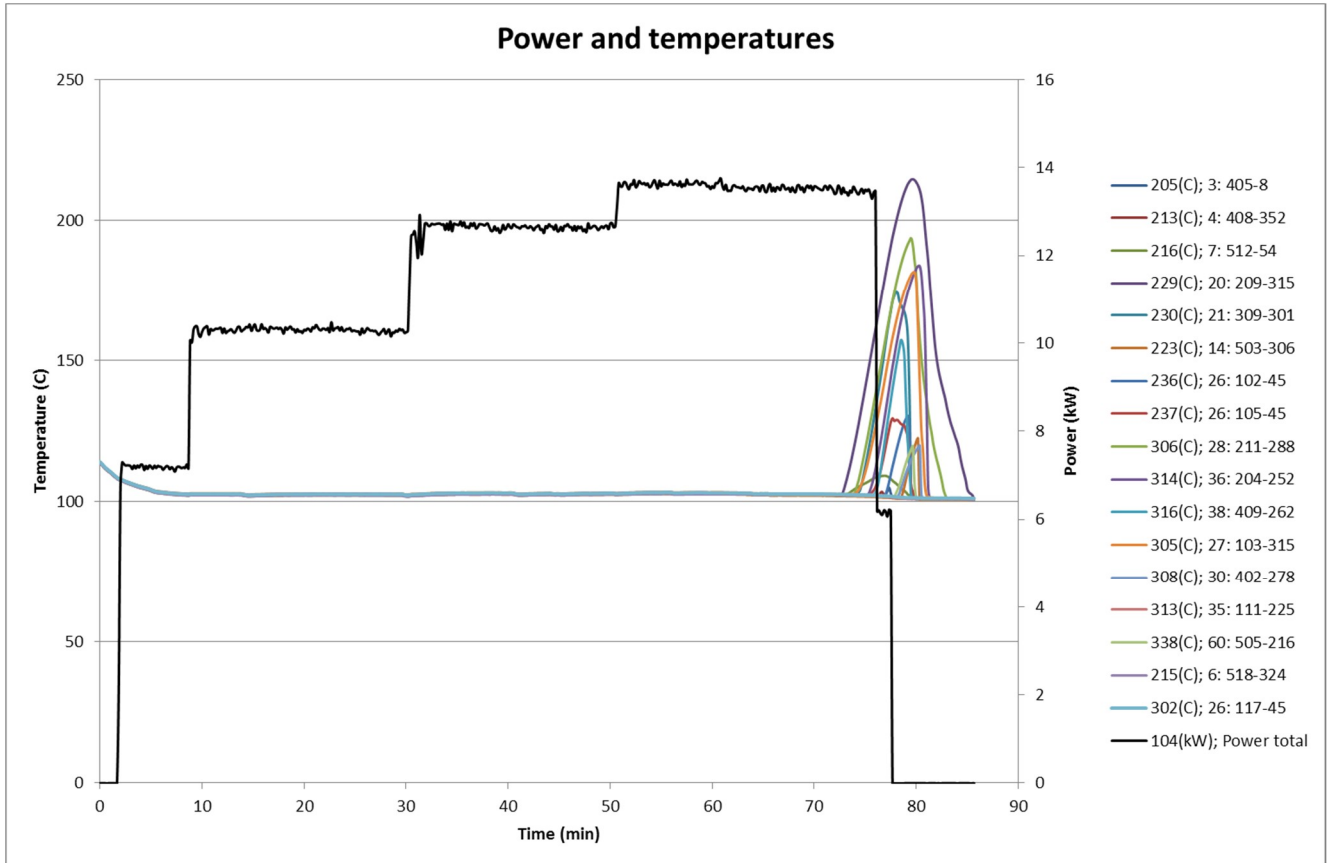


Fig. 8. Control power and temperature log in the COOLOCE-8aR experiment.

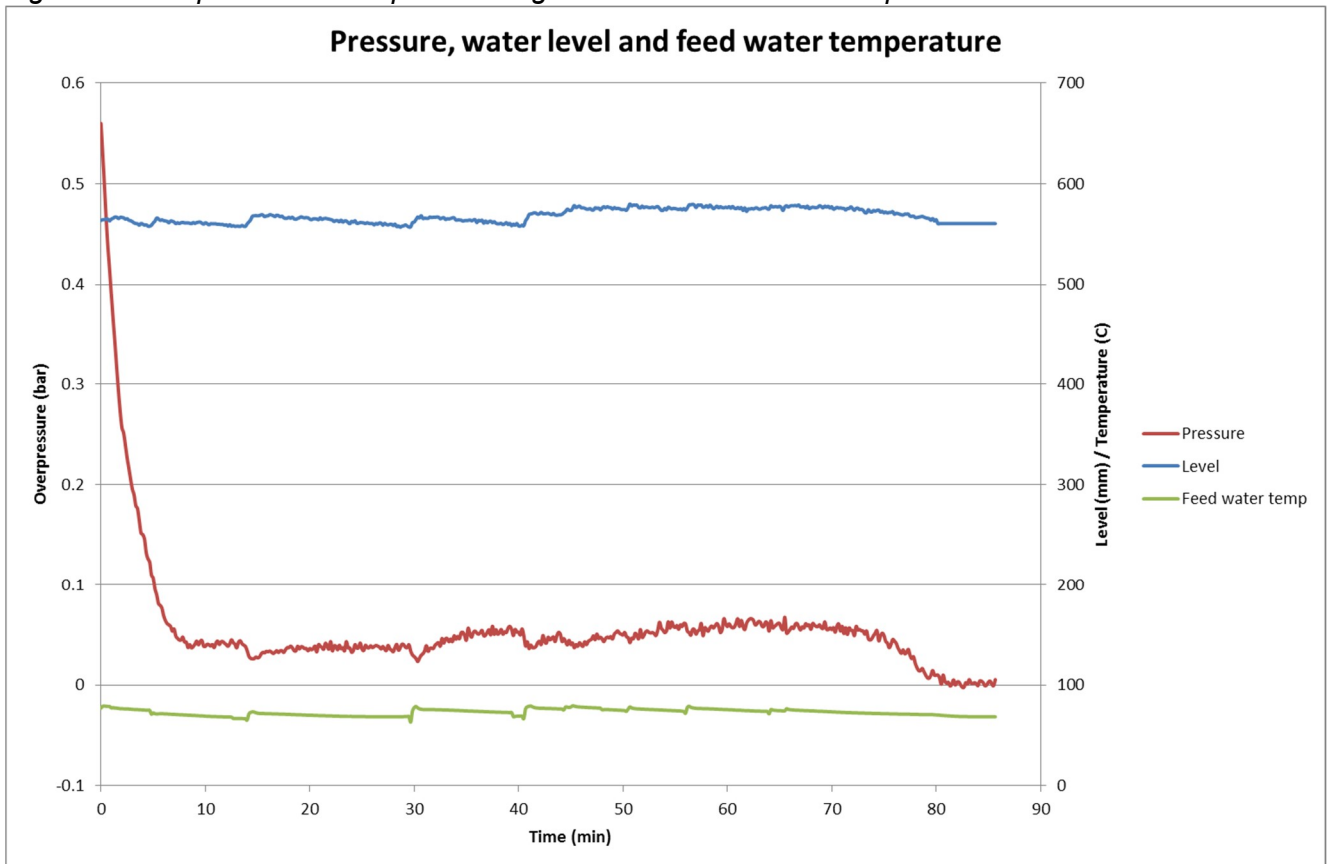


Fig. 9. Pressure and water level in the test vessel and the feed water temperature in the COOLOCE-8aR experiment.

3.2 COOLOCE-8b

The COOLOCE-8b experiment was conducted at approximately 2.1 bar (abs.) pressure. Two attempts were needed to measure the dryout power for this pressure level as the first attempt after a pressure increase from atmospheric to 2 bar after the COOLOCE-8a test run resulted in dryout already at 13 kW. It is suspected that the test bed had not been fully quenched after the first test run. The latter measurement yielded a reasonable value of 17.1 kW for the dryout power. The progress of this test run is illustrated in *Fig. 10* which shows the temperature and power histories and *Fig. 11* which shows pressure, water level and feed water temperature.

The three sensors indicating dryout were located at the height of 30 – 120 mm from the bottom. An increase up to about 150°C was indicated by the sensors 209-315 and 512-54. These sensors are rather far apart from each other, the latter is one of the outermost sensors in the test bed near the wall of the cylinder (opposite to the video camera in Appendix B).

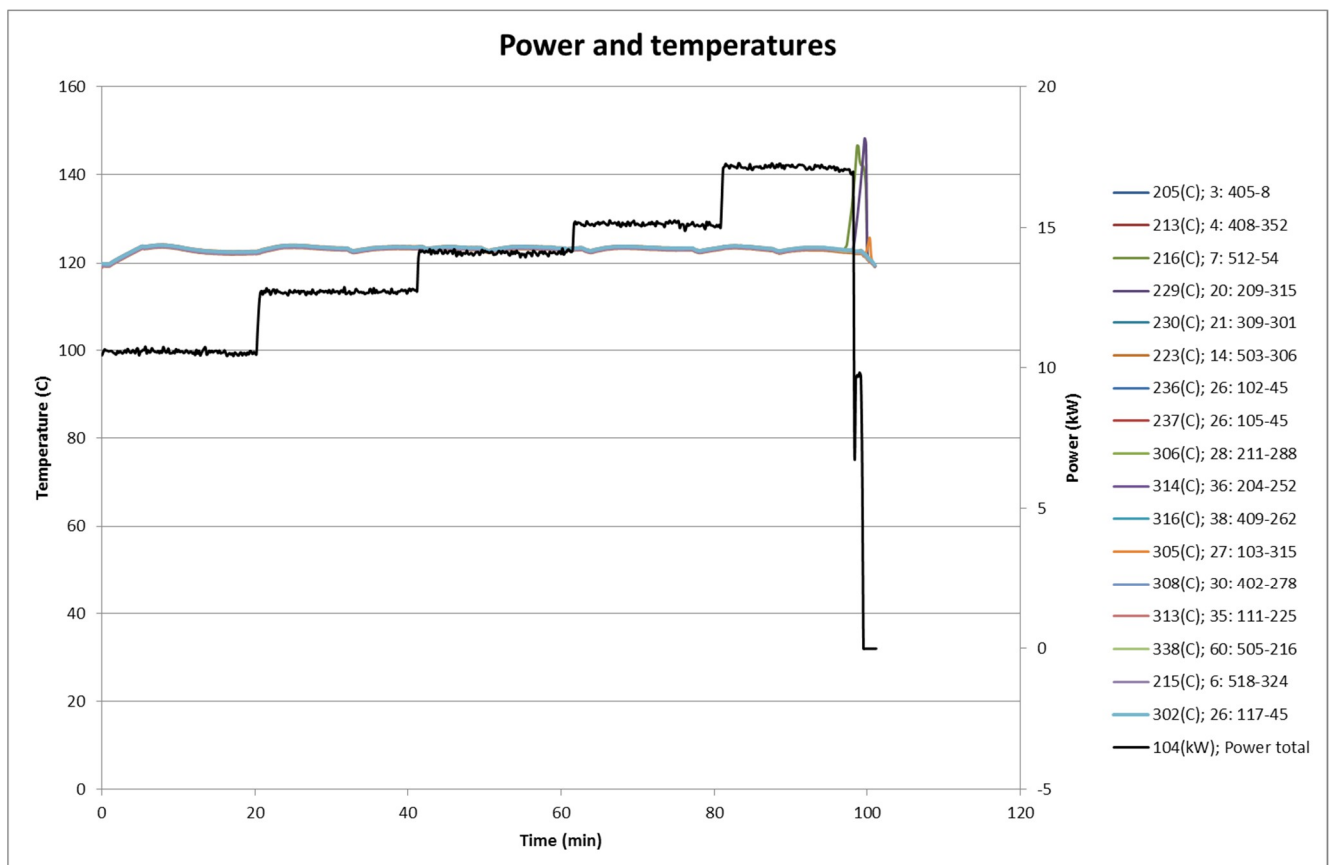


Fig. 10. Control power and temperature log in the COOLOCE-8b experiment.

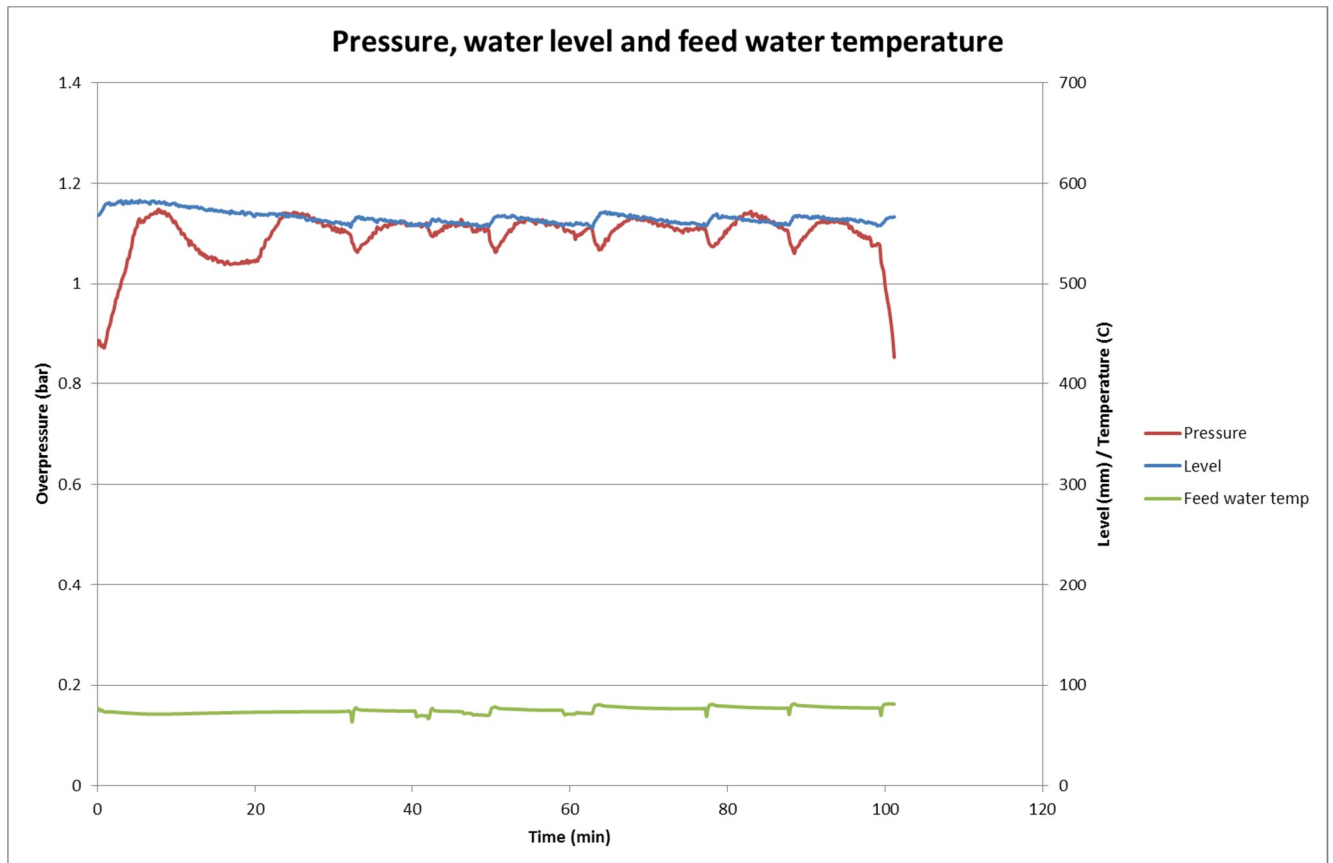


Fig. 11. Pressure and water level in the test vessel and the feed water temperature in the COOLOCE-8b experiment.

3.3 COOLOCE-8c

The experiment at 3.1 bar (abs.) was conducted after the experiments at higher pressures of 5, 7, and 4 bar. The control power and temperature histories in the experiment are shown in Fig. 12 and the pressure, water level and feed water temperature in Fig. 13. Dryout was measured at the power level of 19.1 kW and it was indicated by three sensors at the heights of 30, 40 and 90 mm from the test bed bottom. The sensors are located rather close to each other near the central region of the test bed.

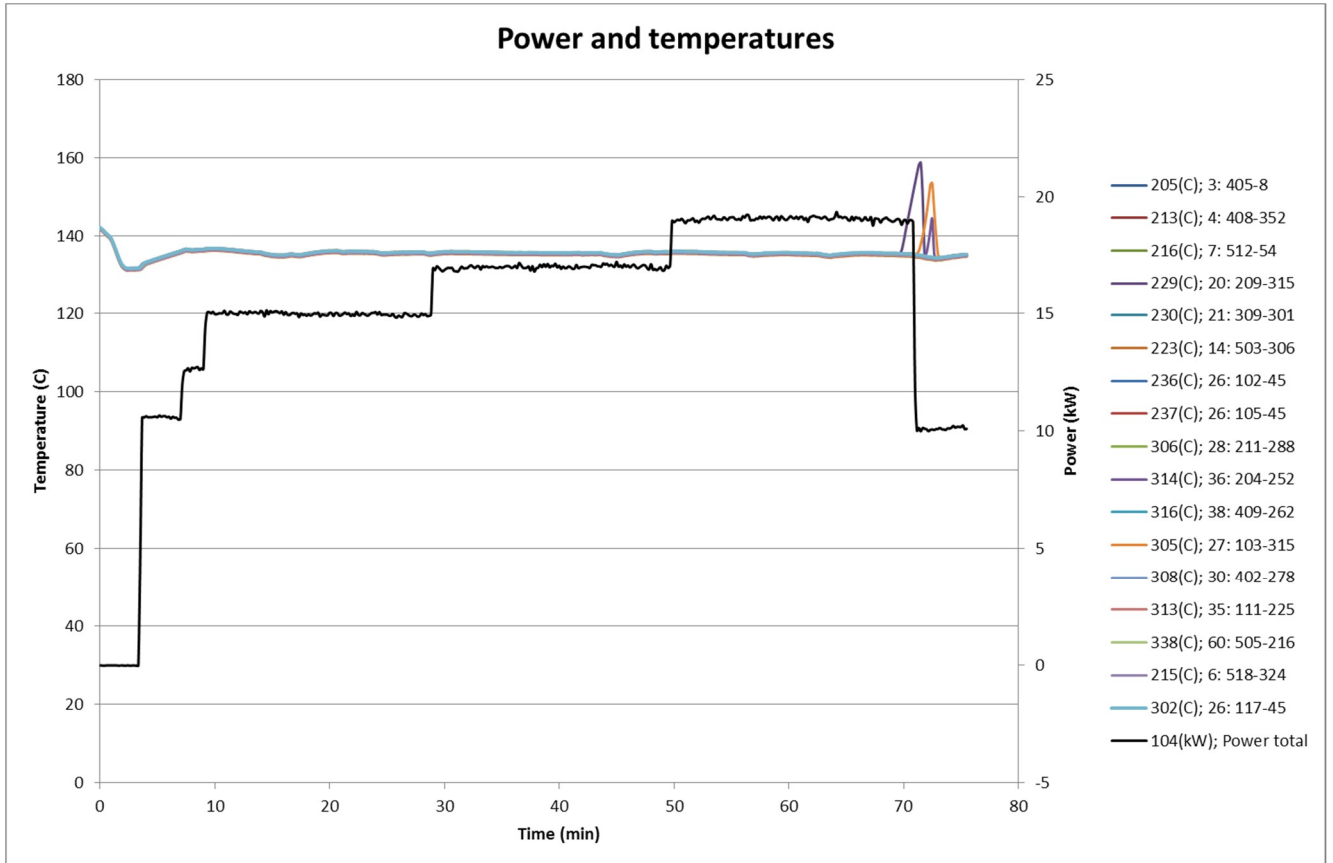


Fig. 12. Control power and temperature log in the COOLOCE-8c experiment.

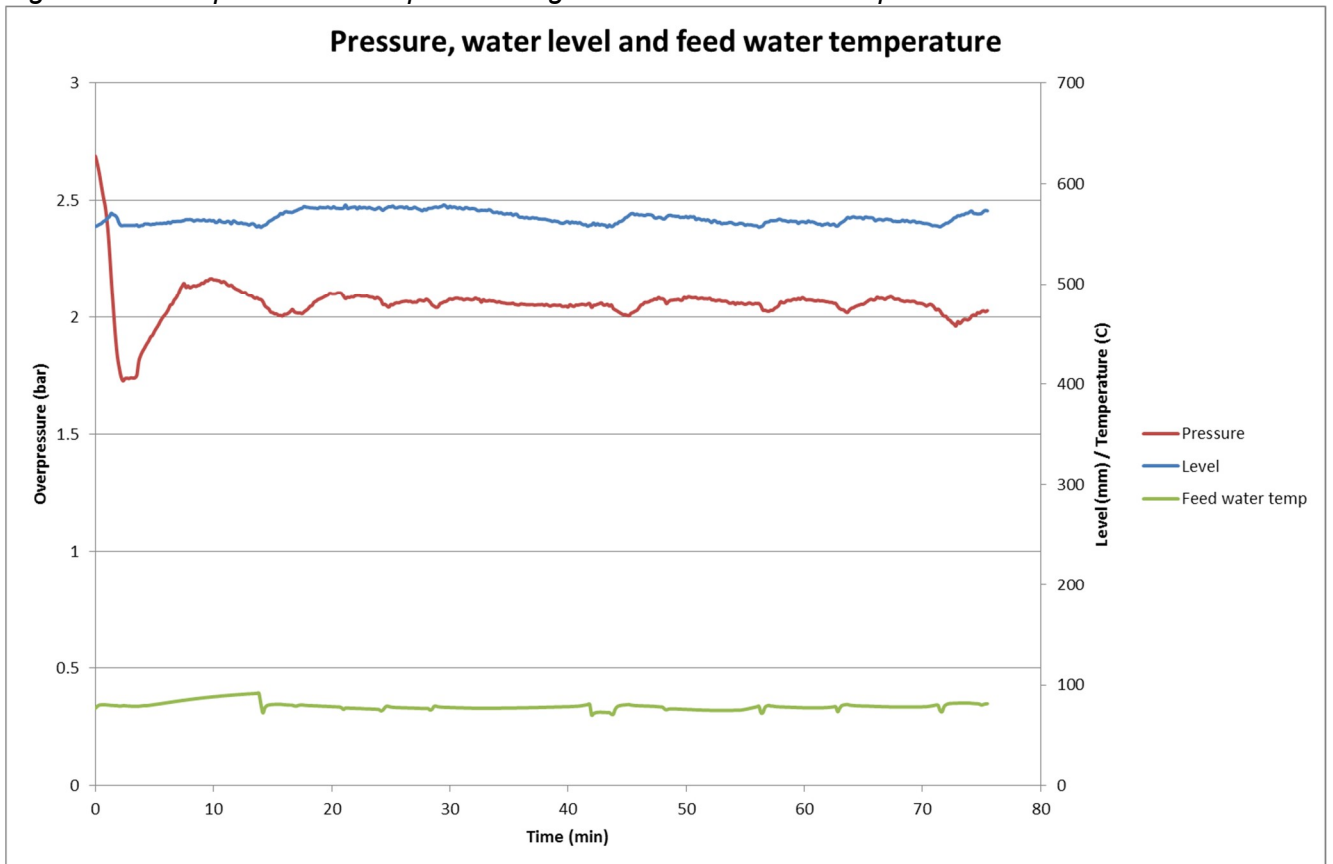


Fig. 13. Pressure and water level in the test vessel and the feed water temperature in the COOLOCE-8c experiment.

3.4 COOLOCE-8d

The COOLOCE-8d experiment at 4.0 bar (abs.) pressure followed the test run at 7.0 bar after a pressure decrease, prior to the 3.1 bar experiment (COOLOCE-8c). The control power and temperature log in the experiment are presented in *Fig. 14*. *Fig. 15* shows the pressure, test vessel water level and feed water temperature during the experiment. Dryout was observed at 21.0 kW control power.

Similarly to the previous test runs, the sensor 209-315 at 90 mm from test bed bottom indicated a clear dryout. In addition, two sensors at 30 and 40 mm indicated a smaller temperature increase of about 5°C. Note that the data for these sensors (204-252 and 103-315) are overlapping in *Fig. 14*.

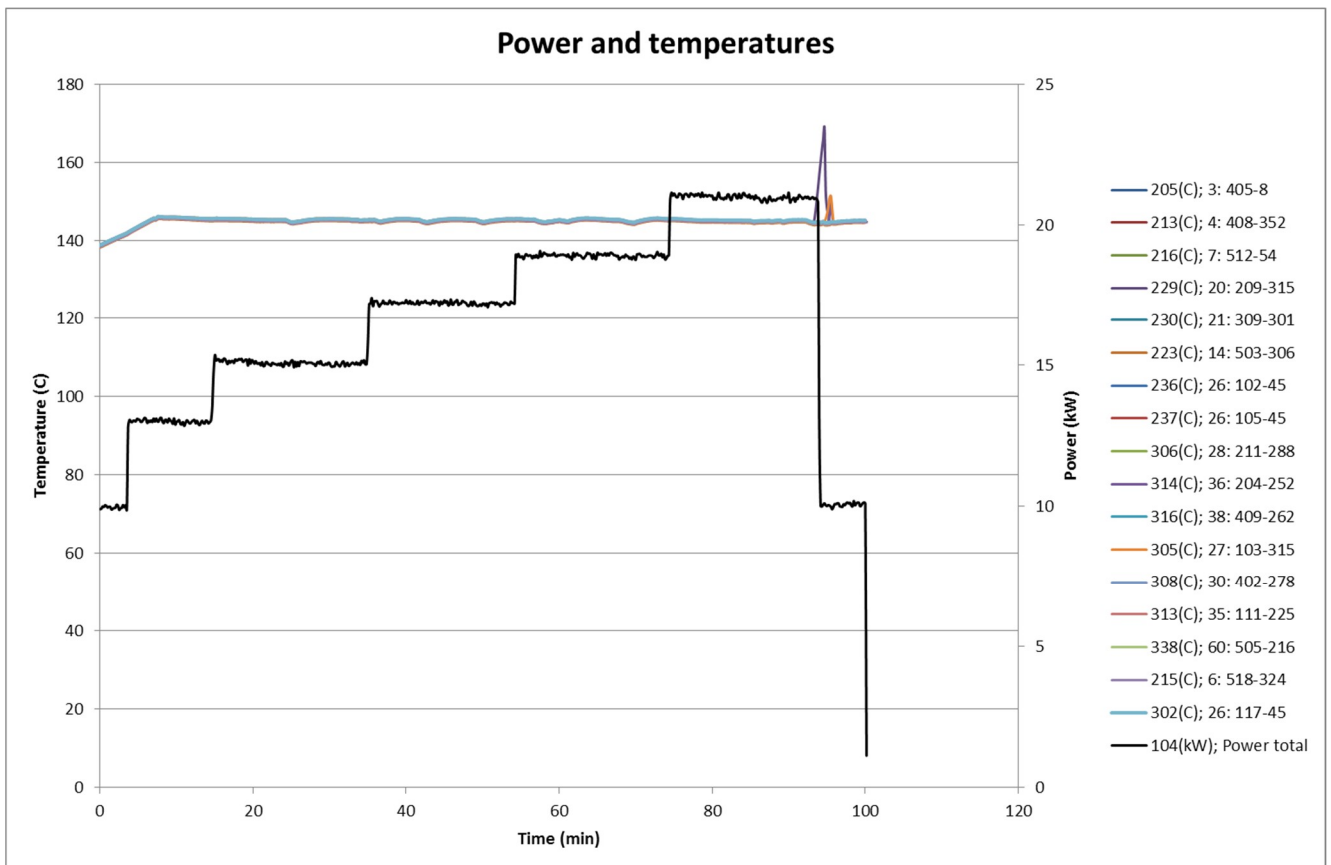


Fig. 14. Control power and temperature log in the COOLOCE-8d experiment.

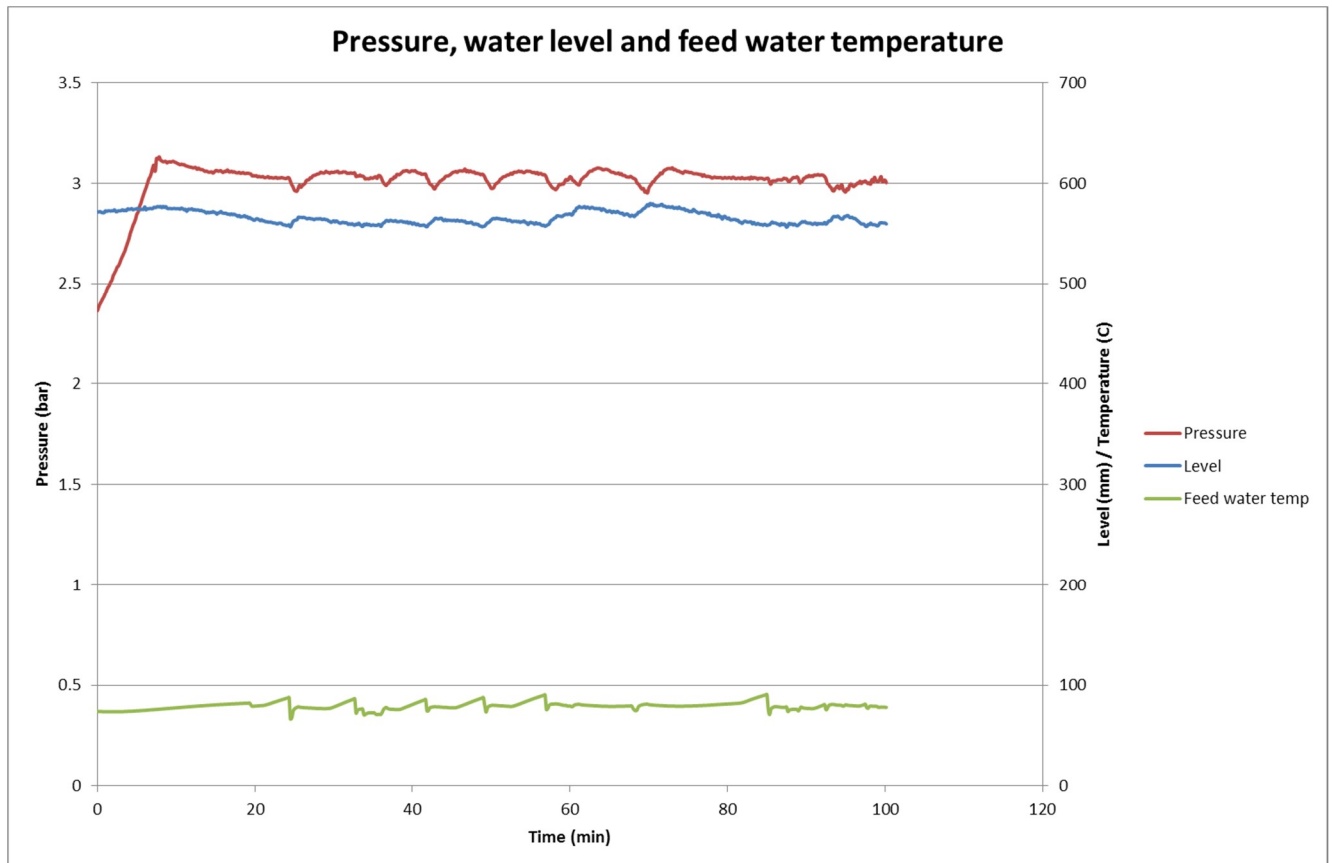


Fig. 15. Pressure and water level in the test vessel and the feed water temperature in the COOLOCE-8d experiment.

3.5 COOLOCE-8e

The COOLOCE-8d test was run at 5.0 bar (abs) pressure, directly after the first attempt to measure dryout at 2 bar. The control power and temperature log in the experiment are presented in Fig. 16. Fig. 17 shows the pressure, test vessel water level and feed water temperature during the experiment. Dryout was indicated by only one sensor at 90 mm height (209-315) at the power level of 23.3 kW.

The power switch-off in Fig. 16 and the pressure drop in Fig. 17 seen between 40 and 60 minutes in the test run were caused by a temporary malfunction in the pressure control. The control system automatically started to open the steam line valve even though the pressure was close to the desired value. This is also seen as a dip in the test bed temperatures which decrease to the saturation temperature for the lower pressure. The test run was continued after the experimental pressure was restored.

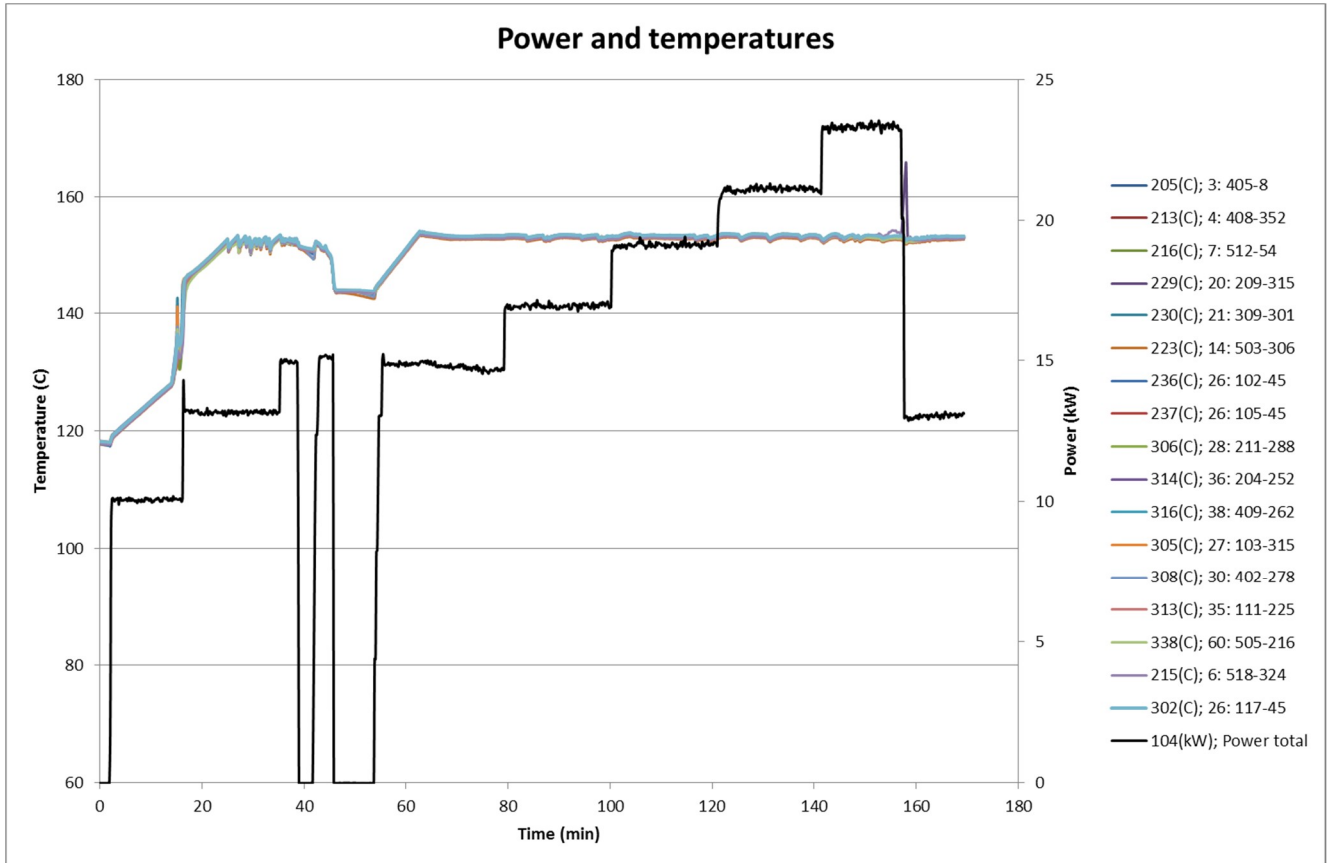


Fig. 16. Control power and temperature log in the COOLOCE-8e experiment.

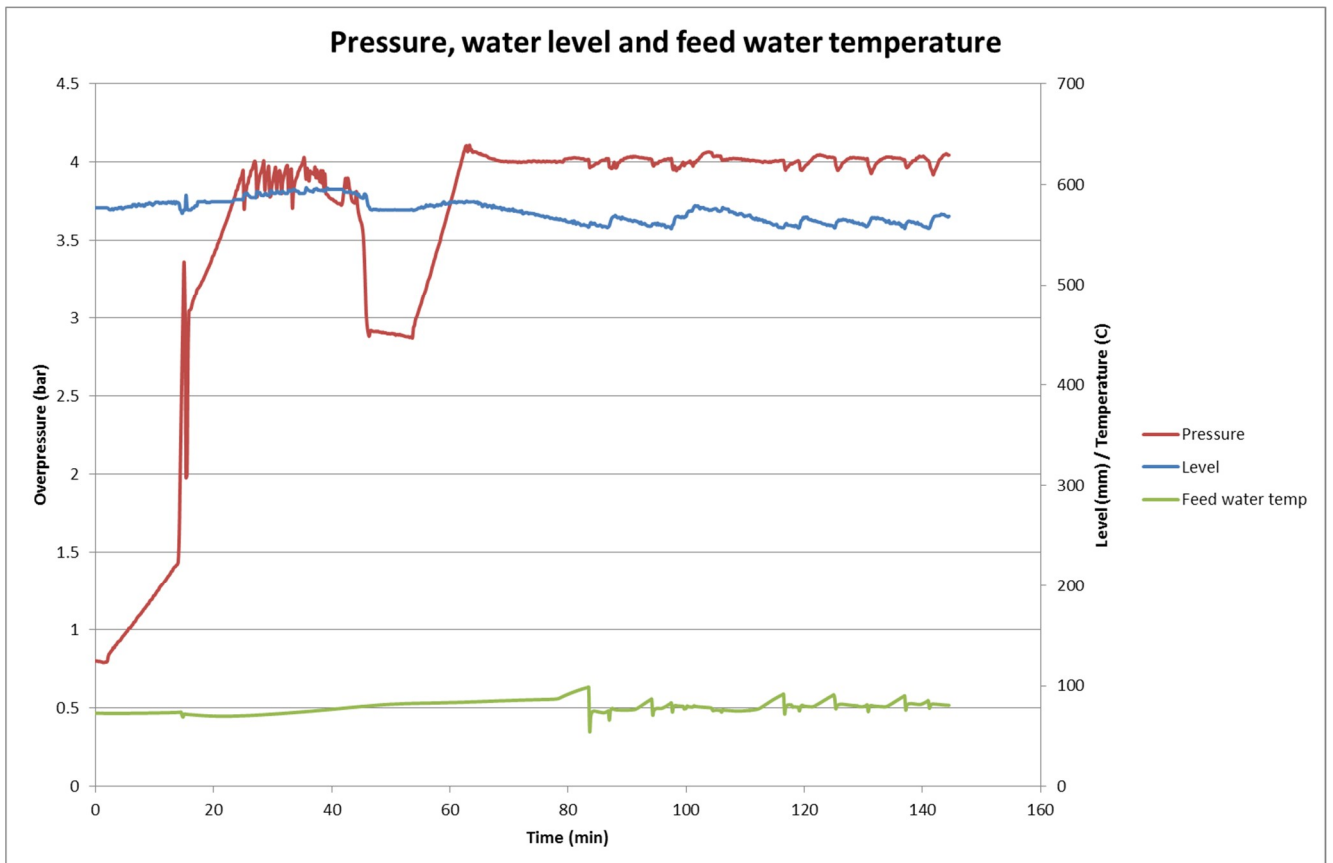


Fig. 17. Pressure and water level in the test vessel and the feed water temperature in the COOLOCE-8e experiment.

3.6 COOLOCE-8f

The COOLOCE-8f experiment was run at 7.0 bar (abs.) after the COOLOCE-8e experiment at 5.0 bar. The control power and temperature histories in the experiment are presented in Fig. 18. Fig. 19 shows the pressure, test vessel water level and feed water temperature during the experiment.

The measured dryout power was 24.9 kW and only one sensor indicated dryout. Curiously, the sensor that indicated dryout was one of the outmost sensors in the central/top region of the test bed, 518-324 at 180 mm from the test bed bottom. The temperature increase remained modest as seen in Fig. 18. At the same time, the heater sensor VY36 increased up to 215°C at which point the test sequence was terminated and the pressure was decreased for the repeatability and verification experiments at 1 and 2 bar pressure (COOLOCE-8b and 8aR).

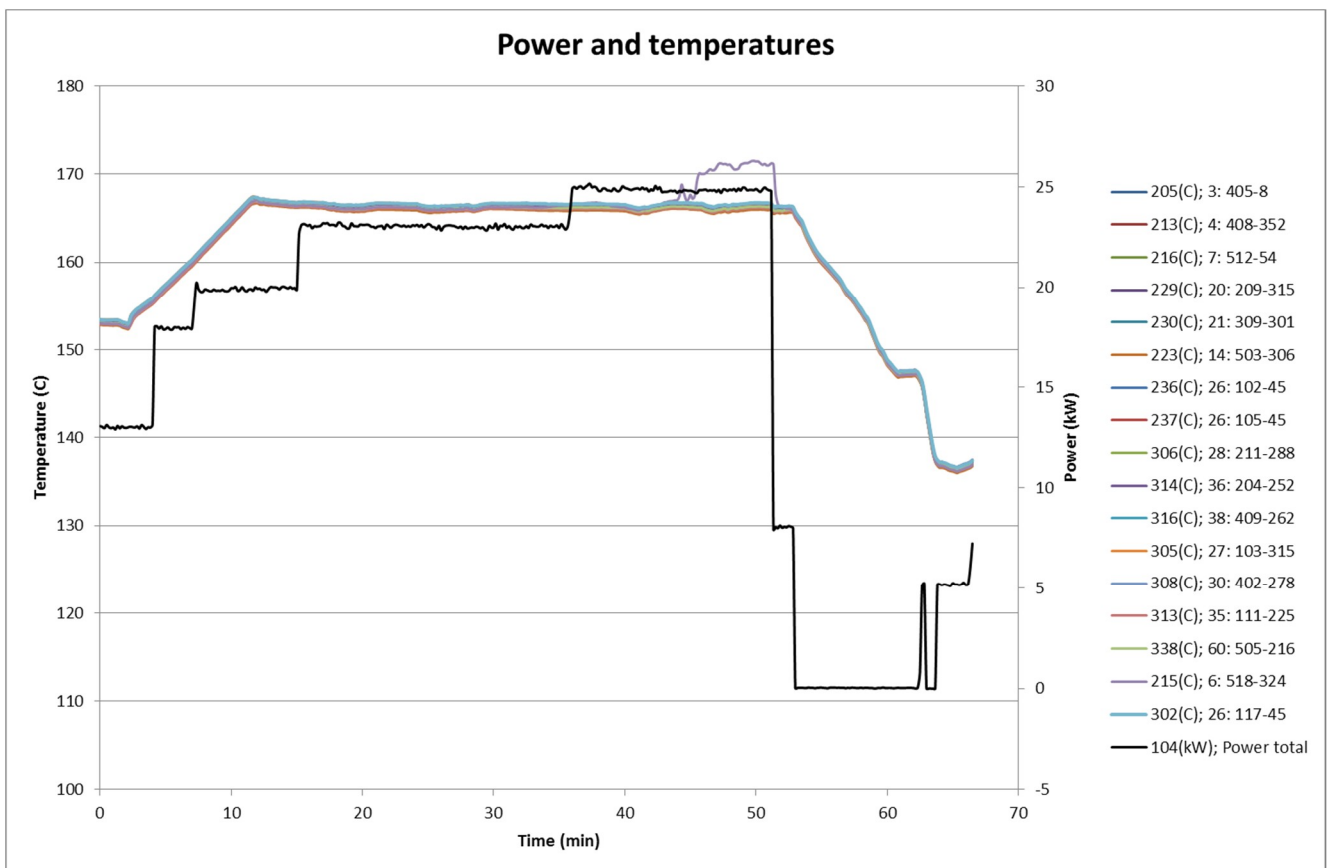


Fig. 18. Control power and temperature log in the COOLOCE-8f experiment.

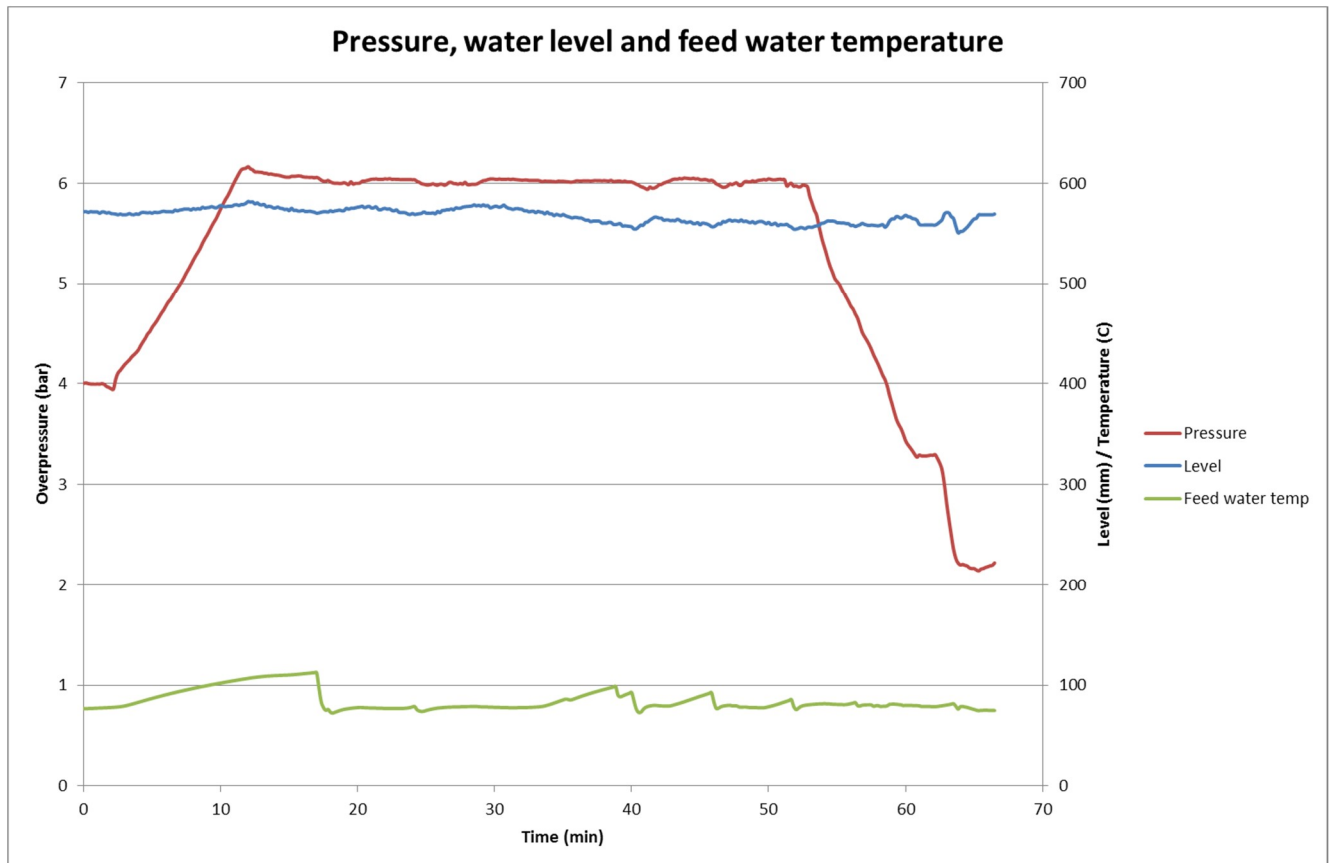


Fig. 19. Pressure and water level in the test vessel and the feed water temperature in the COOLOCE-8f experiment.

3.6.1 COOLOCE-9a

The COOLOCE-9a experiment was the first conducted with a subcooled pool, i.e. with no feed-water pre-heating. The aim was to scope the dryout behavior with the pool water significantly below the saturation temperature. During the experiment, however, it is not possible to control the water temperature in the vessel; it gradually increases (similarly to the heat-up sequence in the previous experiments) because there is no constant injection of cool water to counter the heat generation by the heaters. Because of this, the first experiment was done with short waiting times and comparatively large power steps in order to be able to distinguish the effect of the cooler water before the heat-up to nearly-saturated state.

The initial pool temperature was about 28°C which increased up to 76°C before the termination of the test run (total duration 36 min). The test vessel was not pressurized. The power levels applied were 20, 25 and 27 kW, of which the last one indicated dryout. The waiting time at the power levels prior to dryout was kept at 7 minutes.

The progress of the experiment is illustrated in Fig. 20 – Fig. 22. Fig. 20 shows the histories of control power and pool temperature, the latter measured at 317 mm height above the annular space between the pressure vessel wall and the 270 mm cylindrical test bed. Fig. 10 shows the temperature histories of the sensors that indicated dryout against the control power. There are two dryout points at approximately 16 and 29 minutes into the experiment. At 16 minutes, only one sensor (419-225) at 190 mm (in the upper part of the bed) indicated dryout. After power shutdown and a “re-approach” to 27 kW, the dryout at 29 minutes spread to as many as ten sensors between 120 mm and 220 mm with emphasis on the topmost sensors of the test bed. This means that horizontal spreading was significant.

Such a pronounced dryout in the upper region of the bed was not seen in any of the previous COOLOCE experiments. The measured locations are opposite to those in the COOLOCE-8 series in which the clear majority (15 out of 16) of the dryout locations were between 20 mm and 120 mm. In the experiments conducted with the spherical ceramic particles (cylindrical bed), dryout was generally located in the lower central region, and it was rather central also in the horizontal direction.

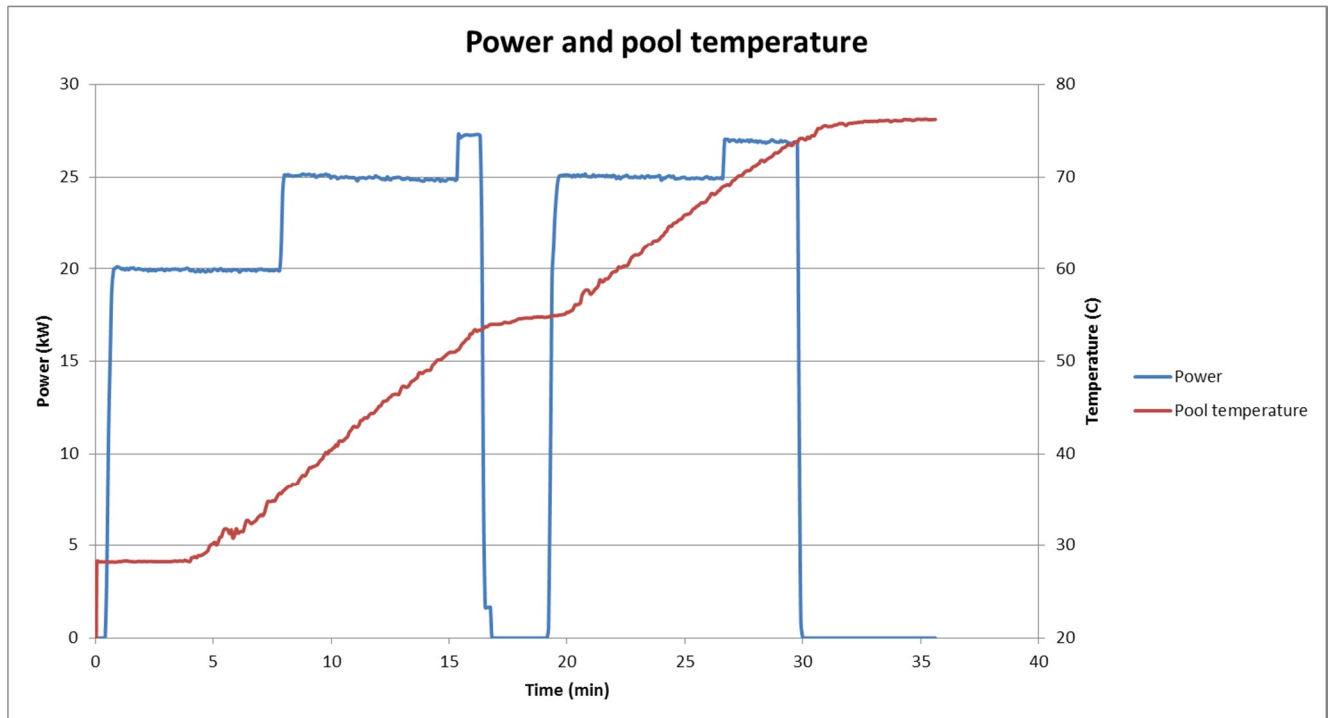


Fig. 20. Control power and water pool temperature measured at 317 mm from the bottom (sensor 339©; 61: Water) in COOLOCE-9a.

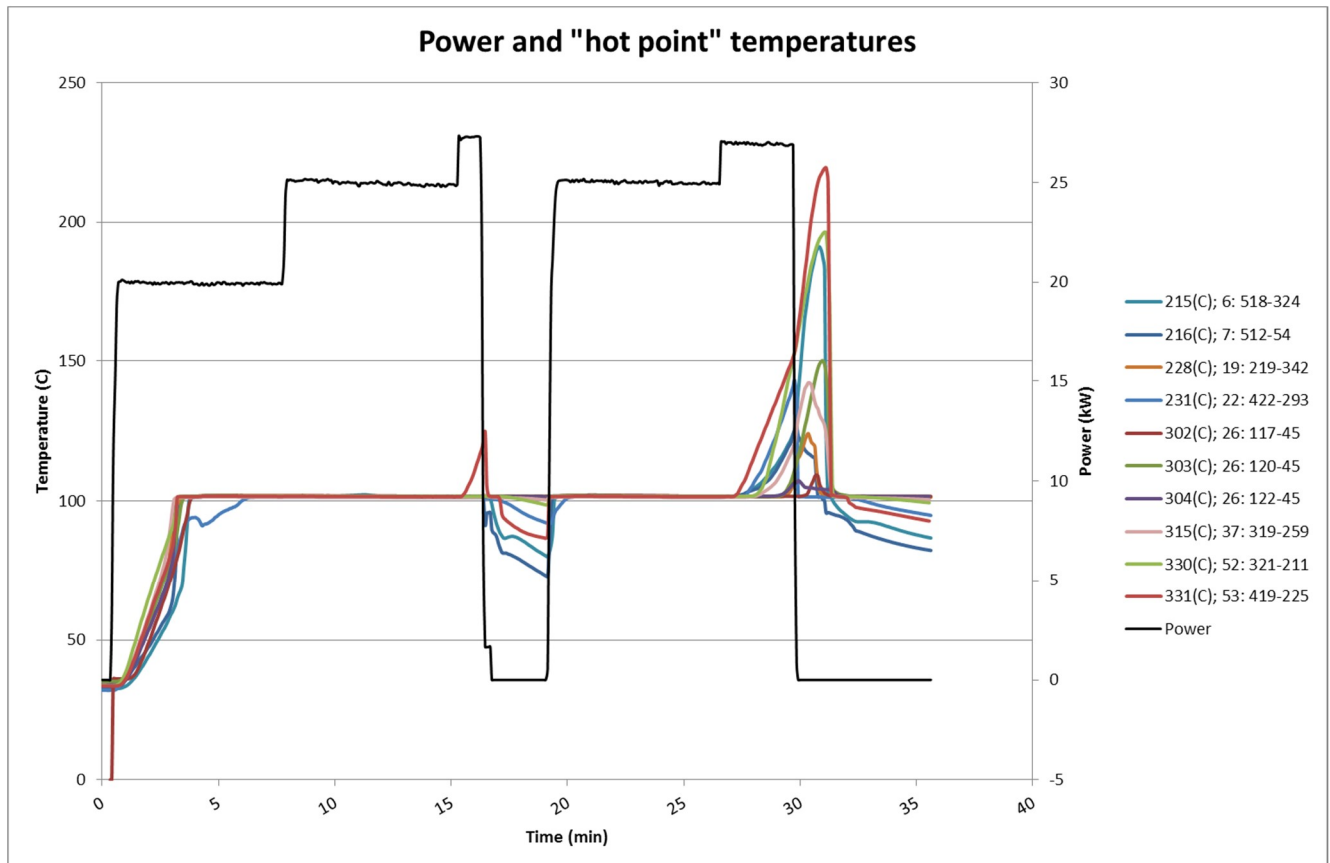


Fig. 21. Control power and temperature of the sensors indicating dryout in COOLOCE-9a.

The temperature histories of all the sensors in the water pool (outside the test bed) and steam volume are presented in Fig. 22. The sensors 117-120 are measuring points in a single multi-point thermocouple. Their distances from the bottom are 67 mm (VESI 2"), 117 mm (VESI 4"), 167 (VESI 6") and 217 mm (VESI TIP). A separate thermocouple denoted *Water* is at 317 mm from the bottom, directly above the multi-point TC. This is the only thermocouple above the height of the cylindrical test bed and its' reading is reported as the pool temperature in Fig. 20. It is seen that, at the end of the experiment, the water temperature range is 62-77°C. The temperature is stratified so that the lowest temperature is found in the bottom and the highest in the topmost sensor.

The vessel pressure control – normally done with the steam line valve – was not used during the experiment. Practically, there is no steam flow exiting the test vessel at pool temperatures below saturation temperature because steam is condensed in the subcooled pool. This can also be observed in the video recordings of the experiments. According to the measurements, pressure and water level in the vessel remained fairly constant under atmospheric conditions.

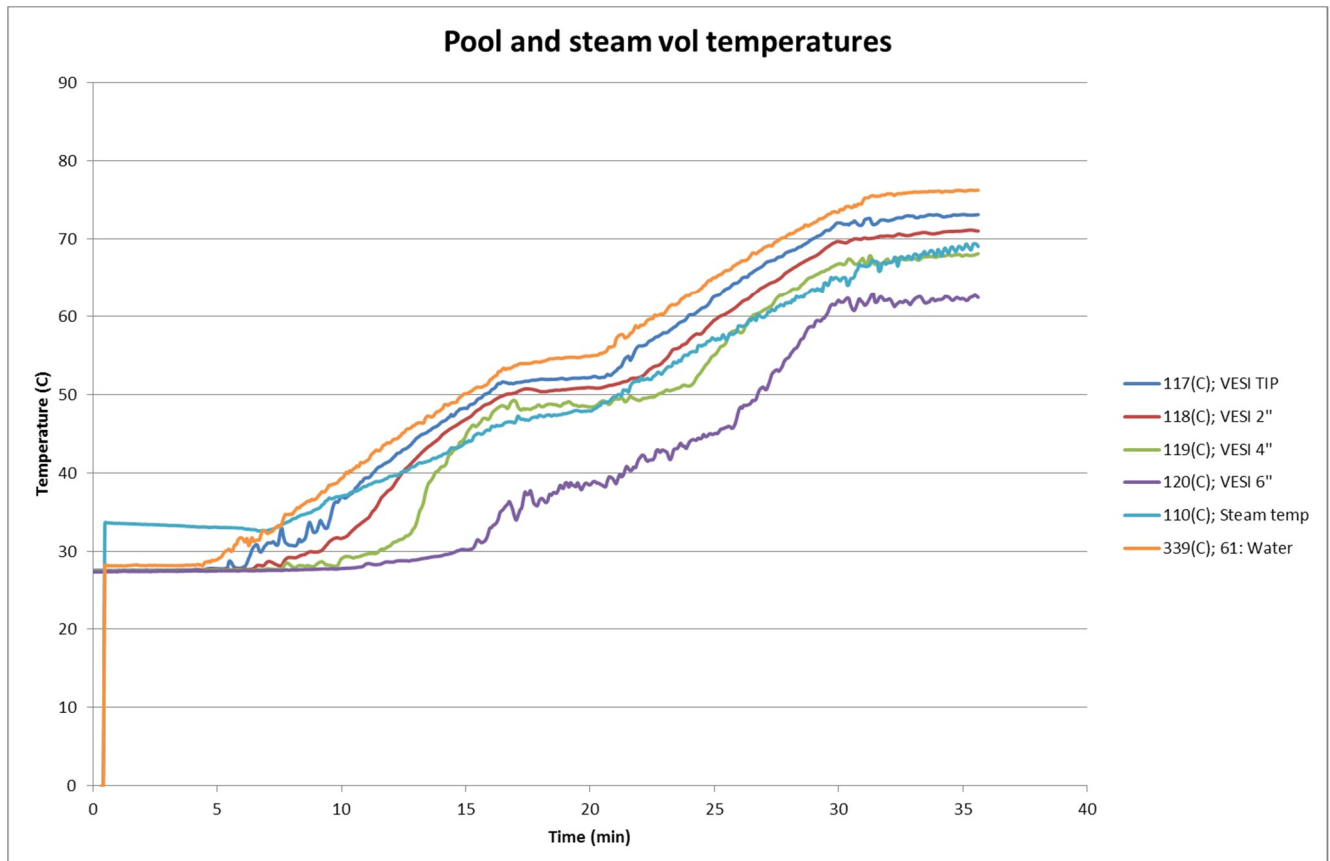


Fig. 22. Temperatures in the water pool and steam volume in COOLOCE-9a. Measured in and above the annular space between the pressure vessel wall and the test bed.

The first dryout is reached at 16 minutes with the power being 20 kW or greater after the start of the experiment. According to the temperature sensors inside the test bed, it takes about five minutes for the debris bed to heat up to saturation temperature. After this, the pool temperature starts to increase gradually. This means that about 10 minutes is allowed for the dryout development in a fully saturated bed. The dryout powers measured in the normal, initially saturated pool experiment were 13.0 kW and 13.7 kW with 20 min waiting time. The currently measured dryout power is twice as high which suggests that the pool subcooling increases dryout power and increases coolability. Even though the waiting time is shorter (indicating some excess in the measured power), it seems unlikely that the excess power for the shorter waiting time could be as high as another 13-14 kW.

3.7 COOLOCE-9b

In the COOLOCE-9a test run, the experimental conditions were not well-controlled due to the transient pool temperature and the varying waiting time and power level. For the second run with no pre-heating, COOLOCE-9b, it was decided to adopt a somewhat different approach: Instead of measuring the dryout power by sequential power increases, the power level was kept constant and the time to dryout was investigated at different pool temperatures. Since no continuous injection of coolant that would help to control the pool temperature is available in the facility, this method of constant power levels was adopted also for the following two experiments (9c and 9d).

Here, the time to dryout is taken as the time interval starting when the bed interior temperature reaches saturation temperature and ending when the first sensor indicating dryout has increased to 107°C. The exact criterion for the saturated conditions was the

average temperature of the test bed sensors reaching 99°C. (After the heating is started, the test bed reaches saturation temperature quickly with the exception of a few bottommost sensors.) The pool temperature increases rather linearly during the waiting time at constant power, and we have examined the average pool temperature (as measured by the sensor named 61:Water) against the time to dryout.

The power level of the expected dryout chosen for this experiment was 27 kW. The progress of the test run is presented in *Fig. 23* and *Fig. 24* which show the control power against the pool temperature and the test bed temperatures, respectively. At this power level (27.0 – 27.1 kW), two dryout points were measured as seen in *Fig. 24*. The time to dryout in the first dryout point was about 9.3 min and the average temperature of the water pool during this time was 36.7°C. The time to dryout for the second dryout point was about 7.2 min and the average water pool temperature about 62.7°C.

The development of the pool and steam volume temperatures is shown in *Fig. 25*. The thermal stratification is clearly seen, similarly to COOLOCE-9a. The temperature is highest in the uppermost sensor, 61: Water.

The cooldown period between the dryout points (20 – 70 min) was long in order to scope the heat transfer and the stabilization of the test bed temperatures since this type of data might be useful in the validation of heat transfer models in simulation codes. It was found that the thermal stratification in the pool as well as in the test bed tends to remain until all parts of the test facility have cooled down to room temperature which can take several days if the facility is left to cool down “normally”. This is due to e.g. the greater heat losses through the bottom plate than through the vessel walls with insulation.

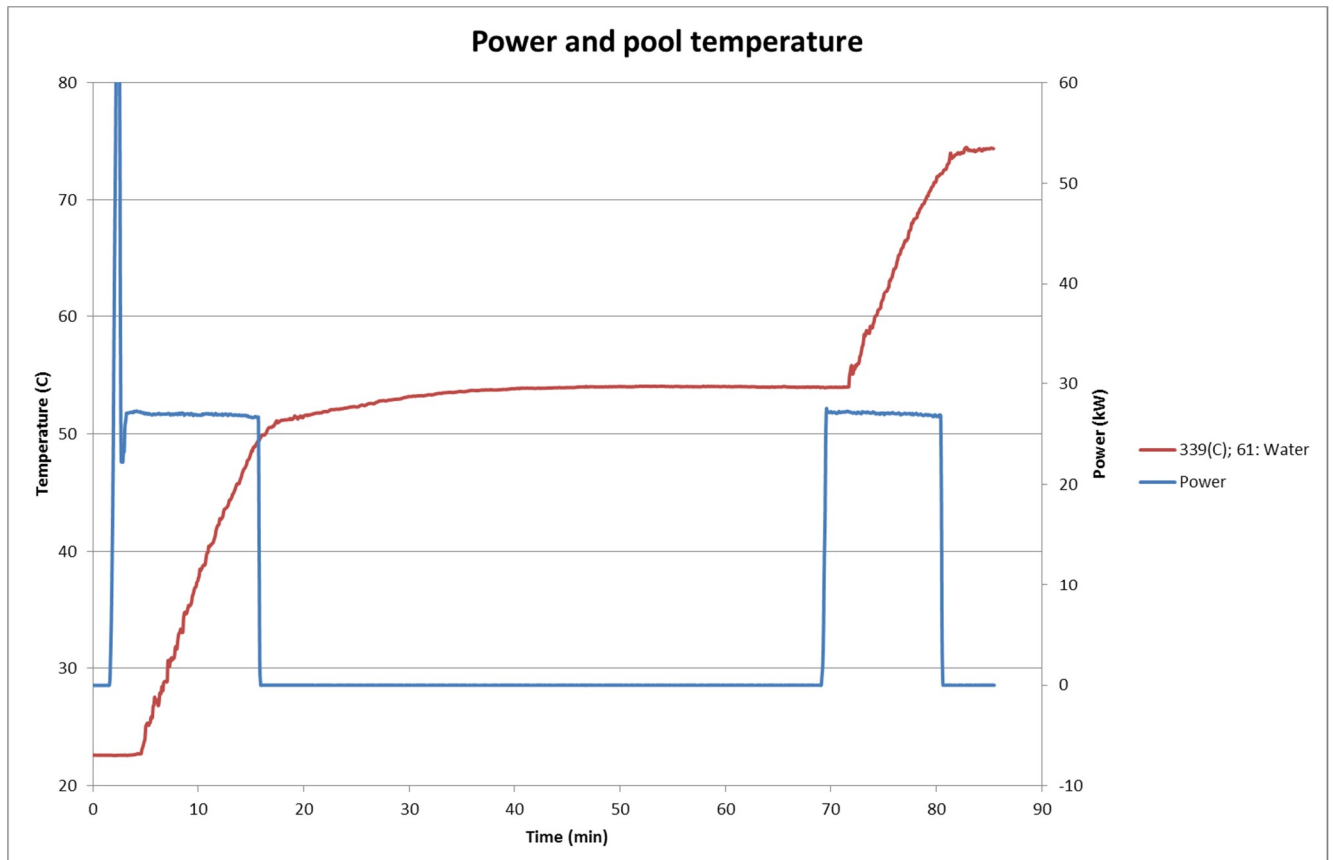


Fig. 23. Control power and water pool temperature measured at 317 mm from the bottom (sensor 339©; 61: Water) in COOLOCE-9b.

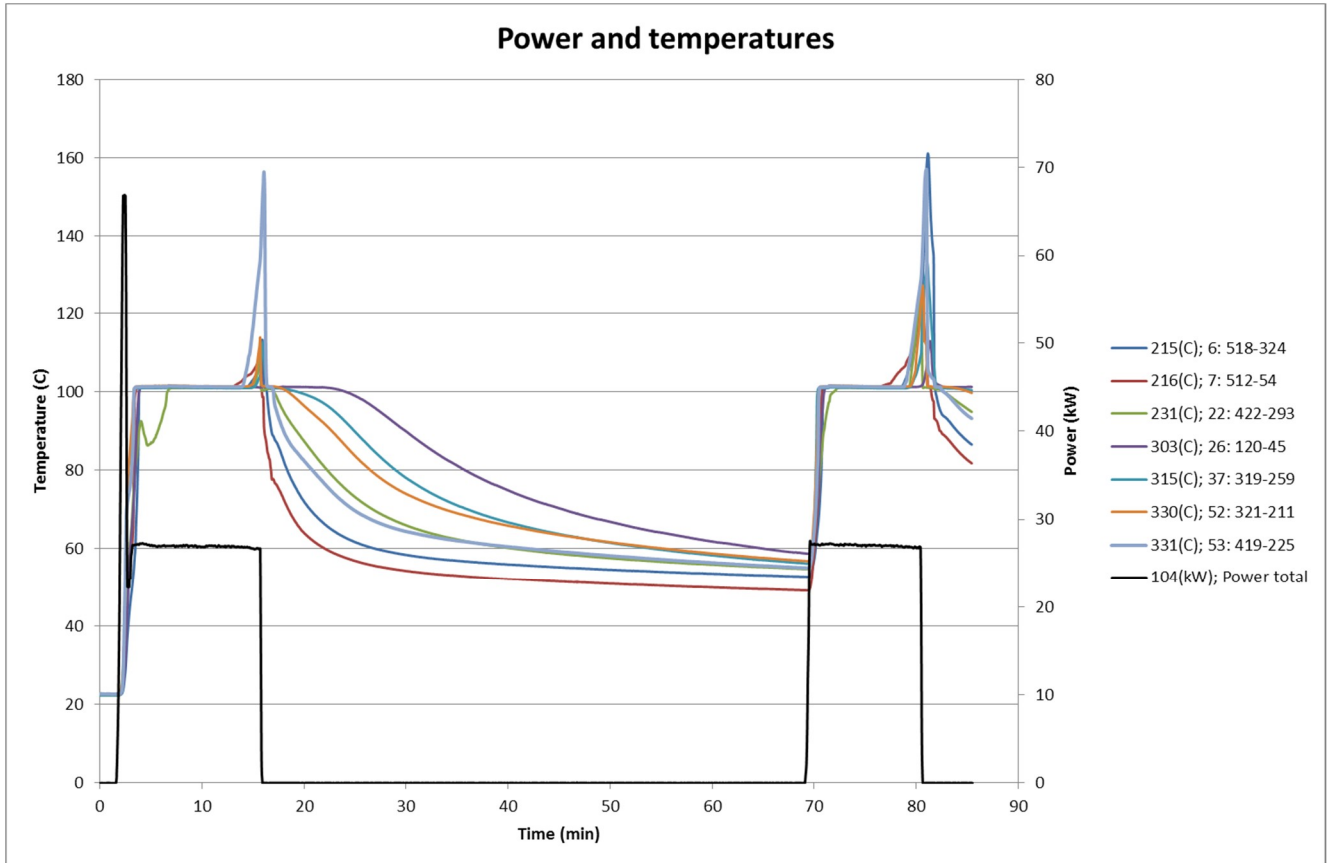


Fig. 24. Control power and temperature of the sensors indicating dryout in COOLOCE-9b.

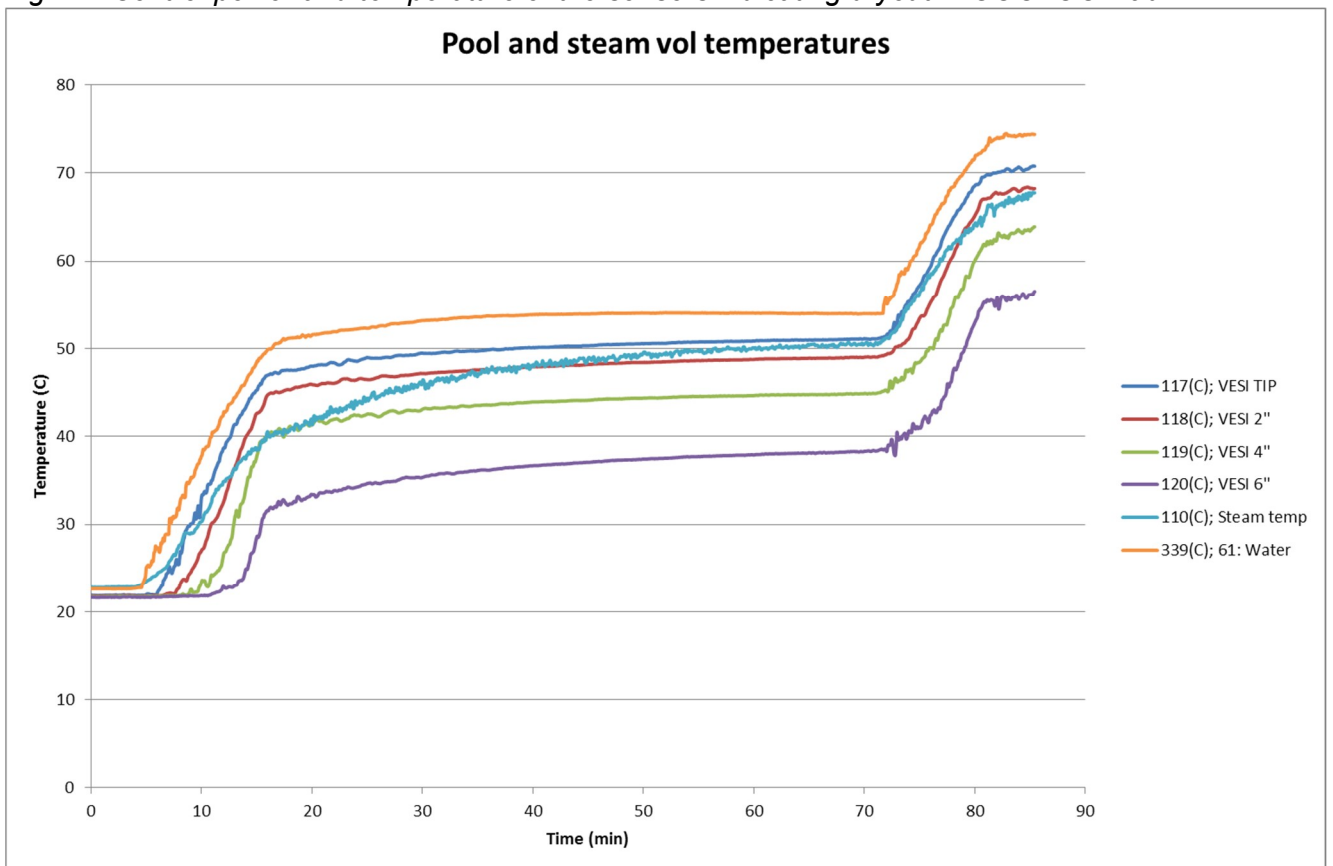


Fig. 25. Temperatures in the water pool and steam volume in COOLOCE-9b. Measured in and above the annular space between the pressure vessel wall and the test bed. 3.8 COOLOCE-9c

The power level examined in COOLOCE-9c with subcooled pool was 20.0 kW. The control power and water pool temperature in the experiment are shown in *Fig. 26*. The control power with the test bed temperatures (sensors indicating dryout) are shown in *Fig. 27*. At this power level, only one dryout point was measured before the pool temperature increased to saturation temperature at about 75 minutes.

Dryout occurred after a 27.1 minute waiting time from the increase of the bed temperature to saturation temperature. During the waiting time, the average pool temperature was 51.6°C. After the first dryout, the power was switched off and the test bed was allowed to reflood according to the normal test procedure. The second measurement at 20 kW did not result in dryout, instead the temperature increased to 100°C in about 22 minutes. This means that the waiting time is longer than 22 minutes for this power level even at the rather high pool temperature between 75-100°C.

The temperatures in the water pool and steam volume are presented in *Fig. 28*. It is seen that the thermal stratification disappears when saturated conditions are reached. Otherwise, the temperature increase generally corresponds to the heating periods (dryout waiting times).

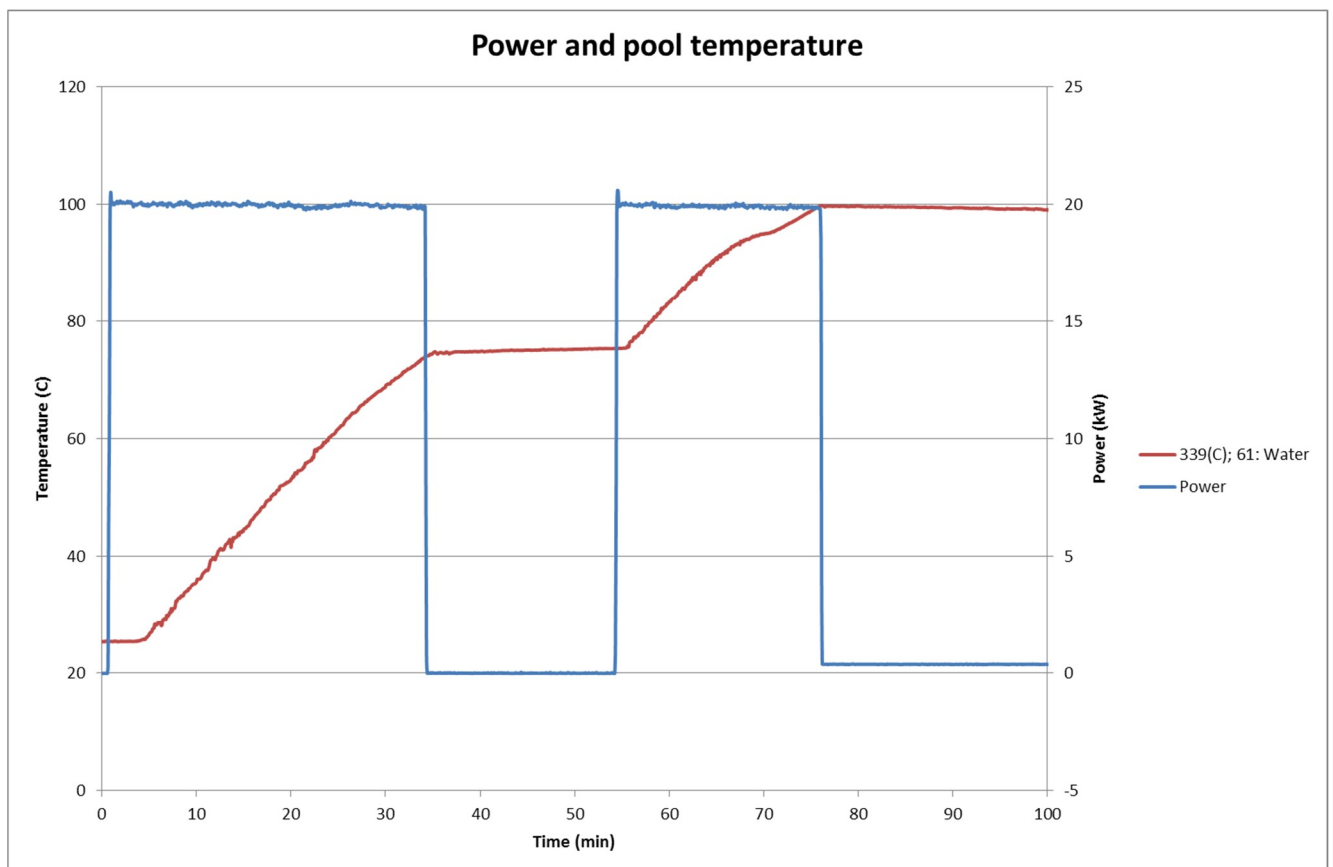


Fig. 26. Control power and water pool temperature measured at 317 mm from the bottom (sensor 339°C; 61: Water) in COOLOCE-9c.

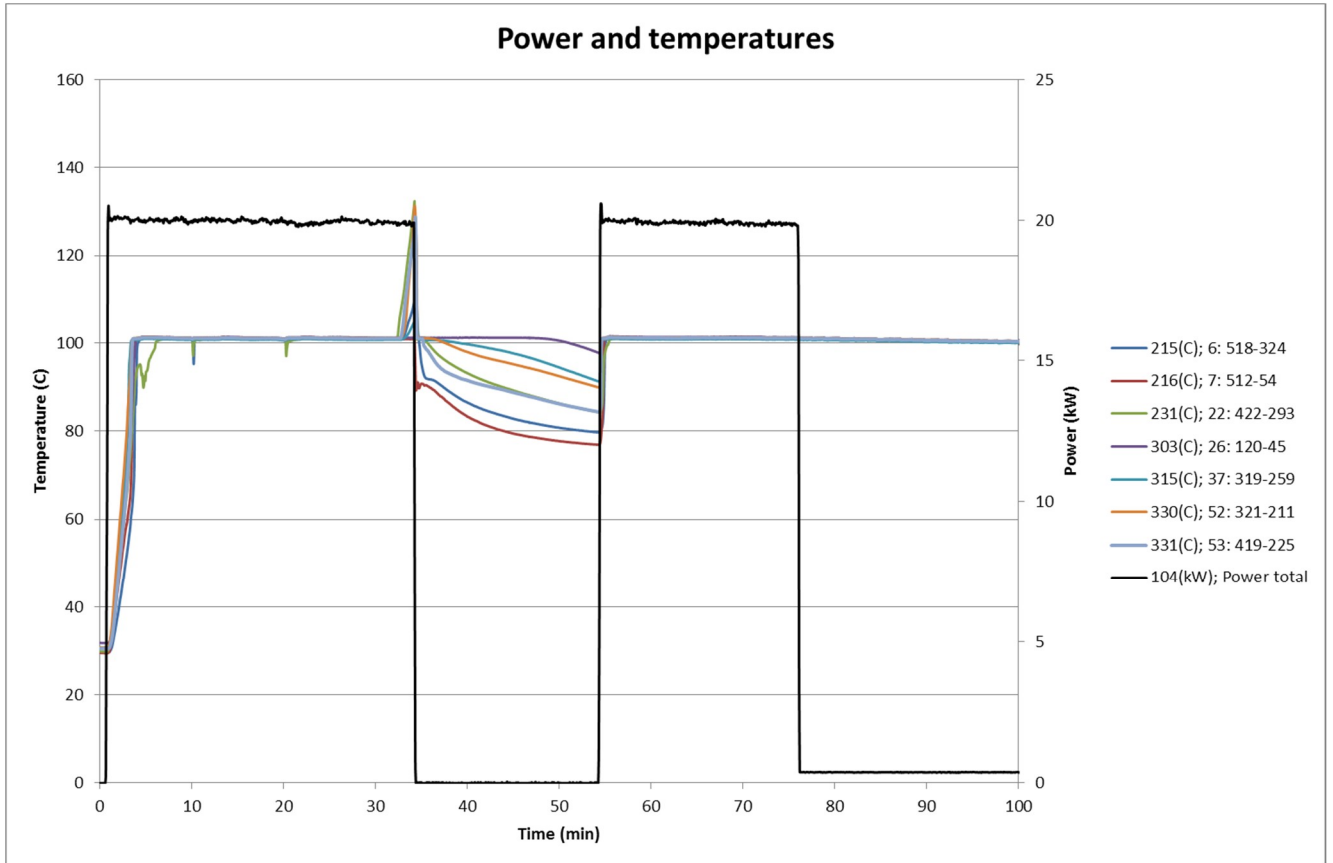


Fig. 27. Control power and temperature of the sensors indicating dryout in COOLOCE-9c.

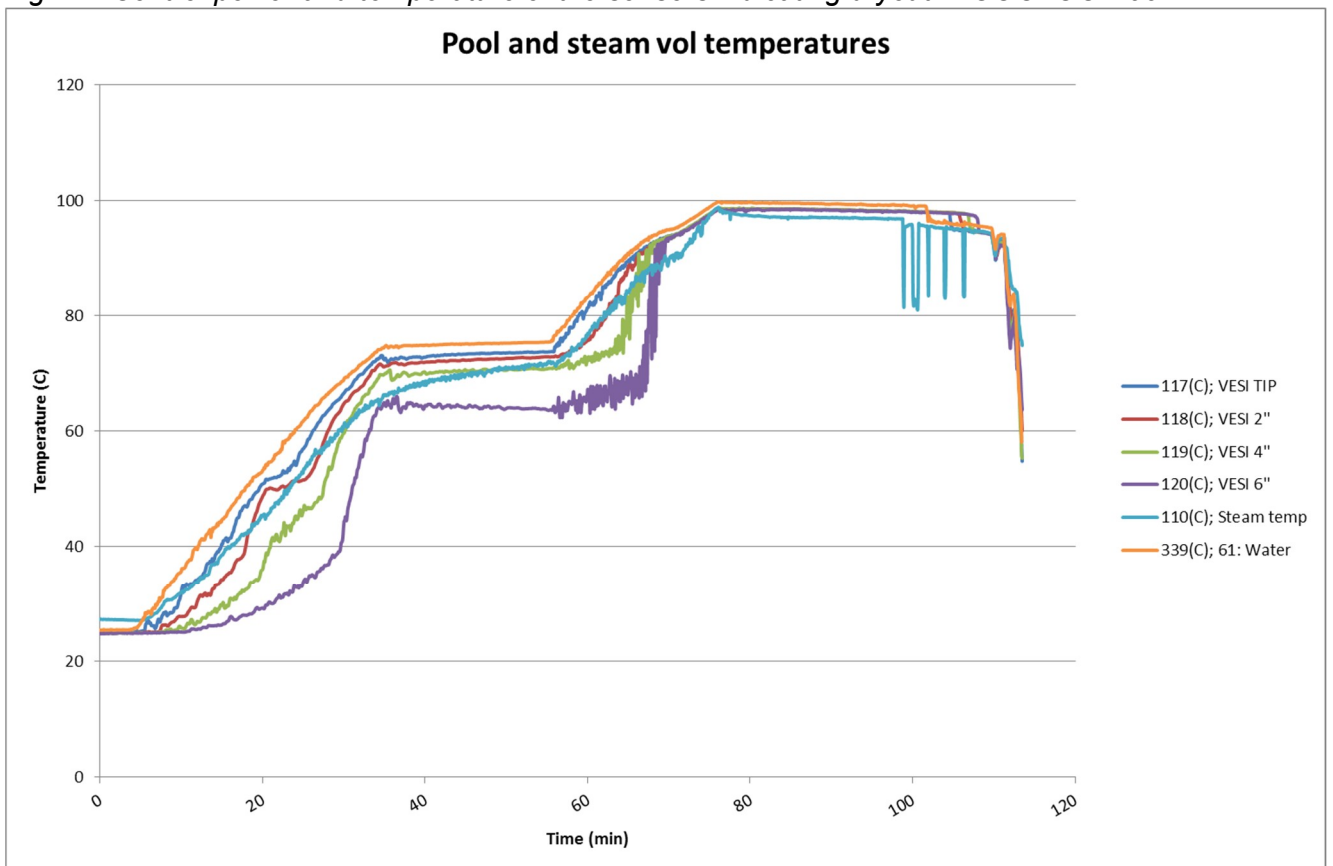


Fig. 28. Temperatures in the water pool and steam volume in COOLOCE-9c. Measured in and above the annular space between the pressure vessel wall and the test bed.
3.9 COOLOCE-9d

The power level chosen for COOLOCE-9d with subcooled pool was 35 kW. The test was run directly after COOLOCE-9c with no long cooling period between the measurements. Instead, the water in the test vessel was replaced with cool water prior to the test run which gives a slightly different initial conditions compared to the previous test runs as the structures of the test facility (including the vessel bottom plate) were still hot following the 9c test run. The control power and the water pool temperature in the experiment are shown in *Fig. 29*. The control power with the test bed temperatures (sensors indicating dryout) are shown in *Fig. 30*.

Because of the short waiting times resulting from the high power level, five dryout points were measured before the pool temperature increased close to saturation temperature. The waiting times to dryout, the average pool temperature during the waiting time and the control power (average of the waiting time) according to the data logger are listed in *Table 2*.

Table 2. Results of the COOLOCE-9d experiment: time to dryout at different pool average temperature.

Dryout waiting time (min)	Power (kW)	Average pool temperature (°C)
3.5	35.1	43.6
2.8	34.8	56.9
2.5	34.9	68.7
2.4	34.9	78.5
2.4	34.8	86.1

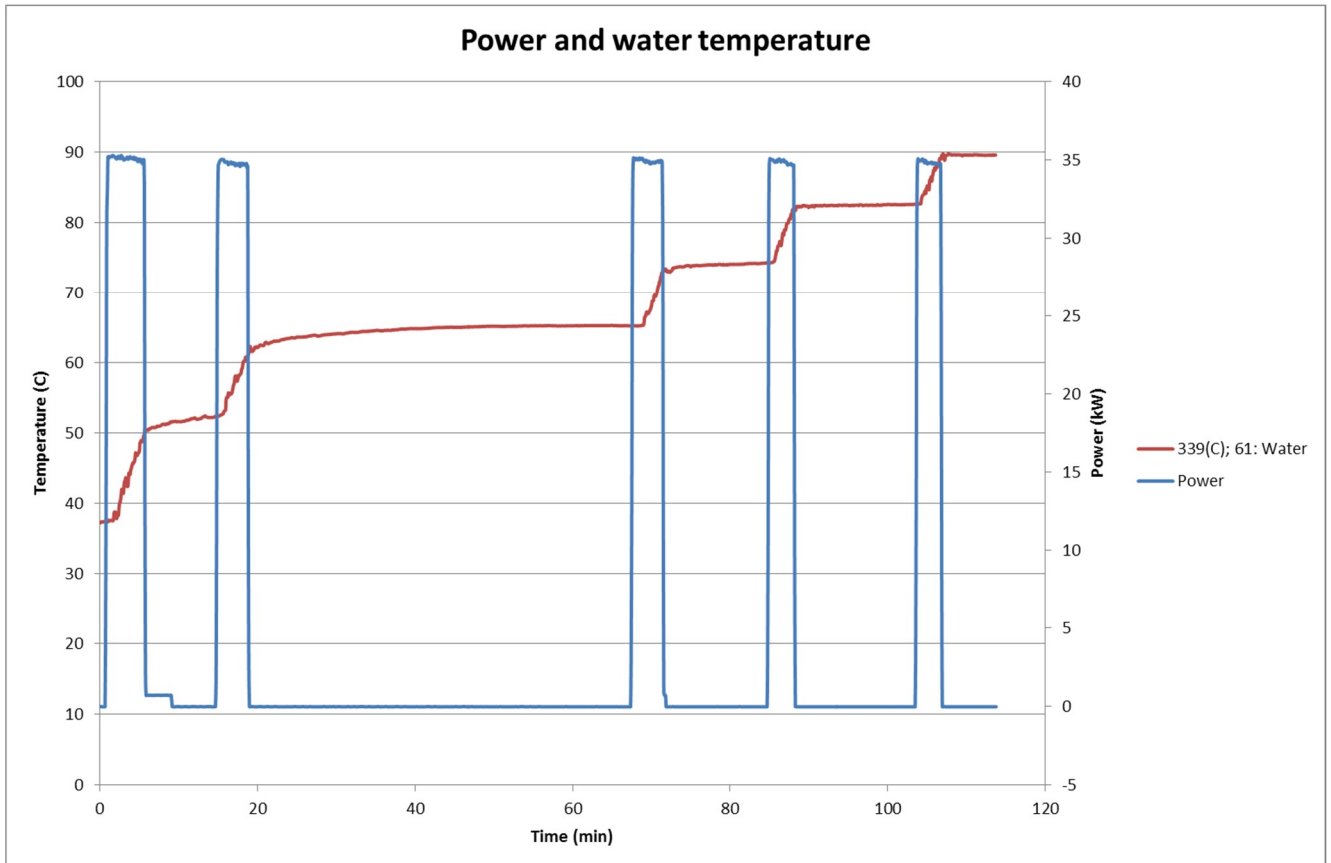


Fig. 29. Control power and water pool temperature measured at 317 mm from the bottom (sensor 339°C; 61: Water) in COOLOCE-9d.

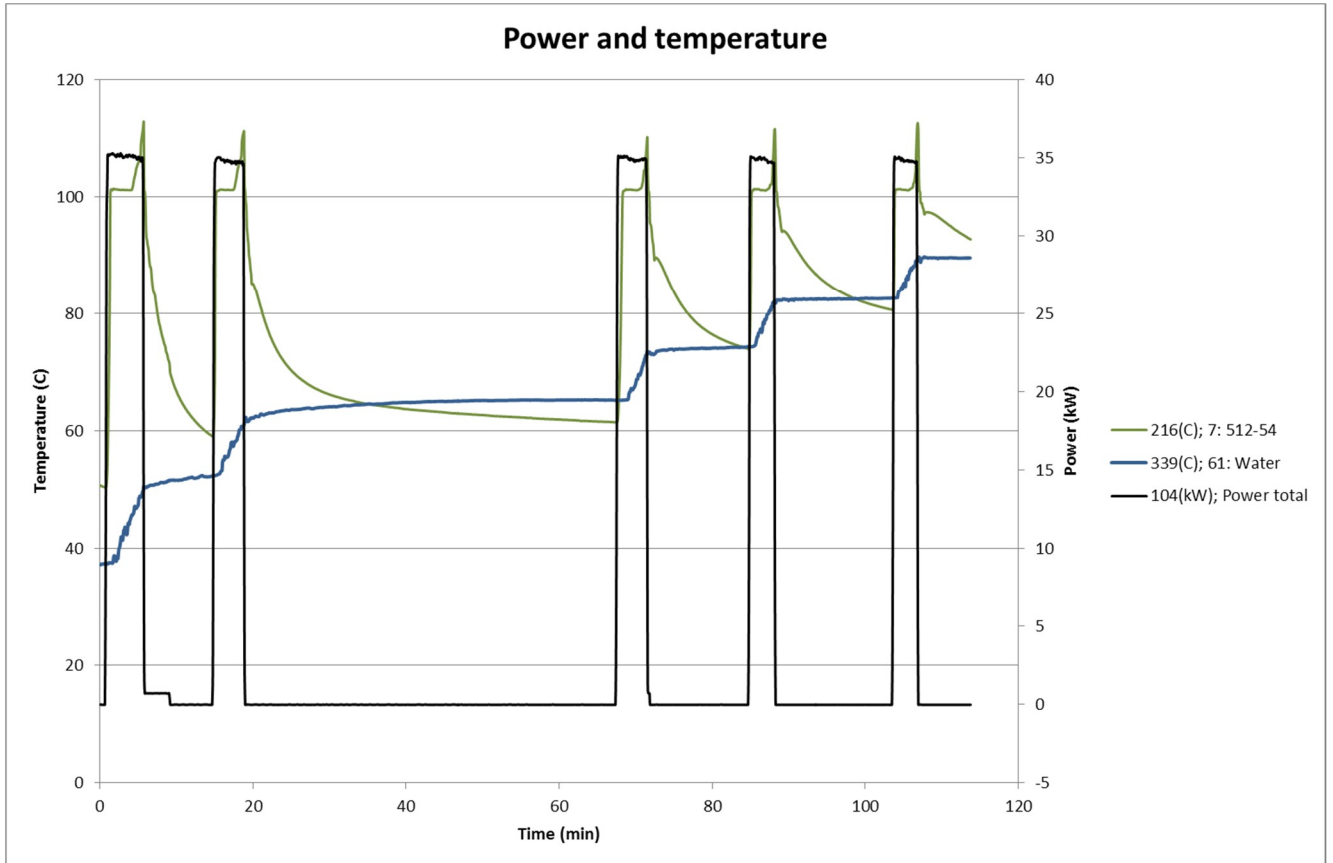


Fig. 30. Control power and temperature of the sensors indicating dryout in COOLOCE-9d.

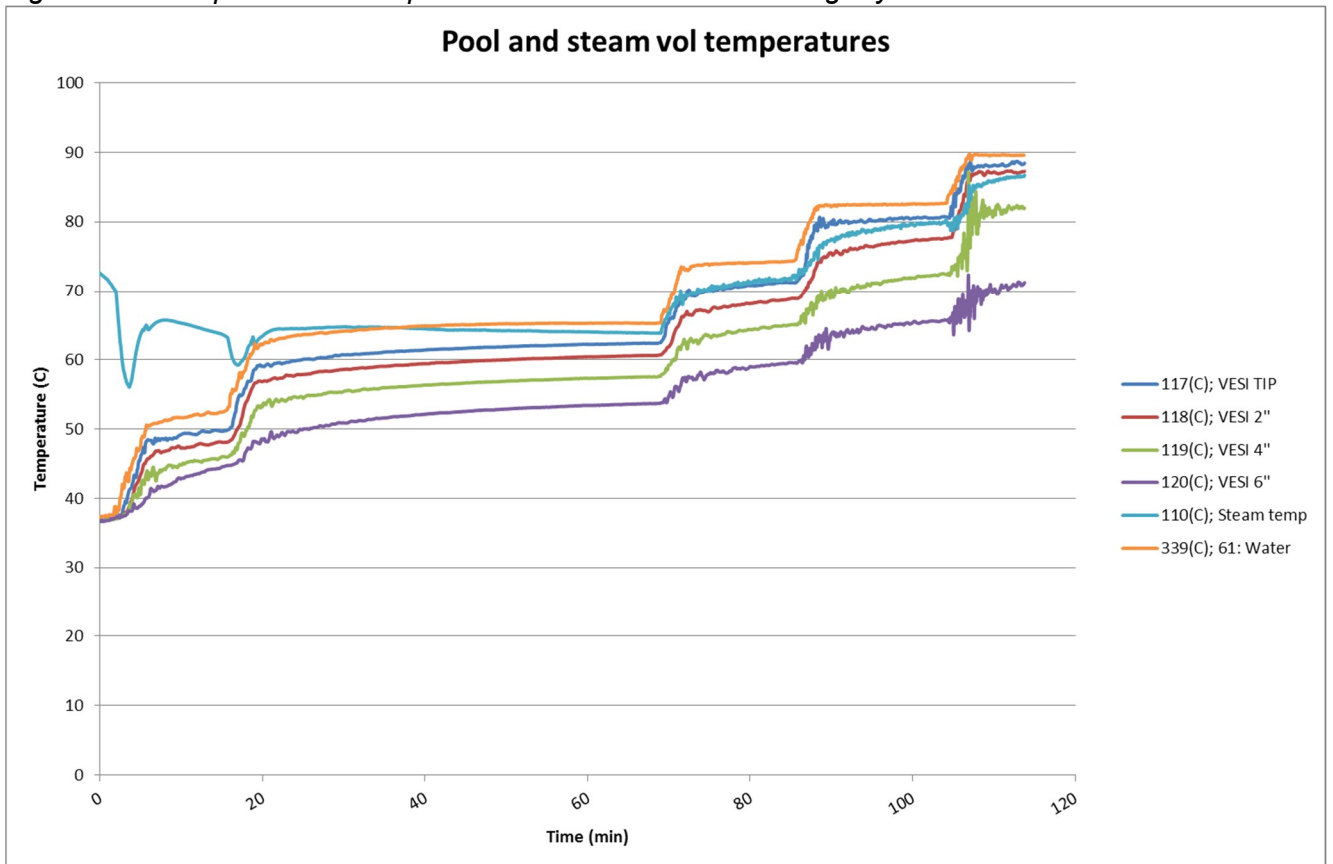


Fig. 31. Temperatures in the water pool and steam volume in COOLOCE-9d. Measured in and above the annular space between the pressure vessel wall and the test bed.

4. COOLOCE-8 and -9 discussion

4.1 Effect of particle material

As stated before, the aim of the COOLOCE-8 test series was to investigate the effect of the particle material on debris bed coolability as well as to scope the possible effect of the heating arrangement. The first of these issues may be addressed by comparing the results of the COOLOCE-8 experiments to the results of COOLOCE- 3 – 5 experiments. The heating and thermocouple locations in the test bed interior in these experiments were the same and both test beds were top-flooded. Instead of the alumina gravel consisting of irregular gravel, the COOLOCE-3 – 5 test runs used spherical ceramic beads as the simulant material.

The comparison of dryout heat flux in COOLOCE-8 and COOLOCE-3 – 5 test series are presented in *Table 3*. Dryout heat flux is the measured dryout power divided by the cross-sectional area of the test bed (W/m^2). It was found that the ceramic beads yielded heat fluxes which were 48% to 64% greater than those with alumina gravel.

Table 3. Dryout heat flux in the COOLOCE experiments with ceramic beads and alumina gravel.

Approx. pressure	Dryout heat flux [kW/m^2]	
	COOLOCE-3-5 (ceramic beads)	COOLOCE-8 (alumina gravel)
1	270	178
2	347	235
3	423	263
4	458	290
5	493	319
7	560	342

The difference is – at least partially – caused by the greater average particle size of the ceramic beads: The average size of the beads is 0.97 mm and the effective diameter of the gravel particles is 0.65 mm. The simulation results presented in Section 7.4 show how the results agree with the results obtained by the open-literature models normally used in dryout heat flux predictions.

In addition to the difference in dryout heat flux, another interesting discrepancy between the two materials appeared in the experiments. In the case of ceramic beads, dryout was limited to the central regions of the test bed, both in radial and vertical directions. Dryout was seen nearer to the bottom (below 120 mm) with the alumina gravel and it was radially somewhat more widespread in different parts of the bed. Even though some of the test runs, especially in the higher pressures, only indicated dryout by a single sensor before the termination of the test run, there was generally more variation in the dryout location compared to COOLOCE-3 – 5 with the ceramic material.

4.2 Effect of experimental set-up

The second important comparison concerns the heat fluxes measured in two different experimental set-ups utilizing the same particles. Here, the main difference is the heating and thermocouple arrangement. This is illustrated in *Fig. 32* which shows the STYX and COOLOCE particle beds in their pressure vessels. In STYX, the heating arrangement

consisted of thin resistance wires arranged in horizontal layers at about 30 mm distance from each other. In COOLOCE, the 6 mm thick vertical heaters are installed 30 mm from each other in a type of square mesh (as seen in Appendix A).

The STYX test bed with the volume of about 42 dm³ was also considerably larger than the COOLOCE test bed of 20.4 dm³. The dryout power density in the two test set-ups cannot be directly compared because of this. (The height of the STYX test bed, 600 mm, is close to what is expected if the debris is evenly spread in the Oikiluoto units 1 and 2 containment drywell.)

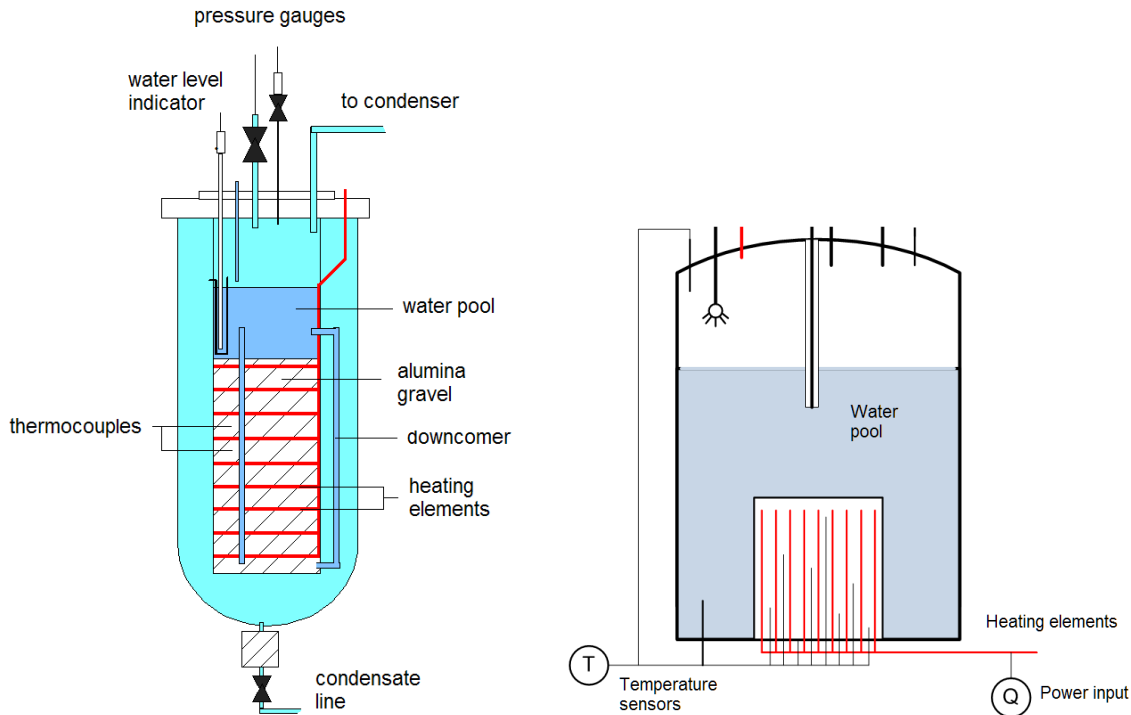


Fig. 32. The particle bed configurations in (a) the STYX tests with horizontal heaters and (b) the COOLOCE tests with vertical heaters.

The dryout heat fluxes measured for cylindrical beds in the COOLOCE and STYX facilities [7] are presented in *Table 4*. It is seen that the COOLOCE-8 heat fluxes are comparatively low. Those measured in the STYX experiments are 16-25% greater than in the new experiments. Considering that the effective particle diameters were 0.80 mm for the STYX test bed and 0.65 mm for the COOLOCE test bed, the difference is reasonable.

Table 4. Dryout heat flux in the COOLOCE and STYX experiments with alumina gravel.

Approx. pressure	Dryout heat flux [kW/m ²]	
	COOLOCE-8 (alumina gravel)	STYX (alumina gravel)
1	178	214
2	235	273
4	263	329
5	290	357
7	342	429

Initially, it was speculated that the COOLOCE heating arrangement might increase coolability due to the local effects caused by the vertical heating arrangement (although it was assumed

that this does not affect the relative coolabilities of the conical and cylindrical beds). However, it is also possible that a *local dryout detectable by the sensors* occurs earlier (with a lower power) than a *global dryout* due to greater local power generation, and the consequently greater fraction of steam in the regions where the power generation is focused. This would be interpreted as decrease of the overall coolability.

The values of the measured dryout heat fluxes thus far do not suggest any drastic effect caused by the heating arrangement on the overall coolability. This is also supported by the rather good predictions of dryout power obtained by simulations concerning the relative coolabilities of the conical and cylindrical beds [16, 17]. However, further analytical work and the comparison of experimental and simulation results are necessary to resolve the remaining uncertainties concerning porosity and the effective particle size.

4.3 Effect of pool subcooling

In the subcooled pool experiments, the time to dryout varied according to the control power. All applied power levels were greater than the one observed in saturated initial conditions. The dryout waiting time as a function of pool subcooling for the dryout points described in the previous Chapter are shown in *Fig. 33*. The pool subcooling (difference from saturation temperature) is taken as the average subcooling during the dryout waiting time.

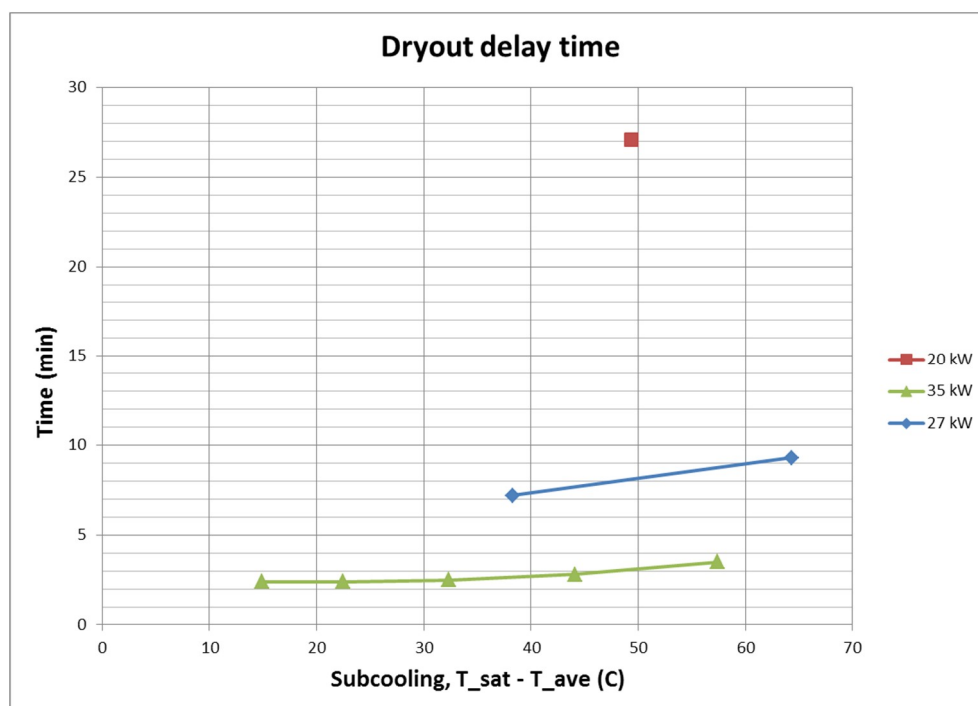


Fig. 33. Time to dryout with different pool subcooling (average subcooling during the dryout delay time) for constant power in COOLOCE-9 test series.

The waiting time to dryout, or dryout delay time, depends on the excess power as described in their experimental study by Hu & Theofanous [15] who found that the critical power “can be uniquely defined as an asymptotic limit (i.e. yielding dryout after an infinitely long delay), and that this limit can be conveniently, and accurately, inferred from a few experimental runs”. The waiting time to dryout increases as the power gets closer to the exact critical power as seen in the example of dryout delay time data by Hu & Theofanous [15] shown in *Fig. 34*.

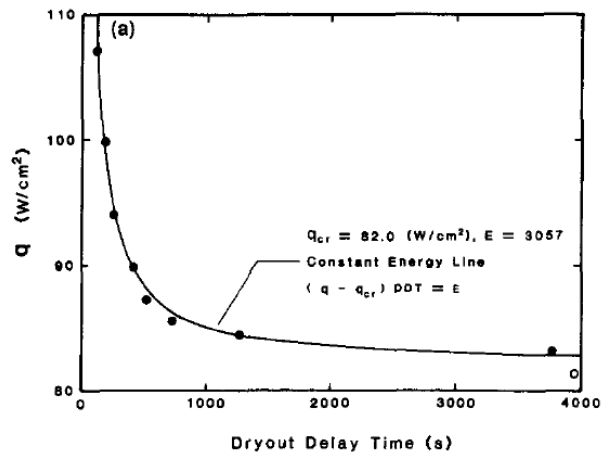


Fig. 34. Power-dryout delay time pairs measured with Purdue's Large Scale Corium Bed Simulation Facility (Hu & Theofanous [15]).

This dependence is consistent with the COOLOCE measurements that showed the longest waiting time for the power level of 20 kW and the shortest for 35 kW, regardless of the increasing pool temperature. Additional data can be obtained from the heat-up sequence of the COOLOCE-8a experiment. Since the 13 kW dryout power in saturated initial conditions was somewhat lower than expected, the authors performed the heat-up sequence at 15 kW which later turned out to be exceeding the dryout power. The heat-up sequence - during which the pool temperature was below the saturation temperature - lasted 47 minutes and no sign of dryout was seen. This is twice the time measured for 20 kW.

Due to the transient pool temperature and the relatively few dryout points, decisive conclusions about the effect of the pool subcooling cannot be made. Moreover, the facility-specific dryout delay times which would help to increase the accuracy of the results have not been measured. However, there are some clear differences between the results with saturated and subcooled initial conditions. The relatively long dryout waiting time at 20 kW and the fact that no dryout was seen at 15 kW with the pool temperature below saturation temperature suggest that the pool subcooling has a measureable effect on dryout power. At least a small coolability increase is achieved based on the results.

Observations of dryout near the top may suggest that the dryout mechanism is different with subcooled pool, possibly affected by the thermal stratification in the water pool. Cooler water is located near the test bed bottom, creating different heat transfer conditions for the bottom parts of the test bed. On the other hand, the excess power itself can cause dryout in the top region.

5. COOLOCE-10 results

5.1 COOLOCE-10a

The COOLOCE-10a experiment was the first test run performed with the laterally flooded cylinder. The power history and temperatures of the thermocouples which indicated temperature increase are shown in *Fig. 35*. As expected, the dryout control power was comparatively high, 34.1 kW.

Dryout was indicated only by a single sensor near the centre of the test bed at the height of 20 cm (26:120-45) while others remained at saturation temperature. However, one of the heater sensors (VY35:111-00) started to show increased temperature already about 90 minutes (at 26 kW power) before the dryout in the test bed sensor 26:150-45. What followed was an increase of a few centigrade in the heater sensor temperature at each power step. This is a clear indication of the loss of liquid cooling at the heater surface but we do not consider this as a valid dryout; only dryouts in the separate test bed sensors between the heaters are accounted for. This is to eliminate the disturbances caused by the heating arrangement to the determination of dryout power. Thus far, this is the only experiment in which such a clear increase in heater temperature was observed without a dryout in the test bed sensors.

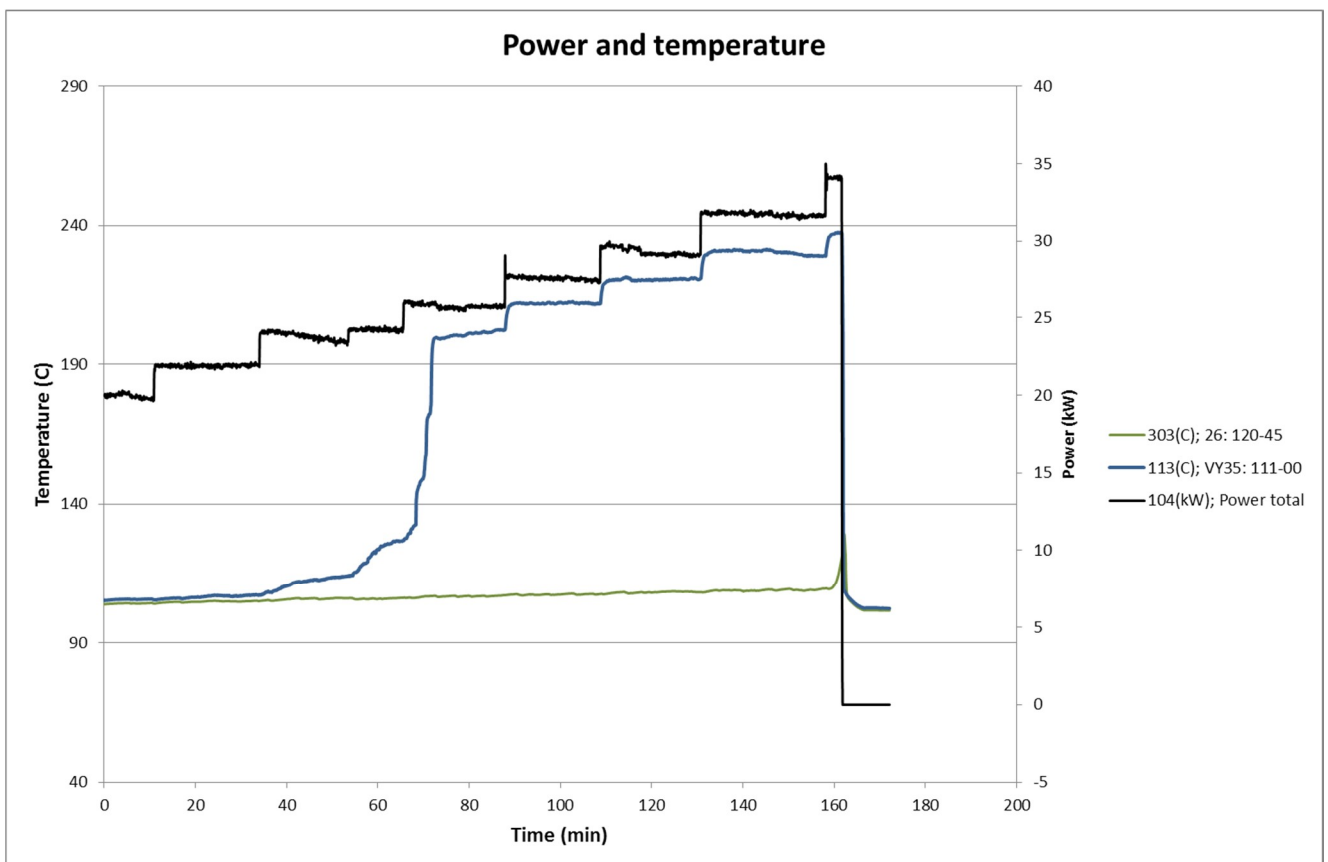


Fig. 35. Control power and temperature log in the COOLOCE-10a experiment.

Pressure and feed water level and temperature in the test vessel during the test run are shown in *Fig. 36*. The final pressure of the experiment was 1.3 bar (absolute). Even though the steam line valve was fully open during the test run, pressure increased from 1.1 bar to 1.3 bar due to the flow resistance in the steam line. Because of the high power levels and the consequential high flow rate in the steam line, the pressure control was somewhat poorer than usual.

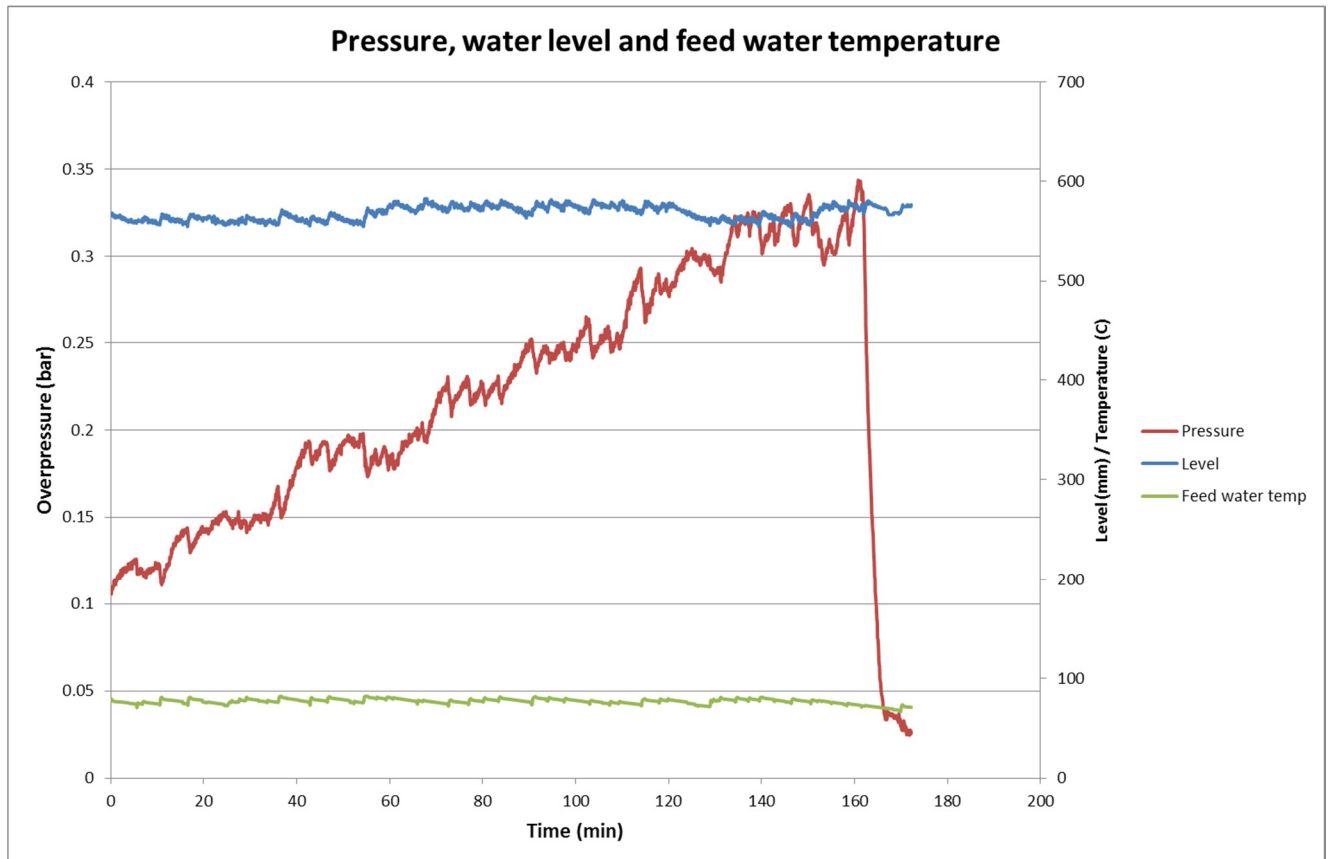


Fig. 36. Pressure and water level in the test vessel and the feed water temperature in the COOLOCE-10a experiment.

5.2 COOLOCE-10b

The COOLOCE-10b test run followed the 10a test run after a pressure increase to 2 bar. Dryout was indicated by the sensor 26:120-45 at 20 cm from the test bed bottom at the power of 40.1 kW. The power and temperature histories are shown in *Fig. 37*. Contrary to the 10a test, the heater temperatures increased only slightly during the final power steps. Pressure and feed water level and temperature in the test vessel during the test run are shown in *Fig. 38*. The pressure was controlled normally with 2 bar set point. The average pressure at the power step leading to dryout was 1.98 bar.

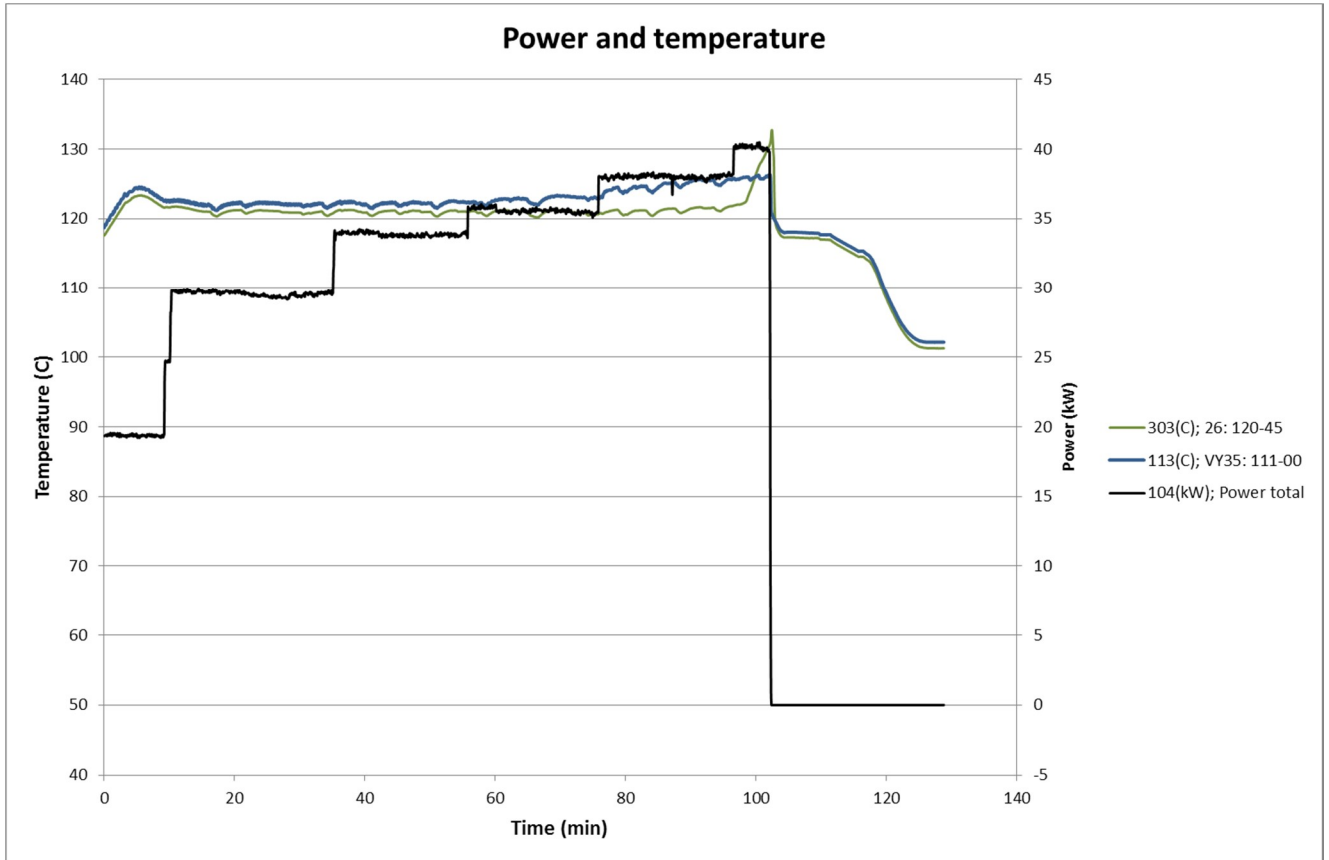


Fig. 37. Control power and temperature log in the COOLOCE-10b experiment.

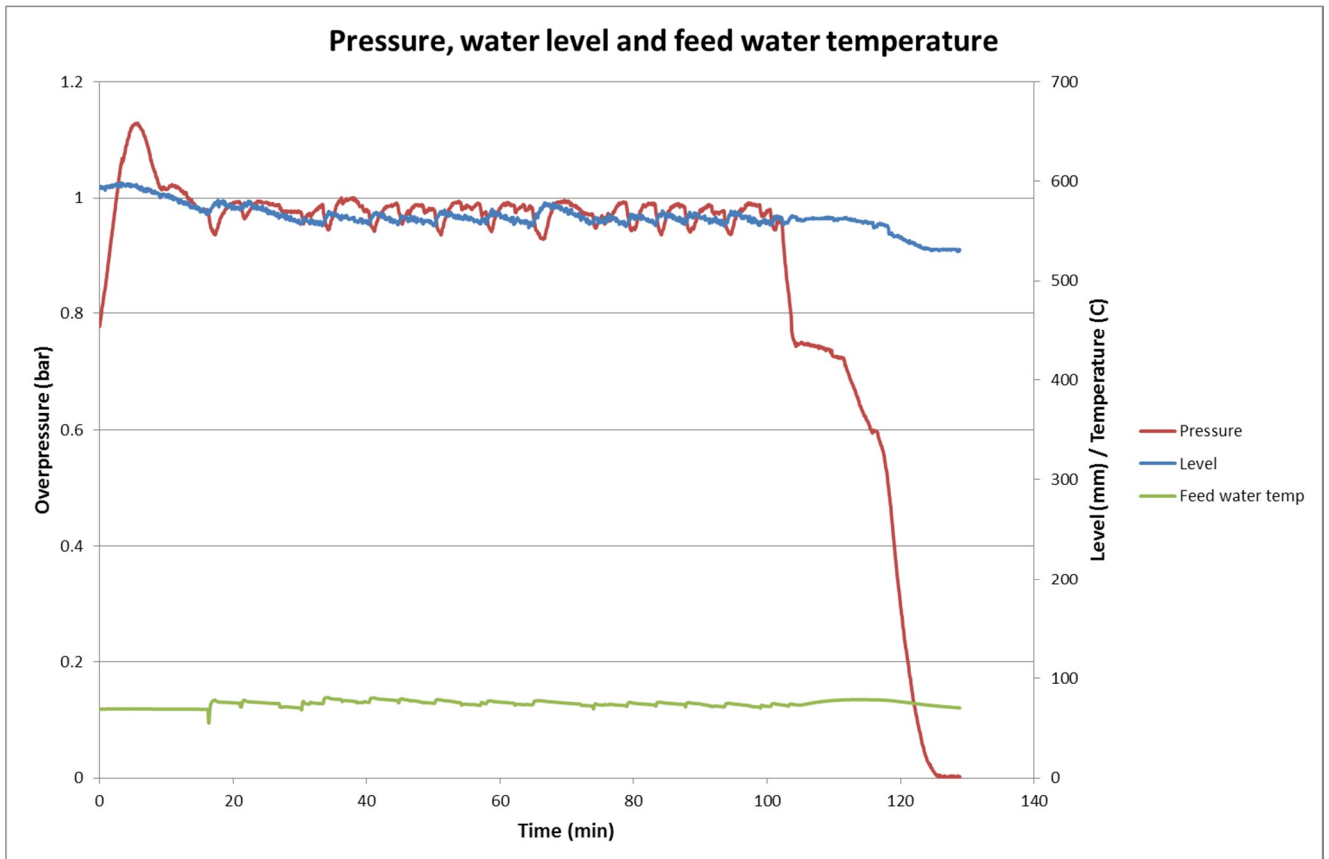


Fig. 38. Pressure and water level in the test vessel and the feed water temperature in the COOLOCE-10b experiment.

5.3 COOLOCE-10c

The COOLOCE-10c test run at 3 bar was started after a heat-up sequence after an overnight break in the experiments. The power and temperature histories are shown in *Fig. 39* (saturated conditions are reached at 50 minutes). The measured dryout power was 46.2 kW, indicated by the sensors 26:122-45 and 26: 120-45. These sensors are the topmost sensors (20 cm and 22 cm) of the multi-point thermocouple near the centre of the test bed. In connection with the dryout, also the heater sensor VY35:111-00 started to increase above saturation temperature. Pressure and feed water level and temperature in the test vessel are shown in *Fig. 40*. The average pressure of the final power step was 2.93 bar.

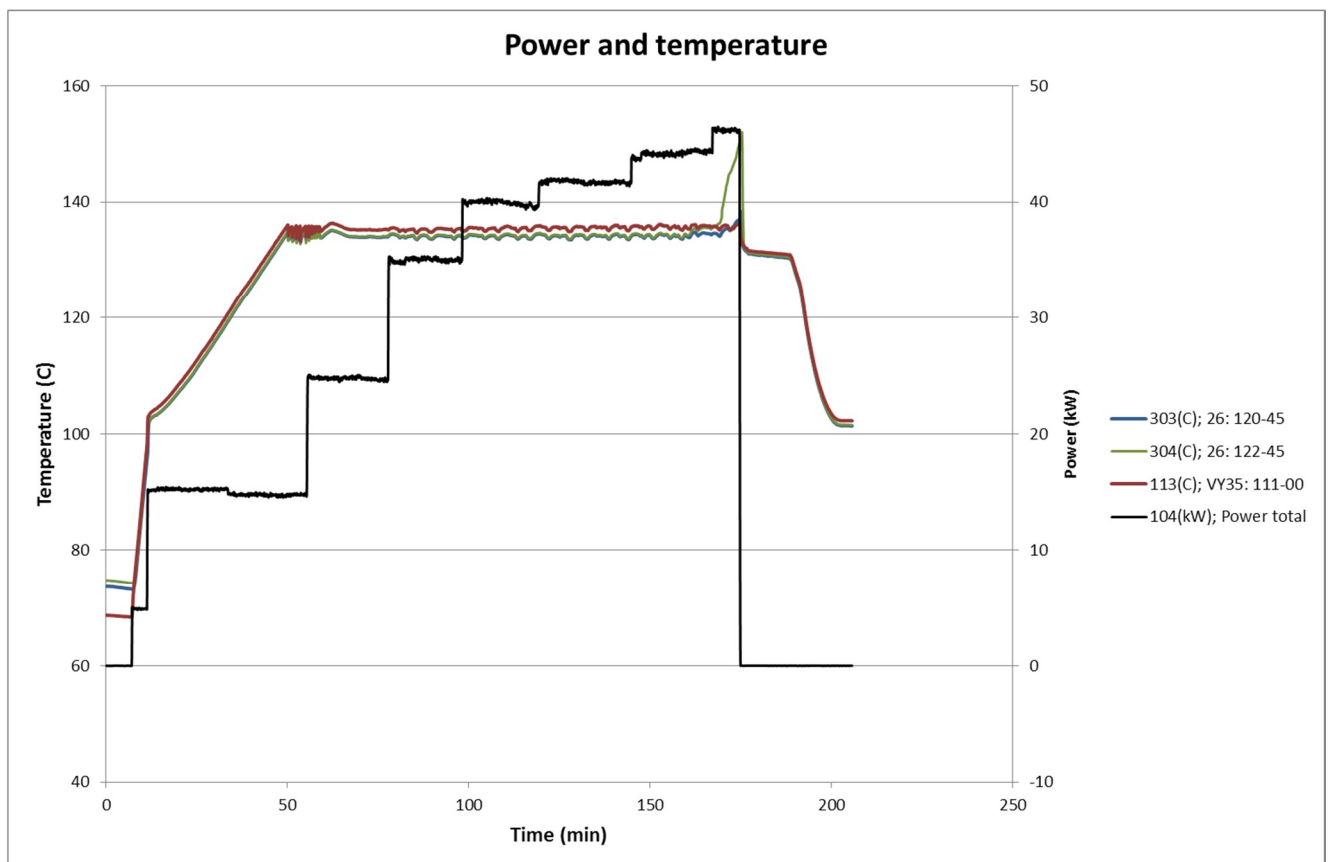


Fig. 39. Control power and temperature log in the COOLOCE-10c experiment.

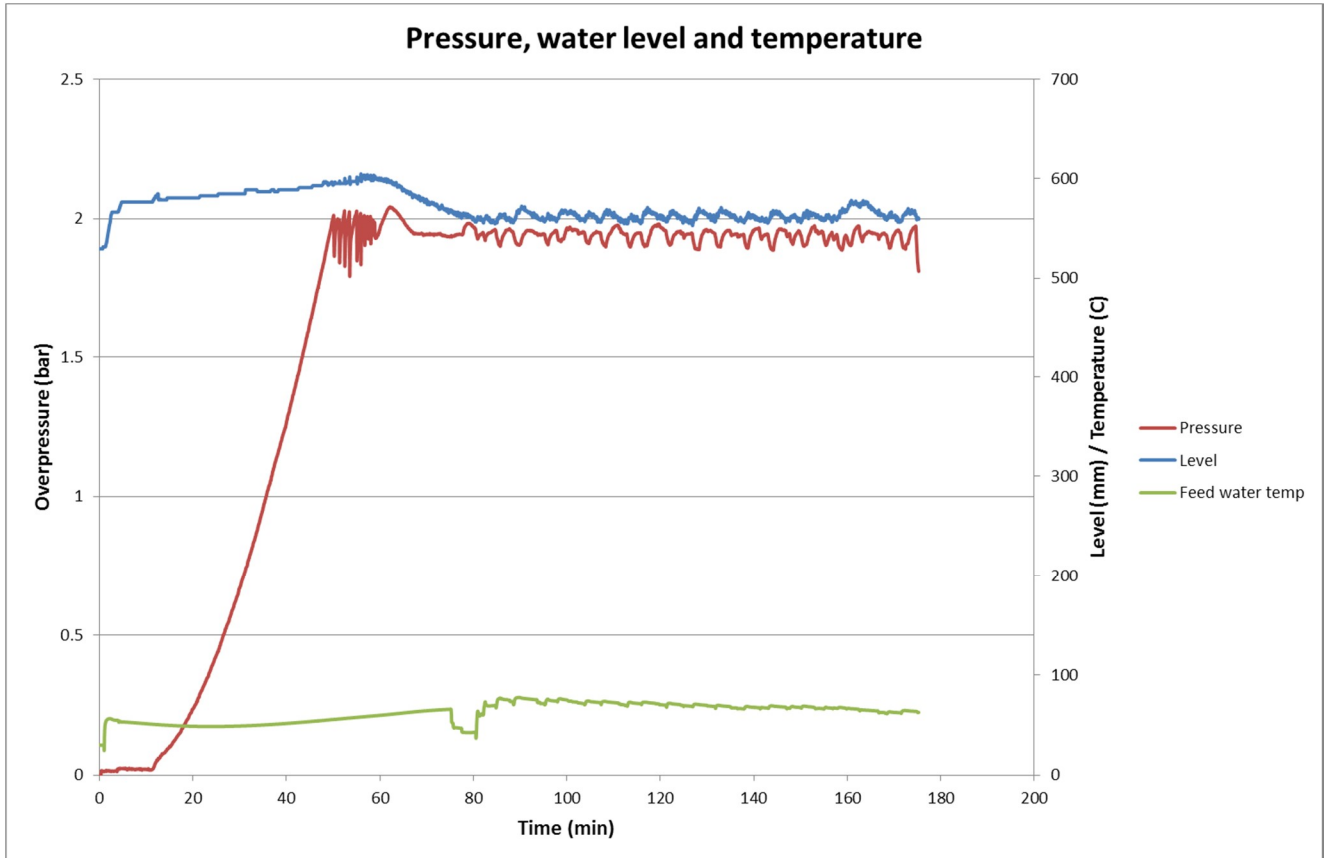


Fig. 40. Pressure and water level in the test vessel and the feed water temperature in the COOLOCE-10c experiment.

6. COOLOCE-10 discussion

Dryout was measured for three pressure points according to the normal test procedures, including initially saturated conditions, stepwise power increases and the termination of test sequences after a verified temperature excursion from saturation temperature. Dryout was located in the upper parts of the test bed and, horizontally, in the centre. Only one or two thermocouples indicated dryout, similarly to several of the previous COOLOCE experiments. However, in the vicinity of the thermocouple showing dryout, there were no sensors at the same height. Thus, the true volume of the dryout zone is not known. Dryout occurred soon after the power increase, in 2-5 minutes.

Considering the lateral flooding, dryout location and the short dryout delay time are reasonable. A prediction of the flow field for a laterally flooded cylinder is given by a pre-test calculation performed by Lubchenko et al. with the DECOSIM code [18]. The simulation result is illustrated in Fig. 41 which shows the void fraction and the water streamlines. The highest void fraction and dryout is formed near the top of the geometry in the centre. Circulation of water through the sidewall keeps the bottom region with the lowest steam fraction (and lowest steam mass flux) cooled as well as the near-wall regions in the upper parts.

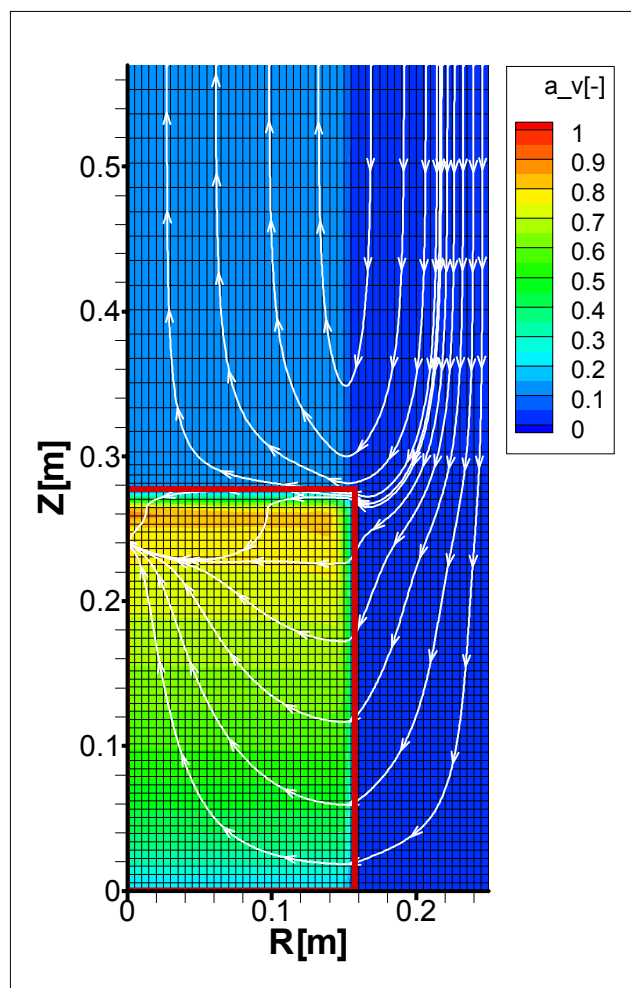


Fig. 41. Spatial distribution of void fraction and streamtraces for water in DECOSIM simulation [18].

The following simulation parameters were used: system pressure 1.1 bar, particle diameter 0.9 mm and porosity 40%. The dryout power in the simulation was 29.3 kW. The agreement

with the experimental power and location in COOLOCE-10a is reasonable considering that the simulation parameters are pre-test estimates.

According to the simulation, the dryout zone is small which means that a difficulty similar to the conical bed geometry may be present in comparing the experimental and simulation results: the dryout zone just above the critical power level might not be captured by the thermocouples even though the geometry does not limit the dryout zone to any specific point in the debris bed (such as the apex of the cone). Rather, it can be said that the dryout zone is small simply because of the increased coolability. Post-test simulations are needed to obtain an estimate of the dependence of dryout zone size on power level.

Similarly to the conical bed, the cylindrical test bed apparently stabilized into a new steady-state with co-current circulation of steam and water, even in post-dryout conditions. This explains the quick formation of dryout after the power increase. A type of demonstration of such a steady-state is the local dryout seen at one of the heaters in COOLOCE-10a in which the temperature increases followed the power steps (with no drastically increasing transient temperature).

6.1 Effect of lateral flooding

As expected, the lateral flooding increases dryout power (as well as heat flux and power density) compared to top flooding only. Comparison of the present test series to the COOLOCE-3 – 5 test series [3] shows that the difference is about 14 kW, corresponding to a difference of 200 kW/m² in heat flux (50-73%). The results are plotted in *Fig. 42*. Note that the correction in bed diameter from 310 mm to 305 mm due to the sidewall wire net is taken into account in the calculation of the dryout heat flux (dryout power per top surface area). The increase in coolability achieved with lateral flooding is significant regardless of the uncertainties in the measurements.

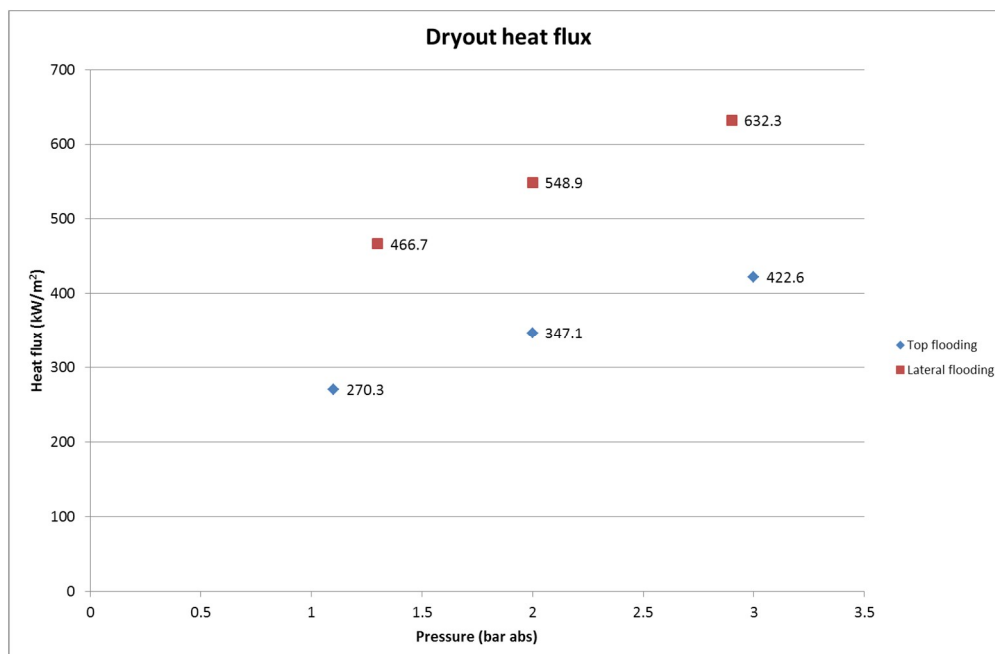


Fig. 42. Dryout heat flux in top flooded (COOLOCE-3-5) and laterally flooded (COOLOCE-10) test bed.

7. 2D simulations of top-flooded beds

An important goal of the COOLOCE-E project is to obtain data for code validation and development. The analyses of the coolability of the molten and/or solidified core in reactor scale are done by severe accident simulation codes. The capabilities of the simulation codes are evaluated by comparing the simulated and experimental results. It is important that this work includes the debris bed configurations that are considered representative based on the latest knowledge of the accident scenarios.

On the other hand, it is often difficult, if not impossible, to accurately reproduce the conditions of a reactor scenario in a laboratory (e.g. the heating methods are different). The limitations of experimental set-ups and instrumentation should be carefully evaluated by comparing results obtained in separate but well-defined experimental conditions. This is one of the tasks of the on-going NKS DECOSE project conducted jointly by VTT and KTH (Royal Institute of Technology, Sweden). Comparisons of experimental results and modelling results with models that have already gone through validation against earlier experiments also help to identify these limitations.

One of the coolability simulation codes is MEWA 2D which has been developed by the IKE institute at Stuttgart University specifically for severe accident assessment [19]. The code has been used at VTT in several previous studies to predict the dryout heat flux in different experiments [20-21]. In the present study, the analysis of the COOLOCE experiments has been continued with the MEWA code. The issues of effective particle diameter and porosity considering two different particle materials used in the experiments have been addressed. Parameter variations have been performed for the simulations of conical and cylindrical debris beds. The cylindrical bed experiment with lateral flooding will be modelled in the future.

7.1 Goal

The objectives of the presented simulations are as follows:

- 1) Modelling of the COOLOCE-8 experiments performed in 2012 with measured effective particle size and estimating
 - a. the effect of the particle material
 - b. the possible test facility specific differences by comparison to STYX experiments
- 2) Re-evaluation of the result of the conical and cylindrical bed experiments conducted in 2011 with
 - a. measured effective particle size and porosity
 - b. variations of particle size and porosity
 - c. improved power step accuracy

7.2 Simulant materials in the experiments

The experiments COOLOCE-3-5 with a cylindrical test bed and COOLOCE-6-7 with a conical test bed were performed with spherical zirconia/silica (ZrO_2/SiO_2) beads with the mean particle size of approximately 0.97 mm. The size was estimated by using image processing software. The follow-up test sequence, COOLOCE-8, was conducted with irregular alumina (Al_2O_3) gravel as the simulant material. Otherwise, the test arrangements in COOLOCE-3-5 and -8 were similar. Samples of the materials are shown in Fig. 43.



Fig. 43. The alumina gravel used in COOLOCE-8 (left) and the zirconia/silica beads used in COOLOCE-3 – COOLOCE-7 (right). Note: the scale of the images is not the same.

The gravel consists of particles of variable size and shape with the size range being 0.25-10 mm. According to measurements performed at Royal Institute of Technology (KTH), the “effective” particle diameter of a batch of the gravel was 0.65 mm [14]. This effective diameter is estimated by single-phase flow pressure loss measurements by fitting the pressure loss at different flow velocities to the Ergun’s equation [13] assuming that porosity is known.

The bed porosity for which the 0.65 mm diameter was obtained was 40.8%. The result is slightly different from a similar type of measurement that was originally conducted for the STYX experiments even though the particle size distribution in COOLOCE-8 was adjusted to closely correspond to the original size distribution. For the STYX experiments, an effective diameter of 0.8 mm was estimated for 40% porosity. The difference might be related to the test set-ups or to minor shifts in the properties of the particle batches in the measurements.

The size range of the spherical beads is 0.815-1.126 mm according to a sample of about 1000 beads. According to the measurement at KTH, the effective particle diameter of the spheres is 0.8 mm and the porosity 39.9% [14]. This means that the representative diameter considering the flow resistance would be close to the smallest particles in the distribution, rather than the mean of 0.97 mm.

The material densities of the gravel and the beads are 3930 kg/m³ and 4230 kg/m³, respectively. The densities were measured based on the mass and volume of the material samples by using a beaker. The approximate thermal conductivities of 20 W/m·K for alumina and 2 W/m·K for zirconia/silica are used in the simulations.

7.3 Simulation specifications

7.3.1 Drag force models for porous medium

The MEWA code models the transient behaviour of the debris bed in 2D with cylindrical or Cartesian geometry by solving the conservation equations for mass, momentum and energy [19]. The momentum conservation equations for the liquid and gas phases appear in a simplified form with no temporal derivatives or viscous shear stress term:

$$-\nabla p_l = \rho_l \vec{g} + \frac{\vec{F}_{pl}}{\varepsilon(1-\alpha)} + \frac{\vec{F}_i}{\varepsilon(1-\alpha)} \quad (1)$$

$$-\nabla p_g = \rho_g \vec{g} + \frac{\vec{F}_{pg}}{\varepsilon \alpha} + \frac{\vec{F}_i}{\varepsilon \alpha} \quad (2)$$

where p is pressure [Pa], ρ is density [kg/m^3], ε is porosity, α is void fraction, \vec{F}_{pl} and \vec{F}_{pg} are the drag forces between the liquid and gas [N/m^3], respectively, and \vec{F}_i is the gas-liquid drag (interfacial drag) [N/m^3].

In the cylindrical bed simulations, we have used the “basic” drag force models derived from the two-phase extension of the Ergun’s equation in which the interfacial drag is not explicitly considered. In this approach, \vec{F}_i is omitted and the particle-fluid drag forces are

$$\vec{F}_{pl} = \varepsilon(1 - \alpha) \left(\frac{\mu_l}{KK_{rl}} \vec{j}_l + \frac{\rho_l}{\eta\eta_{rl}} |\vec{j}_l| \vec{j}_l \right) \quad (3)$$

$$\vec{F}_{pg} = \varepsilon\alpha \left(\frac{\mu_g}{KK_{rg}} \vec{j}_g + \frac{\rho_g}{\eta\eta_{rg}} |\vec{j}_g| \vec{j}_g \right) \quad (4)$$

where \vec{j} is superficial velocity [m/s] and μ is viscosity [kg/m/s]. The relative permeability K_r [-] and relative passability η_r [-] are defined by powers of void fraction as follows

$$K_{rl} = (1 - \alpha)^n, \quad K_{rg} = \alpha^n \quad (5)$$

$$\eta_{rl} = (1 - \alpha)^m, \quad \eta_{rg} = \alpha^m \quad (6)$$

The powers n and m vary depending on the author; Lipinski suggested that $n=3$ and $m=3$ [22], according to Reed $n=3$ and $m=5$ [23] and Hu and Theofanous proposed that $n=3$ and $m=6$ [15]. The assumption of Reed is the most commonly used and has shown to fit most experimental data well. The single-phase permeability K [m^2] and passability η [m] according to Ergun are

$$K = \frac{\varepsilon^3 d_p^2}{150(1 - \varepsilon)^2}, \quad \eta = \frac{\varepsilon^3 d_p}{1.75(1 - \varepsilon)} \quad (7)$$

In all the cylindrical bed simulation cases, we have used the Reed model for relative passability. A model variation is considered in the case of gravel where the simulation with the effective particle diameter ($d_p = 0.65$ mm) and porosity ($\varepsilon = 40.8\%$) is run with the Hu and Theofanous model which yields a somewhat increased pressure drop compared to the Reed model (see the simulation matrix in the next section).

For the conical bed cases, the Tung and Dhir model with the modifications for particles smaller than 6 mm is applied (“modified Tung and Dhir model”) [24, 25]. This model includes a separate expression for the gas-liquid drag \vec{F}_i . The drag forces in this model are dependent on flow regime with weighting functions to account for the transition zones between the flow regimes.

We have chosen this model for the conical bed because it has been well-established that the role of interfacial friction is significant in cases with multi-dimensional flooding, and because the particle size averages addressed are clearly smaller than 6 mm. Since the formulation of the model is rather complex, we do not repeat the model equations here. A summary of the models can be found in [25].

7.3.2 Simulation set-up

The MEWA code as distributed by Stuttgart University in August 2008 to VTT and KTH has been used in the simulations. Minor modifications were done later to e.g. the output files of the code but no changes have been done to the models and numerical solution. Simple 2D axisymmetric grids that have the cell size of 2.5 mm have been used for the spatial discretization. The grids are shown in *Fig. 44*.

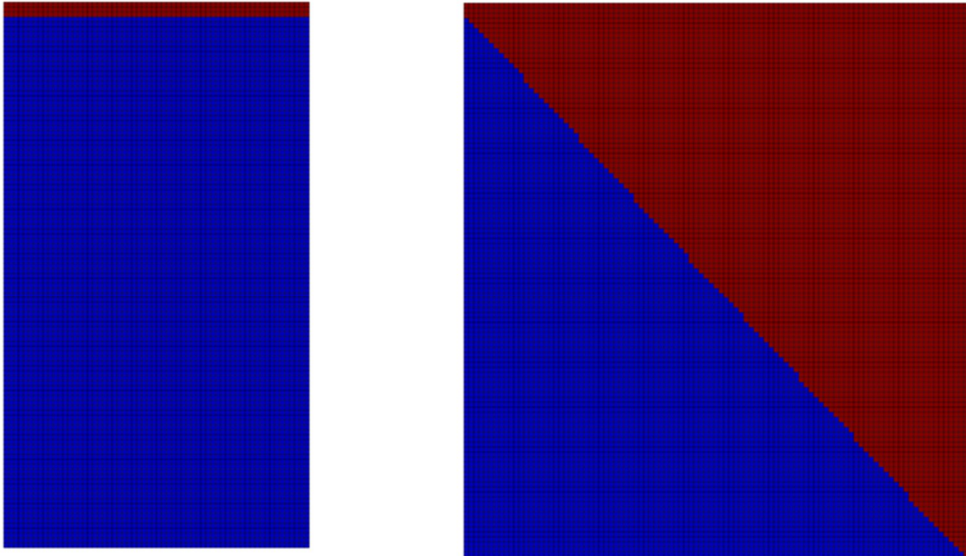


Fig. 44. The computational grids for the COOLOCE simulations: the cylindrical bed (left) and the conical bed (right). The red area is the pool volume and the blue area is the particle bed.

The simulation cases are listed in Table 5. Each case in the table (1-9) contains a set of simulations which cover the pressure levels of the experiments to which the simulation results will be compared, i.e. 1-7 bar for the cylindrical beds and 1-3 bar for the conical bed. The variation range of particle diameter takes into account the different estimates of effective/average particle diameter and the porosity range is kept at a very realistic value (37-40.8%).

It should be emphasized that in the simulations the different sizes and morphology of the ceramic beads and the gravel are accounted for only by the different average diameter and porosity and - concerning heat transfer solution - by different thermal properties. Otherwise, the inputs for the cylindrical bed simulations are similar (cases 1-6). The conical bed cases (7-9) have a different geometry but the material properties are the same as in cases 4-6.

Since the simulations deal with the pre-dryout steady-states without significant temperature gradients and aim to determine the conditions at which such steady-states can no longer be reached, we assume that the differences in thermal properties do not play a significant role in the simulations.

Table 5. The simulation matrix.

Cylindrical bed cases		
Gravel (COOLOCE-8 and STYX)		
Case	Porosity	Particle diameter [mm]
1	0.408	0.65
1b	0.408	0.65
2	0.37	0.65
3	0.38	0.8
Beads (COOLOCE-3-5)		
Case	Porosity	Particle diameter [mm]
4	0.40	0.97
5	0.37	0.97
6	0.40	0.80
Conical bed cases		
Beads (COOLOCE-6-7)		
Case	Porosity	Particle diameter [mm]
7	0.38	0.90
8	0.40	0.80
9	0.38	0.97

The dryout power has been searched by using a stepwise power increase scheme and detecting which power level leads to local dryout. The size of the power step is 0.5 kW (this is the accuracy of the simulations).

The time taken by the development of dryout is dependent on the power level; the greater the excess power, the faster the water remaining in the debris bed is evaporated. According to the simulations, the dryout delay time for the cylindrical debris bed with 0.5 kW accuracy is - in most cases - more than 3400s. In the cases of conical bed, there is no strong dependence of the dryout delay time on power. According to the simulation, the conical bed reaches a new steady-state in about 100-200 s.

The accuracy in the experiments is 2 kW which corresponds to a dryout delay time of 20-30 minutes. Using the aforementioned power steps, the dryout heat flux can be determined with the accuracy of 7 kW/m² in the simulations and 27 kW/m² in the experiments. The dryout heat flux is defined as the dryout power divided by the surface area of the top of the debris bed.

7.4 Simulation results

The experimental and simulation results are presented in this Chapter. The comparisons are arranged correspondingly to the groups of cases in Table 5. In the cases of cylindrical bed, the dryout heat flux (DHF) is presented and in the cases of conical bed, the dryout power density (DPD) as no surface area corresponding to the top of the cylinder can be easily determined for the conical geometry. The exact values of DHF and DPD for each case can be found in Appendix C in which the results are tabulated.

7.4.1 Cylindrical debris beds with gravel (COOLOCE-8 and STYX)

The measured and simulated dryout heat fluxes as a function of pressure in the case of the cylindrical bed and irregular gravel are shown in Fig. 45. It is seen that in near-atmospheric pressure, three of the four cases agree well with the simulation. The lower boundary case with the lowest porosity and particle diameter (37%, 0.65 mm) yields a lower DHF by about 55 kW/m² (30%).

However, the pressure dependence in the experiments deviates from that of the simulations: the greater the pressure, the lower is the measured DHF compared to simulation results. For increased pressure, the three cases which predict the atmospheric DHF well overestimate the dryout heat flux, including the case with the estimated effective particle diameter (40.8%, 0.65 mm) while the closest estimate is given by the lower boundary case (37%, 0.65 mm). The simulated values of DHF at 7 bar vary between 328 and 486 kW/m² with the experimental one being 342 kW/m².

The model variation case calculated using the model of Hu and Theofanous shows a moderate difference compared to the effective diameter case calculated by the Reed model. This is due to the increased drag force in the inertial (quadratic) terms of Eqs. 3-4. The DHF obtained by the Reed model is greater by 7-70 kW/m².

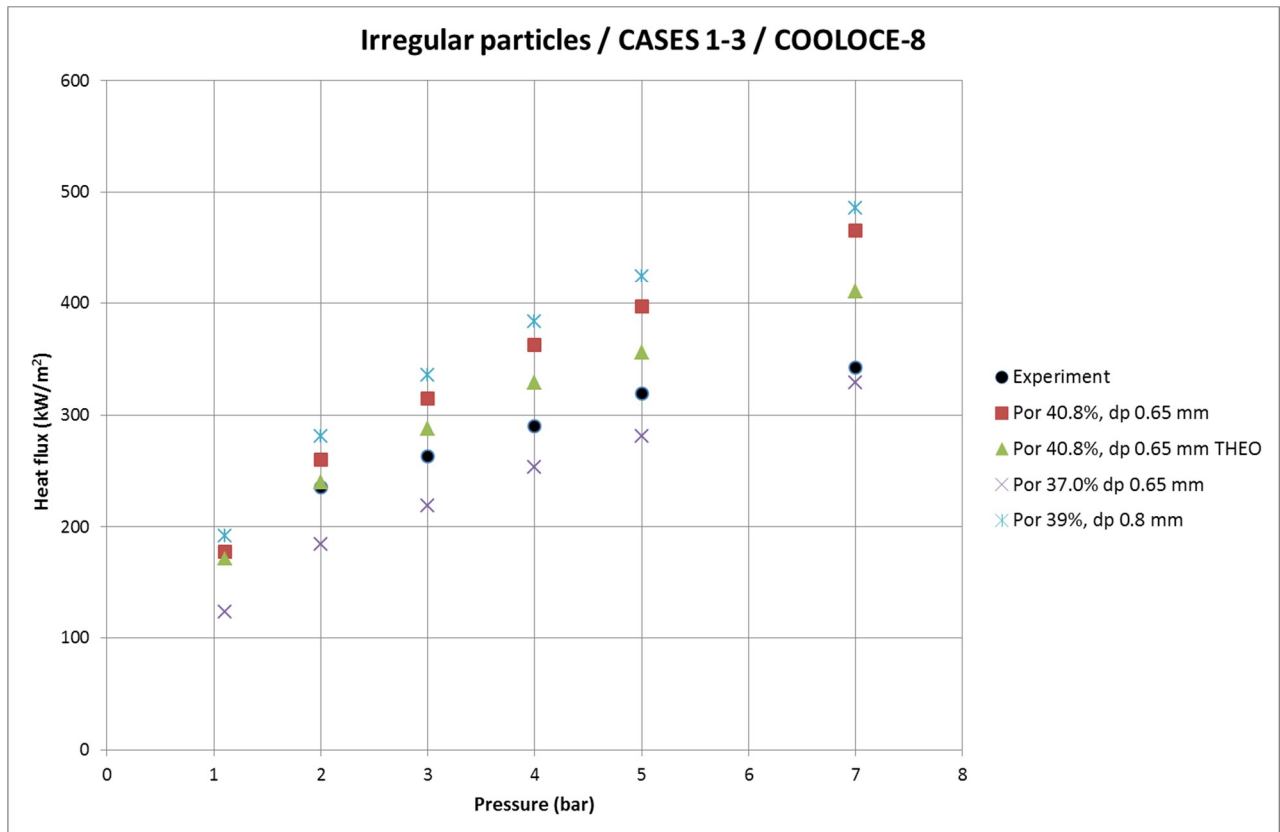


Fig. 45. Experimental and simulated dryout heat flux for the cylindrical bed with irregular particles.

Next, the heat flux obtained by the simulations is compared to that of the STYX-8 experiments in which the same particle material was used [7]. However, the debris bed properties might be slightly different compared to the original ones as suggested by the differences in the estimates of effective particle diameter.

Fig. 46 shows the dryout heat flux of the STYX experiments and the simulation results for the cases with effective particle diameters according to the new estimate (0.65 mm) [14] and the old estimate for the STYX test bed (0.8 mm) [6]. A lower boundary for DHF is represented by the case with 0.65 mm diameter and 37% porosity.

Concerning the pressure dependence, a similar trend is seen as in the COOLOCE experiment. Experimental DHF does not increase as steeply as the simulated one and the models tend to underestimate DHF for lower pressure and overestimate it for higher pressures. However, the 7 bar point in the STYX experiments seems to be more in accordance with the simulation results than the corresponding point in the COOLOCE experiment in which the 7 bar DHF was pronouncedly low. Otherwise, for pressures below 7 bar, the measured DHF in COOLOCE is about 40 kW/m² lower than in STYX. In general, the results are in accordance with previous simulations of the STYX experiments in which the best agreement was found with 37% porosity and 0.8 mm diameter [26].

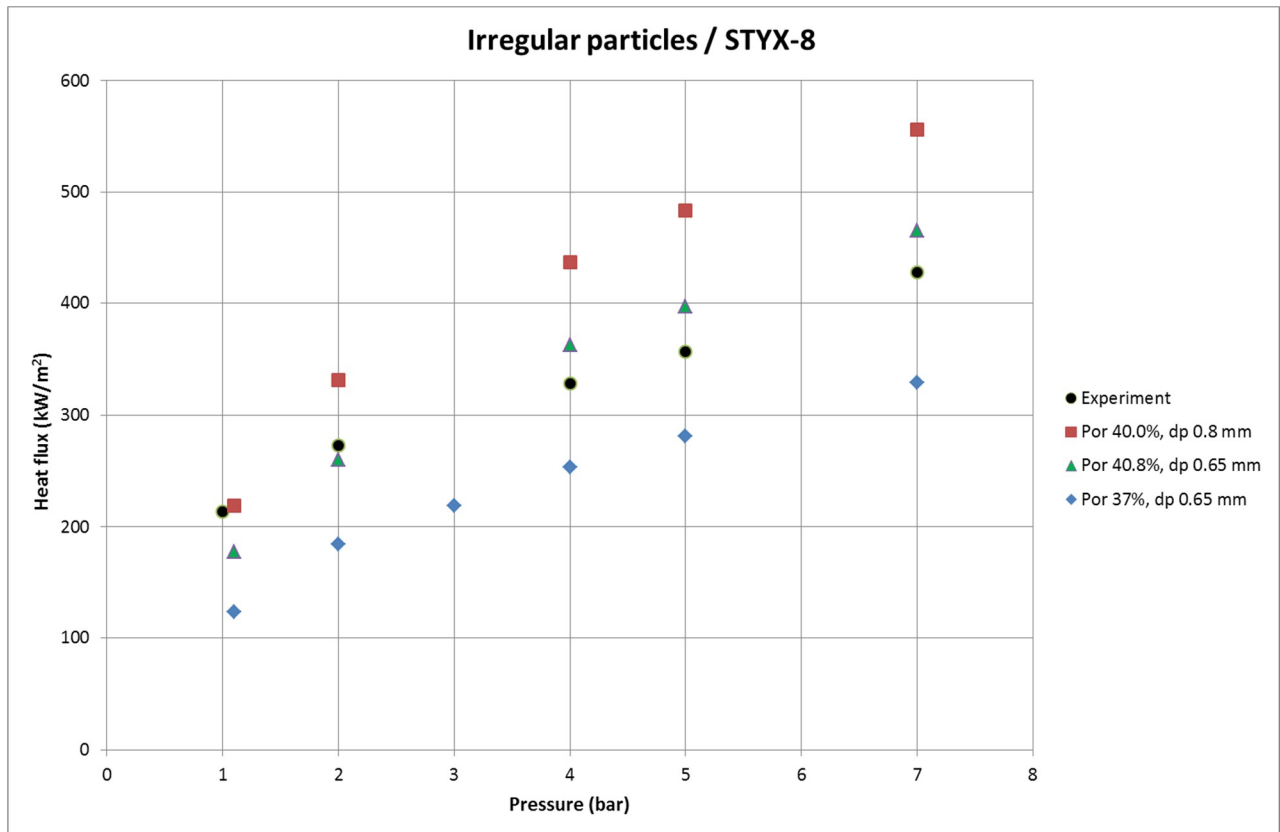


Fig. 46. Experimental and simulated dryout heat flux for the STYX experiments with irregular particles.

7.4.2 Cylindrical debris beds with spherical particles (COOLOCE-3-5)

The comparison of experimental and simulated dryout heat fluxes in the case of cylindrical bed with ceramic beads is presented in Fig. 47. Contrary to the gravel bed, the particle size distribution with the ceramic beads is small and the particles are (nominally) spherical. It is seen that the cases with the separately measured effective diameter (40%, 0.8 mm) and the average diameter with a denser packing (37%, 0.97 mm) yield very similar results, both of which are in a good agreement with the experimental DHF for pressures above 1 bar. Assuming the looser packing of 40% and the arithmetic mean size of the particles, 0.97 mm, the DHF is somewhat overestimated.

The pressure dependence in the experiments does not exactly follow the one in the simulations: at atmospheric pressure, there is a maximum deviation of about 90 kW/m². However, the difference is not as notable as in the case of gravel particles in Fig. 45.

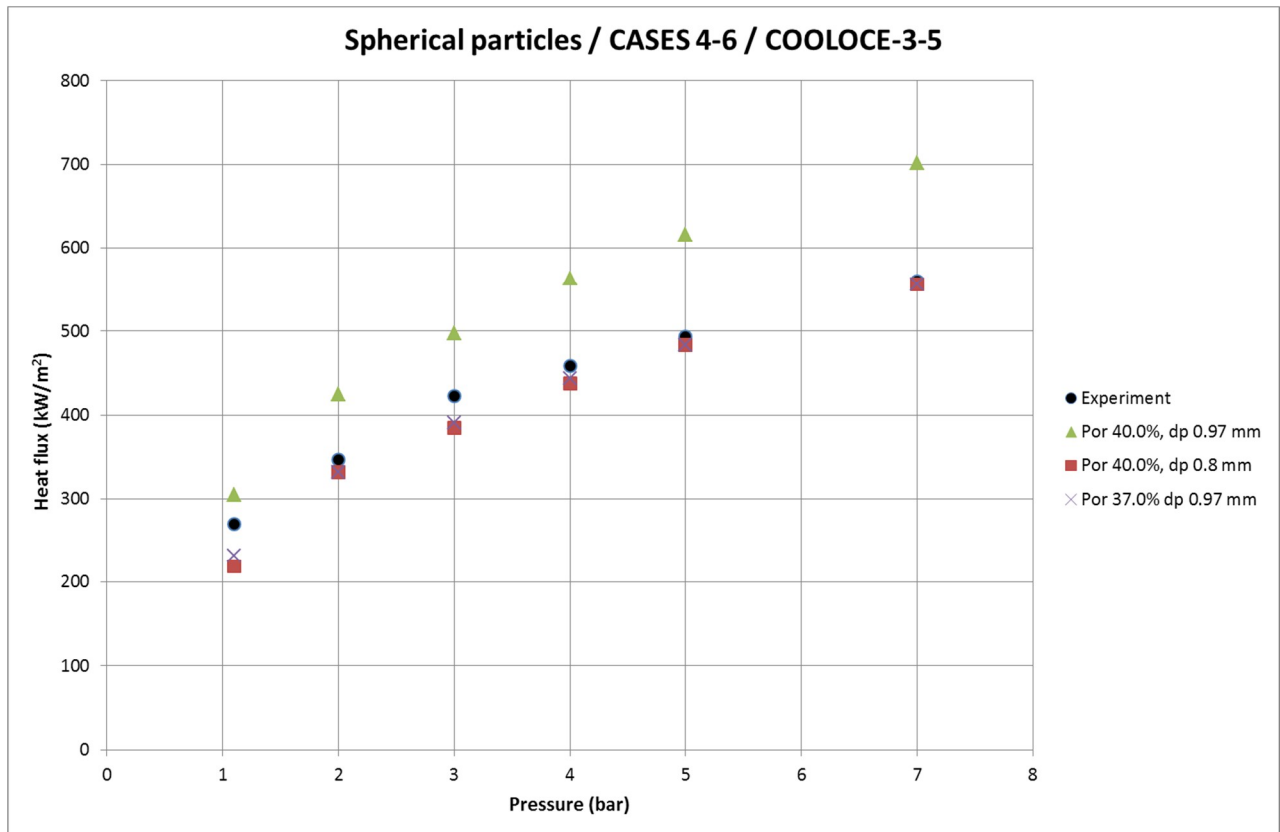


Fig. 47. Experimental and simulated dryout heat flux for the cylindrical bed with spherical particles.

7.4.3 Conical debris bed with spherical particles (COOLOCE-6-7)

The measured and simulated dryout power densities as a function of pressure in the case of the conical debris bed and spherical particles are shown in Fig. 48. By directly comparing the DPD, it is seen that the case with the measured effective diameter and porosity yields a power density 220-310 kW/m³ lower than the measured DPD. The variation with 38% porosity and 0.9 mm diameter results in practically the same DPD. The greatest DPD, and closest to the measurement, is given by the 0.97 mm particle size and 38% porosity.

However, it was seen in Fig. 47 that the case with the effective particle diameter and porosity does not underestimate coolability but yields the closest fit to the experimental data for the top-flooded, cylindrical bed. A similar discrepancy between the conical and cylindrical beds was seen in the other post-test calculations, explained by the different type of flow mode in the two beds and the criterion of dryout [5, 16, 17].

The onset of dryout occurs in an extremely small region near the top of the cone after which the conical bed settles to a new steady-state in which the dryout zone is cooled by the steam flow. The dry zone does not increase in volume until power is further increased. In the simulations, the formation of the first dry zone can be determined with the accuracy allowed by the computational grid and an arbitrarily small power step. It is not possible to detect infinitesimally small dry regions using the test facility; dryout zone volume has to increase at least as much to be captured by one of the thermocouples.

Rather than adjusting the model parameters to fit the experimental DPD data at the critical power level (i.e. minimum power leading to dryout), it is more feasible to examine the dryout zone size and location in the simulations at different power levels and compare them to the experimental dryout power and location. Earlier investigations (not including the full pressure

range) suggest a reasonable agreement between the *experimental dryout conditions* and the *simulations run at the experimental power level*, above the minimum dryout power [16, 17].

Pressure dependence shows a similar trend as the previous case of cylindrical bed with the spherical beads: it is only slightly different from the model predictions with lower DPD in the upper end of the pressure range.

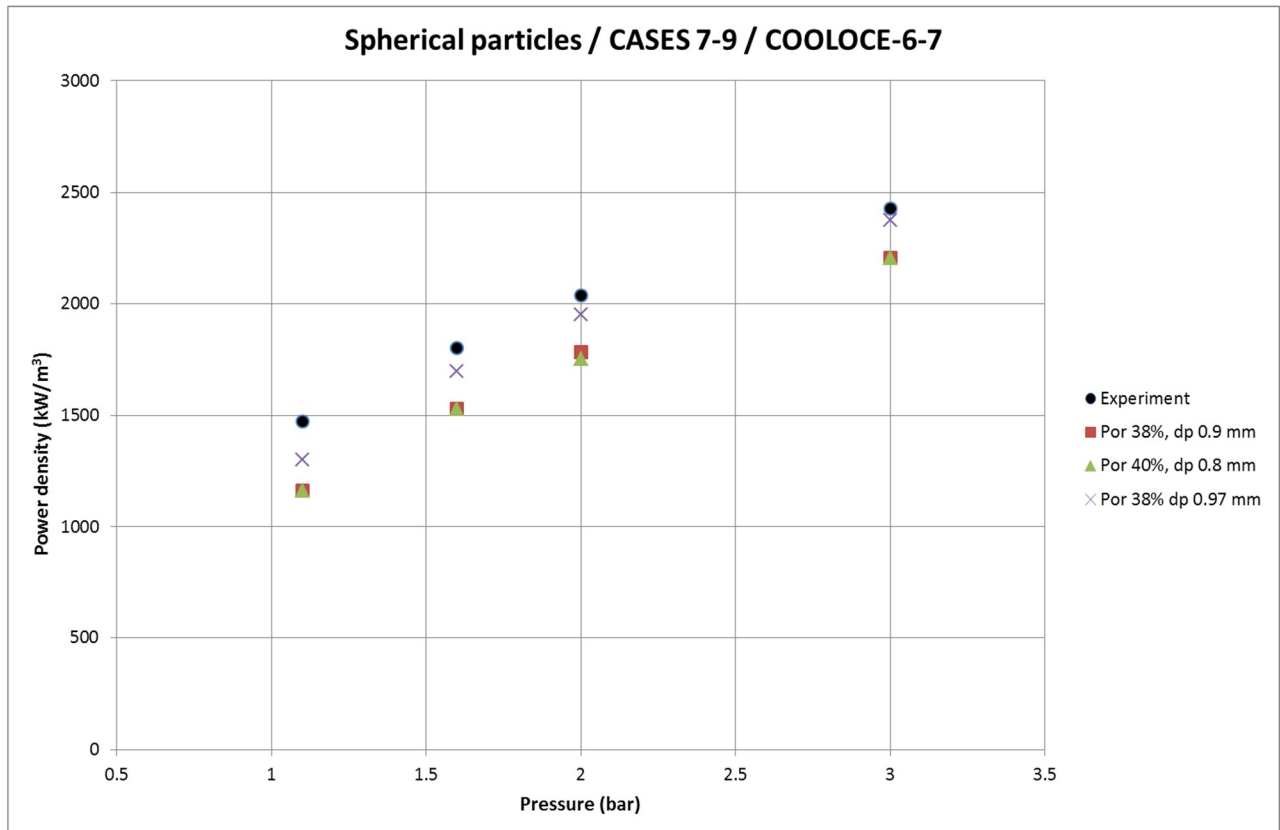


Fig. 48. Experimental and simulated dryout power density for the conical bed with spherical particles.

7.5 Discussion of the simulation results

The MEWA simulations show that a good prediction of DHF is obtained by using the separately measured effective particle diameter (and porosity) in case of the spherical particles. On the other hand, an equally good result is achieved by assuming a smaller porosity and a larger particle diameter (arithmetic mean of the particle size). The latter case may even be better representative of the COOLOCE test bed since its estimated porosity is 38-39.5 % which is slightly smaller than the 40% porosity in the measurement of effective particle diameter with POMECO-FL. This means that the effective particle diameter should be increased to “compensate” the reduced porosity to yield an equal pressure loss as in the measurement with POMECO-FL. (The pressure loss fitted into Ergun’s equation does not distinguish between the contributions of particle diameter and porosity.)

The porosity and particle diameter in both cases are within a realistic range, i.e. porosity is typical for a packed bed but greater than the minimum porosity of randomly packed spheres (~37%) and the diameter is within the particle size variation range.

In the case of irregular particles, the experimental DHF tends to be lower than the simulated DHF with the exception of near-atmospheric pressure. The separately measured effective particle diameter and porosity do not produce as good results as in the case of spherical particles. Uncertainties related to porosity are a likely explanation.

The maximum packing density of the gravel is greater than that of randomly packed spheres because the smallest particles can fill the pores between the larger particles, e.g. for soil gravel the minimum porosity is the order of 25%. In the experiments, the debris bed packing was intentionally left loose to avoid stratification and to simulate a bed formed by pouring of mixed-size particles. It is possible that the bed has shifted during the experiments, gradually creating a denser packing whose true porosity is unknown. (Note that a porosity shift of e.g. from 40% to 37% is so small that it would be difficult to note as a change of gravel surface in the test container). In contrast, the test bed with spherical particles was initially packed as dense as possible.

At 7 bar pressure, the best agreement with the experimental result is given by the case with 0.65 mm effective diameter and 37% porosity. The “basic” case with 0.65 mm diameter and 40.8% porosity notably overestimates the DHF. A somewhat better estimate is apparently given by the Hu & Theofanous model. However, in earlier studies no support has been found for this model to fit experimental data better than the Reed model. On the contrary, recent studies by Yakush et al. [0] suggest that the optimal values for the powers of relative permeability and passability (Eqs. 5-6) could be even lower than in the Reed model.

On its part, the same study confirms by methods of global sensitivity analysis that DHF is highly sensitive to the discussed physical model parameters – porosity and especially particle size. Uncertainty in these parameters can obscure other error sources to DHF. When investigating the uncertainty related to the effects of different test facilities and heating arrangements, the uncertainty of porosity and particle diameter should be minimized, e.g. by using particles as uniform and spherical as possible packed to the maximum packing density (minimum porosity).

7.5.1 Model limitations

In all the simulations, it is assumed that heating is homogenous in the debris bed (constant power density) as in an internally heated debris bed. The test bed heaters are not taken into account in the modelling and, when only the overall coolability is concerned, it is assumed that the test bed behaves similarly to a homogeneously heated bed. The experimental work to distinguish the possible effect of heating arrangements continues within the NKS DECOSE project jointly performed by VTT and KTH. Conclusions will be presented when enough experimental data for comparison of the three test facilities, POMECO-HT, COOLOCE and STYX, is available.

It should be noted that the applied models are designed to solve flows in porous media. The free-flow volume (pool) is not modelled in a detailed, mechanistic manner which would require e.g. the solution of the full momentum equation with the time derivatives and wall friction now omitted from Eqs.1-2. Instead, the pool is treated similarly as the debris bed region but with a large porosity and particle diameter to provide “background friction”. Heat losses are also not taken into account, the wall boundaries are adiabatic.

8. Conclusions

Dryout heat flux experiments that investigate the effects of particle material, heating arrangement, water pool subcooling and lateral flooding have been performed with the COOLOCE test facility. In addition, simulations of the experiments with variations of the important model parameters, porosity and particle size, have been presented.

Alumina gravel previously used in the STYX test programme was used as the debris simulant material in COOLOCE-8 and -9. The experiments were conducted with a top-flooded cylindrical test bed and the pressure range investigated was 1-7 bar. The COOLOCE-8 test series showed that the dryout heat flux for the alumina gravel is relatively low compared to the COOLOCE experiments with spherical beads and to the early experiments with the STYX facility with a different type of resistance heating arrangement. The experiments with initially subcooled pool, COOLOCE-9, suggest that the subcooling may increase dryout heat flux and increase coolability.

The aim of the COOLOCE-10 test series was to investigate the effect of lateral flooding in a test bed with cylindrical geometry, approximating a mound-shaped debris bed. The pressure range was 1-3 bar. It was found that the dryout heat flux and coolability is increased by more than 50% compared to a top-flooded cylinder. Dryout occurred in the upper central region of the test bed which is in agreement with a pre-test simulation.

MEWA 2D simulations aiming to model the debris bed coolability have been assessed against the experiments. The two simulant materials, spherical beads and irregular gravel, have been taken into account in the modelling by variations of particle diameter and porosity. For both materials, the effective particle diameter has also been estimated by separate single-phase pressure loss measurements.

It was found that with the measured effective particle diameter and porosity, the simulation models predict dryout heat flux with a relatively good accuracy in the case of spherical particles. In the case of irregular gravel, there is more discrepancy between the simulations and experiments, especially for higher pressure levels. The uncertainty in the results is greater in the case of gravel because the variation range of true bed porosity and particle diameter are larger. It appears to be well possible that the gravel bed has been shifted towards denser packing during the experiments.

Comparison of the DHFs measured with two test facilities, STYX and COOLOCE, shows that the measured DHF is smaller in COOLOCE. However, it is not certain whether the difference is specific to the test facility or process such as the heating arrangement, or whether the test bed has been more densely packed in COOLOCE.

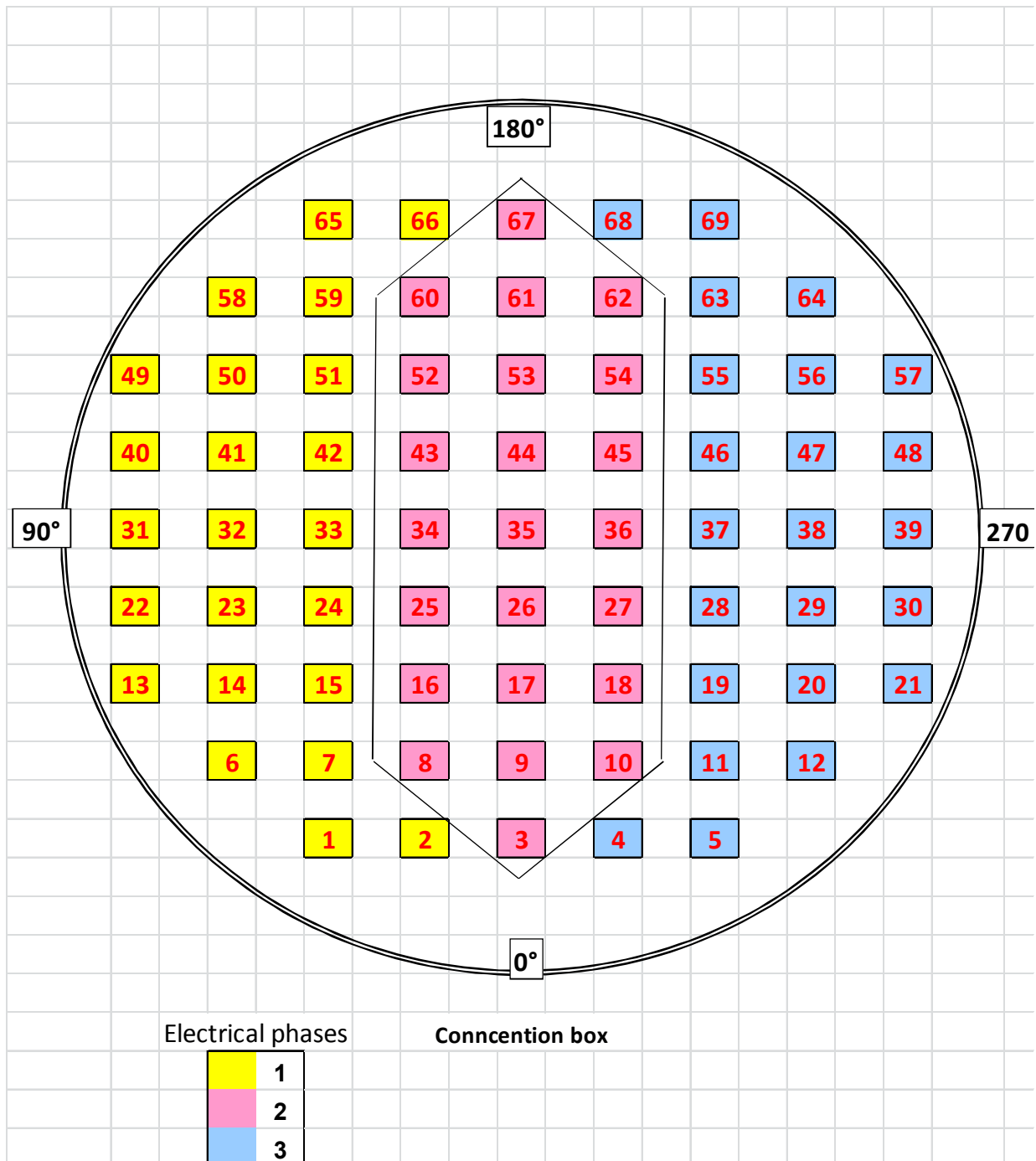
9. References

1. Takasuo, E., Kinnunen, T. Pankakoski P.H., Holmström, S. Description of the COOLOCE test facility – Conical particle bed. Research Report VTT-R-08956-10. Espoo, 2010. 18 p.
2. Takasuo, E., Kinnunen, T. Pankakoski P.H., Holmström, S. The COOLOCE-2 coolability experiment with a conical particle bed. Research Report VTT-R-02427-11. Espoo, 2011. 15 p.
3. Takasuo, E., Kinnunen, T. Pankakoski P.H., Holmström, S. The COOLOCE particle bed coolability experiments with a cylindrical geometry: Test series 3–5. Research Report VTT-R-07099-11. Espoo, 2011. 27 p.

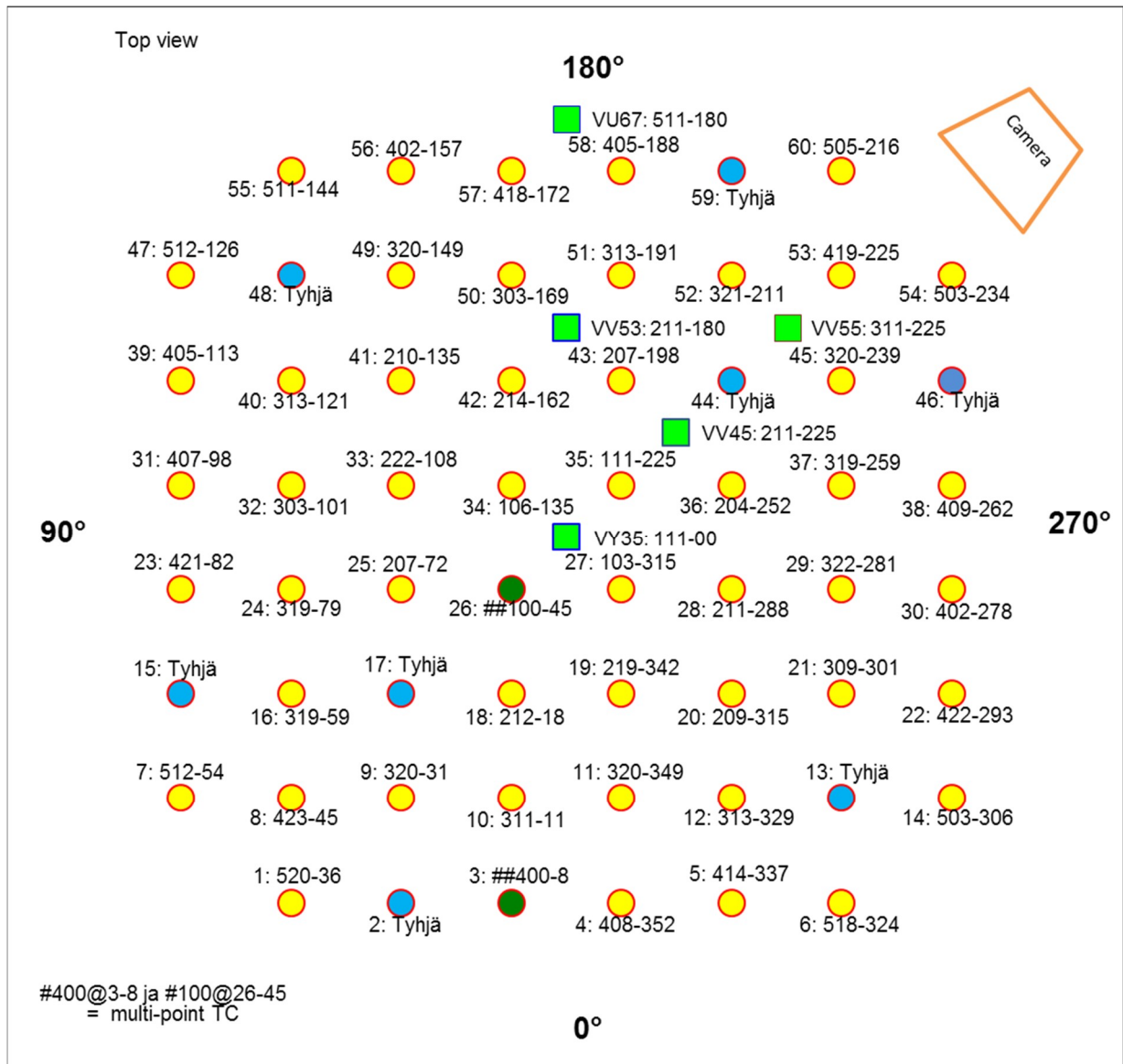
4. Takasuo, E., Kinnunen, T., Pankakoski P.H., Holmström, S. The COOLOCE particle bed coolability experiments with a conical geometry: Test series 6–7. Research Report VTT-R-07097-11. Espoo, 2011. 26 p.
5. Takasuo, E., Holmström, S., Kinnunen, T., Pankakoski, P.H. 2012. The COOLOCE experiments investigating the dryout power in debris beds of heap-like and cylindrical geometries. Nuclear Engineering and Design 250 (2012), p. 687-700.
6. Lindholm, I., Holmström, S., Miettinen, J., Lestinen, V., Hyvärinen, J., Pankakoski, P., Sjövall, H. 2006. Dryout Heat Flux Experiments with Deep Heterogenous Particle Bed. Nuclear Engineering and Design 236 (2006), p. 2060-2074.
7. Holmström, S., Pankakoski, P.H. STYX dry-out heat flux testing with different test bed thicknesses. Part II: homogenous and stratified tests with 600 mm and 400 mm test beds. VTT Industrial Systems, Research Report BTUO74-051381. Espoo, 2005.
8. Takasuo, E., Holmström, S., Kinnunen, T., Pankakoski, P.H., Hosio, E., Lindholm, I. 2011. The effect of lateral flooding on the coolability of irregular core debris beds. Nuclear Engineering and Design 241 (2011), p. 1196–1205.
9. Konovalikhin, M.J. 2001. Investigations on Melt Spreading and Coolability in a LWR Severe Accident. Doctoral Thesis, Royal Institute of Technology, Stockholm, Sweden. ISSN-1403-1701.
10. Bürger, M., Buck, M., Rahman, S., Kulenovic, R., Fichot, F., Ma, W.M., Miettinen, J., Lindholm, I., Atkhen, K. 2010. Coolability of particulate beds in severe accidents: Status and remaining uncertainties. Progress in Nuclear Energy 52, p. 61-75.
11. Yakush, S., Kudinov, P. 2011. Effects of Water Pool Subcooling on the Debris Bed Spreading by Coolant Flow. Proceedings of ICAPP 2011, Nice, France, May 2-5, 2011. Paper 11416.
12. Karbojian, A., Ma, W., Kudinov, P., Davydov, M., Dinh, T.N., 2007. A Scoping Study of Debris Formation in DEFOR Experimental Facility. Proceedings of the 15th International Conference on Nuclear Engineering, Nagoya, Japan, April 22-26, 2007. ICONE15-10620.
13. Ergun, S. 1952. Fluid flow through packed columns. Chemical Engineering Progress 48, p. 89-94.
14. Ma, W. 2012. Study of irregular multi-sized particles bed using POMECO-FL facility (Draft). E-mail communications from Weimin Ma, December 4, 2012.
15. Hu, K., Theofanous, T.G. 1991. On the Measurement and Mechanism of Dryout in Volumetrically Heated Coarse Particle Beds. International Journal on Multiphase Flow, Vol. 17, No. 4, p. 519-532.

16. Takasuo, E., Hovi, V. 2012. MEWA and PORFLO calculations of the COOLOCE experiments. Research Report VTT-R-00967-12. Espoo, 2012. 36 p.
17. Takasuo, E., Hovi, V., Ilvonen, M., Holmström, S. 2012. Modeling of Dryout in Core Debris Beds of Conical and Cylindrical Geometries. Proceedings of the 20th International Conference on Nuclear Engineering, Anaheim, California, USA, July 30 – August 3, 2012. ICONE20-54159.
18. Lubchenko, N., Yakush, S., Kudinov, P. Pre-test calculations for cylinder geometries with open side walls or turned off outer heaters. Unpublished report, email communications, August 20, 2012.
19. Bürger, M., Buck, M., Schmidt, W., Widmann, W. Validation and application of the WABE code: Investigations of constitutive laws and 2D effects on debris coolability. Nuclear Engineering and Design 236 (2006), p. 2164–2188.
20. Takasuo, E., Hovi, V., Ilvonen, M. PORFLO modelling of the coolability of porous particle beds. Research Report VTT-R-09376-10. Espoo, 2011. 41 p.
21. Takasuo, E., Hovi, V. 2012. MEWA and PORFLO calculations of the COOLOCE experiments. Research Report VTT-R-00967-12. Espoo, 2012. 36 p.
22. Lipinski, R.J. 1982. A Model for Boiling and Dryout in Particle Beds. Sandia National Laboratories, SAND 82-9765, NUREG/CR-2646.
23. Reed, A.W. 1982. The effect of channeling on the dryout of heated particulate beds immersed in a liquid pool. PhD. Thesis. Massachusetts Institute of Technology, Cambridge.
24. Tung, V.X. and Dhir, V.K., 1988. A Hydrodynamic Model for Two-Phase Flow through Porous Media. International Journal of Multiphase Flow 14 No. 1, 47-65.
25. Schmidt, W., 2004. Influence of Multidimensionality and Interfacial Friction on the Coolability of Fragmented Corium. Doctoral Thesis, Institut für Kernenergetik und Energiesysteme, Universität Stuttgart, 2004.
26. Takasuo, E. 2009. Numerical analysis of the STYX particle bed coolability tests with different bed thicknesses and downcomers. VTT Research Report VTT-R-06318-09. Espoo, 2009.
27. Yakush, S.E., Kudinov, P., Lubchenko, N.T. 2013. Coolability of heat releasing debris bed. Part 1: Sensitivity analysis and model calibration. Annals of Nuclear Energy 52 (2013), 59-71.

APPENDIX A. Heater arrangement in the COOLOCE cylinder



APPENDIX B. Thermocouple arrangement in the COOLOCE cylinder



Example of how to read the map:

111-225

1 – number of the ring to which the thermocouple belongs to (1 indicates the central sensors, 5 the outermost)

11 – height of the thermocouple from the bottom in cm

225 – angle between the thermocouple location and 0°

APPENDIX C. Dryout heat flux and power density in the experiments and simulations

Units: Heat flux kW/m², power density kW/m³, pressure bar (absolute)

COOLOCE-8 Pressure	Experimental HF	Simulated HF			
		CASE1	CASE1b	CASE2	CASE3
1.1	177.93	177.93	171.09	123.18	191.62
2.0	235.42	260.05	239.52	184.78	280.58
3.0	262.79	314.80	287.43	218.99	335.33
4.0	290.17	362.71	328.49	253.21	383.24
5.0	318.91	396.92	355.86	280.58	424.30
7.0	342.18	465.36	410.61	328.49	485.89

COOLOCE-3-5 Pressure	Experimental HF	Simulated HF		
		CASE4	CASE5	CASE6
1.1	270.28	304.73	231.86	218.61
2.0	347.13	423.97	331.23	331.23
3.0	422.65	496.84	390.85	384.22
4.0	458.42	563.09	443.85	437.22
5.0	492.87	616.08	483.59	483.59
7.0	560.44	702.20	556.46	556.46

COOLOCE-6-7 Pressure	Experimental DPD	Simulated DPD		
		CASE7	CASE8	CASE9
1.1	1471.30	1160.06	1160.06	1301.53
1.6	1799.51	1527.89	1527.89	1697.65
2.0	2037.18	1782.54	1754.24	1952.30
3.0	2427.64	2206.95	2206.95	2376.71

STYX-8 Pressure	Experimental HF
1.0	213.62
2.0	273.04
4.0	328.21
5.0	356.51
7.0	428.66

Title	COOLOCE debris bed experiments and simulations investigating the coolability of cylindrical beds with different materials and flow modes
Author(s)	Eveliina Takasuo, Tuomo Kinnunen, Stefan Holmström, Taru Lehtikuusi
Affiliation(s)	VTT Technical Research Centre of Finland
ISBN	978-87-7893-361-4
Date	July 2013
Project	NKS-R / DECOSE
No. of pages	58
No. of tables	5
No. of illustrations	48
No. of references	27

Abstract

The COOLOCE experiments aim at investigating the coolability of debris beds of different geometries, flow modes and materials. A debris bed may be formed of solidified corium as a result of a severe accident in a nuclear power reactor. The COOLOCE-8 test series consisted of experiments with a top-flooded test bed with irregular gravel as the simulant material. The objective was to produce comparison data useful in estimating the effects of different particle materials and the possible effect of the test arrangement on the results. It was found that the dryout heat flux (DHF) measured for the gravel was lower compared to previous experiments with spherical beads, and somewhat lower compared to the early STYX experiments. The difference between the beads and gravel is at least partially explained by the smaller average size of the gravel particles. The COOLOCE-9 test series included scoping experiments examining the effect of subcooling of the water pool in which the debris bed is immersed. The experiments with initially subcooled pool suggest that the subcooling may increase DHF and increase coolability. The aim of the COOLOCE-10 experiments was to investigate the effect of lateral flooding on the DHF a cylindrical test bed. The top of the test cylinder and its sidewall were open to water infiltration. It was found that the DHF is increased compared to a top-flooded cylinder by more than 50%. This suggests that coolability is notably improved. 2D simulations of the top-flooded test beds have been run with the MEWA code. Prior to the simulations, the effective particle diameter for the spherical beads and the irregular gravel was estimated by single-phase pressure loss measurements performed at KTH in Sweden. Parameter variations were done for particle size and porosity used as input in the models. It was found that with the measured effective particle diameter and porosity, the simulation models predict DHF with a relatively good accuracy in the case of spherical particles. In the case of irregular gravel, for which the uncertainties of porosity and particle diameter are larger, the discrepancy between the simulations and experiments is greater.

Key words severe accident, core debris, coolability, dryout, COOLOCE experiments, MEWA code